HELICON PROPAGATION IN SODIUM AND COPPER

A Thesis Presented to
The Faculty of the Department of Physics
University of Houston

In Partial Fulfillment
of the Requirements for the Degree
Master of Science

BY
Stephanie Dietz Yesavage

December, 1971

ACKNOWLEDGEMENTS

I wish to thank Dr. Lowell T. Wood for the help and encouragement given to me during the preparation of this thesis. I also express my thanks to Victor Yesavage, who helped me find many of my computer errors, and to the Physics Department for support through a Teaching Fellowship.

HELICON PROPAGATION IN SODIUM AND COPPER

An Abstract of a Thesis

Presented to

the Faculty of the Department of Physics

Univeristy of Houston

In Partial Fulfillment

of the Requirements for the Degree

Master of Science

BY

Stephanie Dietz Yesavage

December, 1971

ABSTRACT

Helicons and Gantmakher-Kaner oscillations were observed for the sodium metal. For a cylindrically symmetric Fermi surface approximation for copper, we observed the beating of two Gantmakher-Kaner waves for the [111] direction of copper and helicon propagation for the [001] direction of copper. Using the true Fermi surface of copper, we observed helicon propagation in the [001] direction. In all instances of helicon propagation, we found that a relaxation time of 10^{-10} sec. produced smooth sinusoidal shaped helicon curves, whereas a relaxation time of 10^{-9} sec. produced a delta-function shaped curve.

TABLE OF CONTENTS

INTRODUCTION

An electromagnetic wave striking a metal surface is generally damped to 1/e of its initial amplitude within a distance of δ, the skin depth. However, if a static magnetic field is present and the metal is pure, it is possible under certain conditions for the wave to propagate through the metal. This propagated wave is called a helicon.

Given a slab of metal of thickness Q upon which an electromagnetic wave of frequency ω is incident in the presence of a static magnetic field $\vec{B}$, we calculate in this paper the ratio of the transmitted to incident electric fields, E_t/E_i. The expression E_t/E_i is a complex quantity, thus supplying an amplitude and a phase factor.

The metals chosen for investigation were sodium and copper. The calculation of E_t/E_i requires the knowledge of the Fermi surface of the metal. Whereas, such calculations have been done for a spherical Fermi surface which sodium possesses and for approximate Fermi surfaces of copper, no calculation has yet been done using the exact Fermi surface of copper. It is the main purpose of this thesis to calculate E_t/E_i using the correct Fermi surface of copper and to thus make data available for comparison with experimental data recorded previously by others. A second purpose of this paper was an investigation of the effect of the relaxation time τ on the shape of the curve produced by a plot of E_t/E_i versus B.

The sodium metal was investigated because of the simplification of the calculations brought about by its spherical Fermi surface. After finding that the sodium data was in good agreement with experimental data, we advanced to a cylindrically symmetric Fermi surface for copper and, at last, to the true non-cylindrically symmetric Fermi surface. The former Fermi surfaces provide an accuracy check for the final copper calculations.

THEORY

Let us first describe the condition for helicon propagation. Suppose an electromagnetic wave with wave number $\vec{q}$ and frequency ω is propagating in a metal in the presence of a static magnetic field $\vec{B}$. Suppose, also, that $\vec{q}$ and $\vec{B}$ are both parallel to the Z-axis. Now the force $\vec{F}_e$ on an electron in the metal with an average velocity in the Z-direction, $\overline{V}_z$, due to the B field is found from

$$\vec{F}_e = e(\vec{V} \times \vec{B}) \; . \qquad (1)$$

The electron will move in a helix about an axis parallel to the Z-axis due to the initial velocity of the electron. The cyclotron frequency of the electron is given by

$$\omega_c = (eB)/(mc) \; . \qquad (2)$$

Now, the electron sees the electromagnetic wave as having the Doppler shifted frequency ω_e given by

$$\omega_e = \omega + q\overline{V}_z \; . \qquad (3)$$

Let τ equal the relaxation time of the electron. If $\omega_c\tau \gg 1$, then the electron makes many spirals of its orbit before it has a collision. In this time, it would be able to absorb energy from the electric field, if the condition $\omega_e = \omega_c$ is satisfied. This is called Doppler shifted cyclotron resonance. Thus, we have two required conditions for energy absorption,

$$\omega_e = \omega_c \quad , \tag{4}$$

and

$$\omega_c \tau \gg 1 \quad . \tag{5}$$

Let the maximum value of $\bar{V}_z$ of an electron in the metal be denoted by $\bar{V}_{zMAX}$. Thus, the maximum Doppler shifted frequency seen by an electron is given by

$$\omega_{eMAX} = \omega + q \bar{V}_{zMAX} \quad . \tag{6}$$

Now, for a given B field, ω_c is constant. Thus, if $\omega_c < \omega_{eMAX}$, then some electrons with a $\bar{V}_z < \bar{V}_{zMAX}$ will be able to satisfy the condition $\omega_c = \omega_e$, and energy will be absorbed from the electromagnetic wave or helicon. If $\omega_c = \omega_{eMAX}$, only the electrons with $\bar{V}_z = \bar{V}_{zMAX}$ would be capable of absorbing energy. We call the condition $\omega_c = \omega_{eMAX}$ the absorption edge. Now, if we increase the value of B such that $\omega_c > \omega_{eMAX}$, then no electron could absorb energy, and the helicon would propagate with no cyclotron damping effects.

For three-fold symmetry about the magnetic field direction, we have the following expression for E_t/E_i from Antoniewicz, et al.[1]:

$$\frac{E_t}{E_i} = \frac{-i4\omega}{Qc} \sum_{m=1}^{\infty} \frac{(-1)^m}{\left(\frac{m\pi}{Q}\right)^2 - \left(\frac{\omega}{c}\right)^2 \epsilon_+\left(\frac{m\pi}{Q}\right)} + \frac{i4c}{Q\omega\epsilon_+(0)} \quad , \tag{7}$$

where

Q = thickness of metal slab,

C = speed of light,

K = ionic dielectric constant,

$$\overleftrightarrow{\sigma} = \text{conductivity tensor} = \begin{pmatrix} \sigma_{xx} & \sigma_{xy} & \sigma_{xz} \\ \sigma_{yx} & \sigma_{yy} & \sigma_{yz} \\ \sigma_{zx} & \sigma_{zy} & \sigma_{zz} \end{pmatrix}, \tag{8}$$

$$\sigma_+ = \sigma_{xx} - i\sigma_{xy} , \tag{9}$$

and

$$\epsilon_+\left(\frac{m\pi}{Q}\right) = \frac{4\pi}{i\omega}\sigma_+\left(\frac{m\pi}{Q}\right) + K . \tag{10}$$

Now, $K \ll \frac{4\pi}{i\omega}\sigma_+$, and we ignore the term $\frac{i4c}{Q\omega\,\epsilon_+(0)}$ because of its negligible contribution. Thus, we have

$$\frac{E_t}{E_i} = \frac{-i4\omega}{QC}\sum_{m=1}^{\infty}\frac{(-1)^m}{\left(\frac{m\pi}{Q}\right)^2 + \frac{i\omega 4\pi}{c^2}\sigma_+\left(\frac{m\pi}{Q}\right)} , \tag{11}$$

and

$$\frac{E_t}{E_i} = \frac{-i4\omega}{QC}\sum_{m=1}^{\infty}\frac{(-1)^m}{\left[\left(\frac{m\pi}{Q}\right)^2 + \frac{\omega 4\pi}{c^2}\sigma_{xy}\right] + \frac{i\omega 4\pi}{c^2}\sigma_{xx}} . \tag{12}$$

Now, let us denote the real and imaginary parts of σ_{xx} and σ_{xy} as follows:

$$\text{Real } \sigma_{xx} = \text{ANSRX} , \tag{13}$$

$$\text{Imaginary } \sigma_{xx} = \text{ANSIX} , \tag{14}$$

$$\text{Real } \sigma_{xy} = \text{ANSRY} , \tag{15}$$

and

$$\text{Imaginary } \sigma_{xy} = \text{ANSIY} . \tag{16}$$

Then we have,

$$\frac{E_t}{E_i} = -\frac{i4\omega}{QC}\sum_{m=1}^{\infty}\frac{(-1)^m}{\left\{\left(\frac{m\pi}{Q}\right)^2 - \frac{\omega 4\pi}{c^2}[\text{ANSIX} - \text{ANSRY}]\right\} + i\left\{\frac{\omega 4\pi}{c^2}[\text{ANSRX} + \text{ANSIY}]\right\}} \quad . \tag{17}$$

Let $S = \left\{\left(\frac{m\pi}{Q}\right)^2 - \frac{\omega 4\pi}{c^2}[\text{ANSIX} - \text{ANSRY}]\right\}$, (18)

and $V = \left\{\frac{\omega 4\pi}{c^2}[\text{ANSRX} + \text{ANSIY}]\right\}$. (19)

Thus, we have for the real and imaginary parts of E_t/E_i,

$$\text{REAL}\left(\frac{E_t}{E_i}\right) = \frac{4\omega}{QC}\sum_{m=1}^{\infty}\frac{(-1)^{m+1}V}{S^2+V^2} \quad , \tag{20}$$

and

$$\text{IMAGINARY}\left(\frac{E_t}{E_i}\right) = \frac{4\omega}{QC}\sum_{m=1}^{\infty}\frac{(-1)^{m+1}S}{S^2+V^2} \quad . \tag{21}$$

Now, we have stated that E_t/E_i gives the amplitude, $|E_t/E_i|$, and the phase θ of the E_t/E_i ratio. Thus, we have

$$|E_t/E_i| = \left(\left[\text{Real}\left(\frac{E_t}{E_i}\right)\right]^2 + \left[\text{Imaginary}\left(\frac{E_t}{E_i}\right)\right]^2\right)^{1/2} \quad , \tag{22}$$

and

$$\text{ARCTAN}\ \theta = \frac{\text{Imaginary}\left(\frac{E_t}{E_i}\right)}{\text{Real}\left(\frac{E_t}{E_i}\right)} \quad . \tag{23}$$

However, we are concerned only with Real E_t/E_i, since this is the only part seen experimentally.

From the development of Mertsching[2], we have the following expressions:

$$\overleftrightarrow{\sigma}_{a,b}(\vec{q}) = \frac{e^2}{2\pi\hbar^2}\int_{-\text{KMAX}}^{+\text{KMAX}} m_c\, dk_z \sum_{m=-\infty}^{\infty}\frac{\vec{V}_{ma}\,\vec{V}_{mb}^{\,*}}{\frac{1}{\tau} + i(\vec{q}\cdot\bar{\vec{v}} - \omega - m\omega_c)} \quad , \tag{24}$$

and

$$\vec{V}_{ma} = \frac{1}{2\pi}\int_0^{2\pi}\vec{V}_a(\theta)\, e^{-\frac{i}{\omega_c}\int_0^{\theta}[\vec{q}\cdot\{\vec{V}(\theta'') - \bar{\vec{v}}\} + m\omega_c]d\theta''}\, d\theta \quad , \tag{25}$$

where

$\overleftrightarrow{\sigma}$ = conductivity tensor,

KMAX = maximum value of k_z on the Fermi surface,

ω = frequency of electromagnetic wave,

τ = relaxation time,

$\hbar$ = Planck's constant,

e = charge of electron,

m_c = cyclotron mass,

ω_c = cyclotron frequency

Q = thickness of metal slab,

q = wave vector = $\frac{m\pi}{Q}$ $\quad m = 0, 1, 2 \cdots$,

n = an integer,

a = indice for X, Y, or Z component,

b = indice for X, Y, or Z component,

$\vec{V}_a(\theta)$ = a-component of electron velocity at Fermi surface,

and $\overline{V}$ = average electron velocity at Fermi surface.

In our calculation of E_t/E_i, we need expressions for σ_{xx} and σ_{xy}. Thus, we have, assuming that $\vec{q}$ is in the Z-direction,

$$\sigma_{xx} = \frac{e^2}{2\pi\hbar^2}\int_{-KMAX}^{+KMAX} m_c \, dk_z \sum_{m=-\infty}^{\infty} \frac{\vec{V}_{mx}\vec{V}_{mx}^*}{\frac{1}{\tau} + i\left(\frac{m\pi}{Q}\overline{V}_z - \omega - m\omega_c\right)}, \tag{26}$$

$$\vec{V}_{mx} = \frac{1}{2\pi}\int_0^{2\pi} V_x(\theta)\, e^{-\frac{i}{\omega_c}\int_0^{\theta}\left[\frac{m\pi}{Q}\{V_z(\theta') - \overline{V}_z\} + m\omega_c\right]d\theta''} d\theta, \tag{27}$$

$$\sigma_{xy} = \frac{e^2}{2\pi\hbar^2}\int_{-KMAX}^{+KMAX} m_c \, dk_z \sum_{m=-\infty}^{\infty} \frac{\vec{V}_{mx}\vec{V}_{mx}^*}{\frac{1}{\tau} + i\left(\frac{m\pi}{Q}\overline{V}_z - \omega - m\omega_c\right)}, \tag{28}$$

and $$\vec{V}_{my}^* = \frac{1}{2\pi}\int_0^{2\pi} V_y(\theta)\, e^{\frac{i}{\omega_c}\int_0^{\theta}\left[\frac{m\pi}{Q}\{V_z(\theta'') - \overline{V}_z\} + m\omega_c\right]d\theta''} d\theta. \tag{29}$$

We have the following dispersion relation for a circularly polarized electromagnetic wave in a metal, such as a helicon:

$$q^2 = \frac{4\pi\omega}{c^2}\left(\text{IMAGINARY } \sigma_+ - i \text{ REAL } \sigma_+\right) \quad . \tag{30}$$

Since

$$\sigma_+ = (\text{ANSRX} + \text{ANSIY}) + i(\text{ANSIX} - \text{ANSRY}) \ , \tag{31}$$

we have

$$q^2 = \frac{4\pi\omega}{c^2}\left\{(\text{ANSIX} - \text{ANSRY}) - i(\text{ANSRX} + \text{ANSIY})\right\} . \tag{32}$$

We may express $|\vec{q}|^2$ in polar form as:

$$q^2 = \left\{\left(\frac{4\pi\omega}{c^2}\text{Img. }\sigma_+\right)^2 + \left(\frac{4\pi\omega}{c^2}\text{REAL }\sigma_+\right)^2\right\}^{1/2} e^{i\theta} \ , \tag{33}$$

where

$$\theta = \arctan\frac{-\text{Real }\sigma_+}{\text{Img. }\sigma_+} = \arctan\frac{(-\text{ANSIX} + \text{ANSRY})}{(\text{ANSRX} + \text{ANSIY})} \quad . \tag{34}$$

Let us call the roots of q^2, q_1 and q_2. Then we have that

$$q_1 = \left\{\left(\frac{4\pi\omega}{c^2}\text{Img }\sigma_+\right)^2 + \left(\frac{4\pi\omega}{c^2}\text{Real }\sigma_+\right)^2\right\}^{1/4}\left(\cos\frac{\theta}{2} + i\sin\frac{\theta}{2}\right), \tag{35}$$

and

$$q_2 = \left\{\left(\frac{4\pi\omega}{c^2}\text{Img }\sigma_+\right)^2 + \left(\frac{4\pi\omega}{c^2}\text{Real }\sigma_+\right)^2\right\}^{1/4}\left(\cos\left[\frac{\theta}{2}+\pi\right] + i\sin\left[\frac{\theta}{2}+\pi\right]\right) . \tag{36}$$

An electromagnetic wave propagates as $e^{i(\vec{q}\cdot\vec{r}-\omega t)}$. If $\text{Img }\sigma_+ \gg \text{Real }\sigma_+$, then θ is close to zero. This makes q_1 and q_2 mostly real, and there is a negligible damping factor. As the $Real\ \sigma_+$ increases, θ approaches $-\frac{\pi}{2}$ which means that the imaginary part of $\vec{q}$ is increasing which causes the damping factor to increase. At $\theta = -\frac{\pi}{2}$, we have

$$q_1 = \left\{ \left(\frac{4\pi\omega}{c^2} \mathrm{Img.}\ \sigma_+ \right)^2 + \left(\frac{4\pi\omega}{c^2} \mathrm{Real}\ \sigma_+ \right)^2 \right\}^{1/4} \left(\frac{1}{\sqrt{2}} - i \frac{1}{\sqrt{2}} \right) , \qquad (37)$$

and

$$q_2 = \left\{ \left(\frac{4\pi\omega}{c^2} \mathrm{Img.}\ \sigma_+ \right)^2 + \left(\frac{4\pi\omega}{c^2} \mathrm{Real}\ \sigma_+ \right)^2 \right\}^{1/4} \left(-\frac{1}{\sqrt{2}} + i \frac{1}{\sqrt{2}} \right) . \qquad (38)$$

The root q_1 is discarded because the imaginary part of q_1 carries a minus sign giving rise to an exponentially increasing wave. Thus, q_2 would be our solution.

Therefore, when helicon propagation exists, we will expect the condition $\mathrm{Img}\ \sigma_+ \gg \mathrm{Real}\ \sigma_+$, greater than implying at least one order of magnitude.

It will be noticed that the expression for E_t/E_i contains a sum going from one to infinity over the variable m. The following explains the approach taken to approximate this sum.

When cylindrical symmetry about the magnetic field direction exists, we have from Wood[3] the following expression for σ_+, for the local regime $(qL \ll 1)$:

$$\sigma_+ = \frac{m e c \left(\frac{1}{\omega_c \tau} + i \right)}{B \left(\left(\frac{1}{\omega_c \tau} \right)^2 + 1 \right)} , \qquad (39)$$

where L = the mean free path of the electron, and

n = density of electrons per unit volume of real space.

When: $\omega_c\tau >> 1$, this reduces to

$$\sigma_+ = \frac{nec}{B}\left[\frac{1}{\omega_c\tau} + i\right] \quad . \tag{40}$$

Now we have the equations

$$\text{Real } \sigma_+ = \frac{nec}{B}\,\frac{1}{\omega_c\tau} \ , \tag{41}$$

and

$$\text{Img. } \sigma_+ = \frac{nec}{B} \quad . \tag{42}$$

The real part of E_t/E_i is largest when

$$\left\{\left(\frac{m\pi}{Q}\right)^2 - \frac{\omega 4\pi}{c^2}\,\text{Img.}\,\sigma_+\right\} = 0 \quad . \tag{43}$$

Thus, solving for that M* which makes this expression equal to zero, we obtain

$$M^* = \frac{Q}{c}\left(\frac{\omega 4 nec}{\pi B}\right)^{1/2} \quad . \tag{44}$$

With the assumption that our finite relaxation time still gives a sufficiently large $\omega_c\tau$, we sum over a finite number of m's centered about M*. The contribution to E_t/E_i made by an m decreases as its distance from M* increases.

From McGroddy, et. al.[4], we have the following expressions for the case of spherical symmetry:

$$\text{Real } \sigma_+ = \begin{cases} (3\omega_p^2/16 V_F q)(1 - 1/x^2) & x \geq 1 \\ 0 & x < 1 \end{cases} \ , \tag{45}$$

$$\text{Img. } \sigma_+ = (\omega_p^2/4\pi(\omega_c - \omega))\, F(x) \ , \tag{46}$$

where
$$X = \frac{q V_F}{\omega_c \left(1 - \frac{\omega}{\omega_c}\right)} , \tag{47}$$

$$F(x) = \frac{3}{x^2}\left[\frac{1}{2} - \frac{1-x^2}{4x} \ln\left|\frac{1+x}{1-x}\right|\right] , \tag{48}$$

$$\omega_p^2 = 4\pi n e^2 / m^{**} , \tag{49}$$

and
$$\omega_c = eB / m^{**} c . \tag{50}$$

The effective mass of the electron at the Fermi surface is denoted by m^{**} and the velocity by V_F .

These expressions hold for an infinite value of $\omega_c \tau$. Thus, we have that when $x < 1$, helicons propagate without attenuation, and when $x \geq 1$, the helicons are damped so severely they disappear.

It should be noted that McGroddy's expressions for σ_+ can not be substituted into our expression for E_t/E_i for any meaningful results. This is brought about because McGroddy lets the real part of σ_+ equal zero during propagation. For a finite relaxation time, for which E_t/E_i is derived, we never have a zero real part of σ_+ . Thus, we will always get a real part of E_t/E_i . If we do assume the real part of σ_+ is zero during helicon propagation, then we have

$$\frac{E_t}{E_i} = \frac{-i 4\omega}{Q c} \sum_{m=1}^{\infty} \frac{(-1)^m}{\left\{\left(\frac{m\pi}{Q}\right)^2 - \frac{\omega 4\pi}{c^2} I_{mg.}\sigma_+\right\}} , \tag{51}$$

which gives us a zero real part of E_t/E_i . Thus, we would conclude that there is no helicon propagation, when we know that according to McGroddy, there is helicon propagation. In our calculations for copper and sodium, it will be found that the real part of σ_+ is smaller than the imaginary part by at least one order of magnitude during propagation. This nonzero real part is necessary to exhibit Real E_t/E_i.

We now have a means of predicting at what approximate value of magnetic field we should expect to see helicon propagation start. Setting $X=1$ and using $m = M^*$, we find that

$$B=\left(\frac{m^{+*2} V_F^2 \pi \omega 4 m c}{e}\right)^{1/3} . \qquad (52)$$

It was stated that the knowledge of the Fermi surface is necessary for the calculation of E_t/E_i . This is because we must know the velocity of an electron on the Fermi surface. If $\varepsilon(\vec{k})$ is the equation of the Fermi surface, then we can relate the Fermi velocity to this surface by

$$(V_x, V_y, V_z) = \frac{1}{\hbar}\left(\frac{\partial \varepsilon(\vec{k})}{\partial k_x}, \frac{\partial \varepsilon(\vec{k})}{\partial k_y}, \frac{\partial \varepsilon(\vec{k})}{\partial k_z}\right) . \qquad (53)$$

In addition to the helicons, we will encounter Gantmakher-Kaner oscillations which are caused by electrons with an extremum in $m_c V_z$ along the magnetic field. The period of the oscillations is a constant and is defined by the equation

$$\left[m_c \bar{v}_z \right]_{ex.} = \frac{eQ}{2\pi c} \left(\frac{B}{n} \right) \qquad n = \text{integer}, \quad (54)$$

where the period (B/n) is measured in units of the magnetic field.

REAL E_t/E_i FOR SODIUM

Sodium has a spherical Fermi surface. Now we have

$$\overleftrightarrow{\sigma}_m = \frac{e^2}{2\pi^2\hbar^2}\int_{-KMAX}^{+KMAX} m_c\, dk_z \sum_{m=-\infty}^{\infty} \frac{\vec{V}_m \vec{V}_m^{*}}{\frac{1}{\tau}+i(\vec{q}\cdot\vec{\bar{v}} - \omega - m\omega_c)} , \qquad (55)$$

and

$$\vec{V}_m = \frac{1}{2\pi}\int_0^{2\pi}\vec{V}(\theta)\, e^{-\frac{i}{\omega_c}\int_0^{\theta}[\vec{q}\cdot\{\vec{V}_z(\theta'')-\vec{\bar{V}}_z\}+m\omega_c]d\theta''}\, d\theta . \qquad (56)$$

Now $\overleftrightarrow{\sigma}_m$ is an integral over the variable k_z and will be calculated by numerical integration methods. We must evaluate the integrand for a finite (preferably odd) number of values in order to this integral numerically. This means we must evaluate $\vec{V}_m$ at these particular k_z values also.

We will use a cylindrical co-ordinate system where z, θ, and ρ correspond to k_z, θ, and $k_\perp$ where $k_\perp=(k_{FX}^2+k_{FY}^2)^{1/2}$. A spherical Fermi surface is drawn in such a co-ordinate system below.

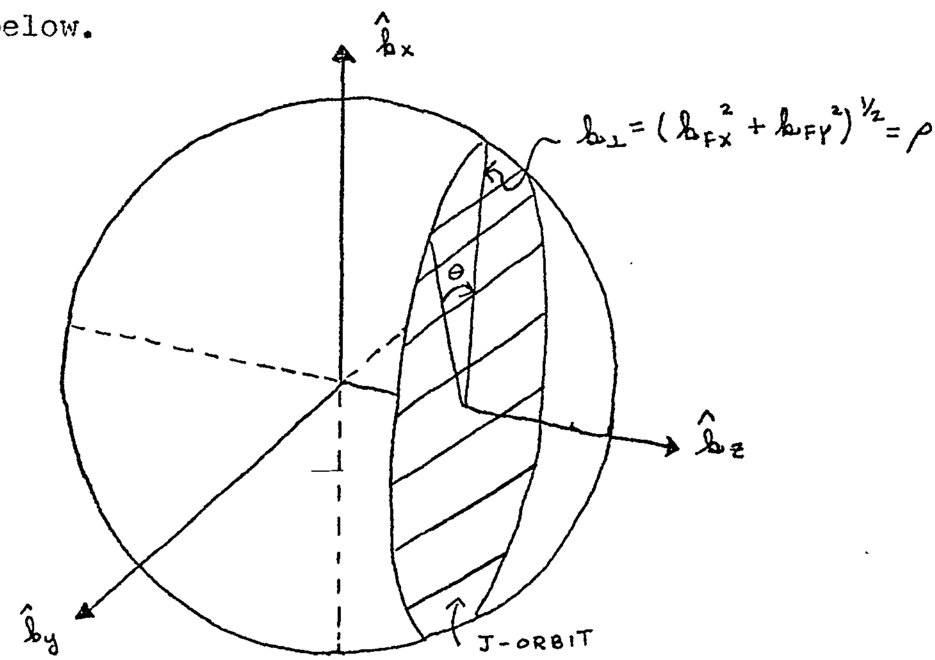

A j-orbit will be designated as a path of intersection of the Fermi surface with a plane k_z = constant. If we evaluate the integrand of $\overleftrightarrow{\sigma}_m$ at j* number of values of k_z , then we will have to deal with j* number of j-orbits. The expression $\vec{V}_m$ involves an integration over θ around a j-orbit. To evaluate $\vec{V}_m$, we would again use numerical methods. Each j-orbit would be divided into N intervals. The integrand of $\vec{V}_m$ would be evaluated at the N+1 points in the interval $[0, 2\pi]$.

For a spherical Fermi surface, however, it is possible to simplify matters so that the $\vec{V}_m$ integrations will not have to be done.

Knowing that for a Fermi sphere we have

$$\mathcal{E}(k) = \frac{\hbar^2}{2m}(k_x^2 + k_y^2 + k_z^2) , \tag{57}$$

and recalling Equation (53), we find that $\vec{V}_F$, the velocity of an electron on the Fermi sphere, and the wave vector, $\vec{k}_F$, are related by

$$m\vec{V}_F = \hbar\vec{k}_F \quad . \tag{58}$$

Now for any j-orbit $k_{Fz_j}(\theta) = k_{FzJ}$ = constant. Thus, we have

$$\overline{V}_{Fz_j} = \frac{1}{2\pi}\int_0^{2\pi}\frac{\hbar}{m}k_{Fz_j}(\theta)d\theta = \frac{1}{2\pi}\frac{\hbar}{m}\int_0^{2\pi}k_{Fz_j}\,d\theta \ , \tag{59}$$

and

$$\overline{V}_{Fz_j} = \frac{\hbar}{2\pi m}\frac{m}{\hbar}V_{Fz_j}\int_0^{2\pi}d\theta = V_{Fz_j} \ . \tag{60}$$

Therefore, we have that

$$\left\{ V_z(\theta'') - \bar{V}_z \right\} = 0 \quad , \tag{61}$$

which simplifies $\vec{V}_m$ to

$$\vec{V}_m = \frac{1}{2\pi}\int_0^{2\pi} \vec{V}(\theta)\, e^{-im\theta}\, d\theta \quad . \tag{62}$$

Also, we have that

$$m_c = \frac{\hbar}{2\pi}\int_{\text{PERIOD}} \frac{dk_s}{V_\perp} \quad , \tag{63}$$

where

$$V_\perp = (V_{xF}^2 + V_{yF}^2)^{1/2} \, , \tag{64}$$

and

$$dk_s = \frac{m}{\hbar} V_\perp d\theta \quad . \tag{65}$$

Thus,

$$m_c = \frac{\hbar}{2\pi}\int_0^{2\pi} \frac{m}{\hbar} V_\perp \left(\frac{1}{V_\perp}\right) d\theta \tag{66}$$

and

$$m_c = m \, . \tag{67}$$

Hence, we also have

$$\omega_c = \text{cyclotron frequency} = \frac{eB}{m_c C} = \frac{eB}{mC} \quad . \tag{68}$$

In the evaluation of $\vec{V}_m$, we note that

$$V_{Fxj}(\theta) = V_F \sin\theta_j \cos\theta \quad , \tag{69}$$

$$V_{Fyj}(\theta) = V_F \sin\theta_j \sin\theta \quad , \tag{70}$$

and

$$V_{Fzj}(\theta) = V_F \cos\theta_j \quad . \tag{71}$$

Recalling that

$$2\pi\,\delta_{m,m} = \int_0^{2\pi} e^{i(m-m)\theta}\, d\theta \, , \tag{72}$$

we obtain

$$V_{mxj} = (V_F \sin\theta_j/2)\left[\delta_{m,1} + \delta_{m,-1}\right] \quad , \tag{73}$$

$$V_{myj} = (V_F \sin\Theta_j/2i)\,[\delta_{m,1} - \delta_{m,-1}] \;, \tag{74}$$

and $$V_{mzj} = V_F \cos\Phi_j \,\delta_{m,0} \;. \tag{75}$$

From this, we see that the only contribution to the sum in $\overleftrightarrow{\sigma}_m$ will be from the integers n=1 and n= -1. Computing σ_{xx} and σ_{xy}, we get

$$\sigma_{xx} = \frac{-e^2 V_F^2 k_F m}{4\pi^2\hbar^2}\int_0^\pi \frac{a\sin^3\phi\, d\phi}{a^2+b^2} \;, \tag{76}$$

and

$$\sigma_{xy} = \frac{e^2 V_F^2 k_F m}{4\pi^2\hbar^2}\int_0^\pi \frac{b\sin^3\phi\, d\phi}{a^2+b^2} \;, \tag{77}$$

where
$$a = \frac{1}{\tau} + iq\bar{V}_z - i\omega \;,$$
and
$$b = \omega_c \;. \tag{78}$$
Now
$$\sigma_\pm = \sigma_{xx} \mp i\sigma_{xy} \;; \tag{79}$$
so we obtain

$$\sigma_\pm = -\frac{3}{4}\sigma_0\int_0^\pi \frac{\sin^3\phi\, d\phi}{1 + i\tau(\pm\omega_c - \omega + qV_F\cos\phi)} \;, \tag{80}$$

where $$\sigma_0 = ne^2\tau/m \;. \tag{81}$$
This integral can be evaluated as follows:
$$x = \cos\phi \;,$$
and
$$\sin\phi = (1-x^2)^{1/2} \;. \tag{82}$$
Such a substitution will give us

$$\sigma_+ = \frac{3i\sigma_0}{4qV_F\tau}\left\{2\Omega - (\Omega^2-1)\log\left(\frac{\Omega+1}{\Omega-1}\right)\right\} \;, \tag{83}$$

where
$$\Omega = \left((i/\tau) - \omega + \omega_c\right)/q\,V_F \;. \tag{84}$$

We now put σ_+ into E_t/E_i and obtain

$$\frac{E_t}{E_i} = \frac{-i4\omega}{Qc} \sum_{m=1}^{\infty} \frac{(-1)^m}{\left(\frac{m\pi}{Q}\right)^2 - \left(\frac{\omega}{c}\right)^2 \frac{4\pi}{i\omega}\sigma_+} \quad , \tag{85}$$

and

$$\frac{E_t}{E_i} = -\frac{i4\omega}{Qc} \sum_{m=1}^{\infty} \frac{(-1)^m}{\left[\left(\frac{m\pi}{Q}\right)^2 - \frac{\omega 4\pi}{c^2} \mathrm{Imag.}\,\sigma_+\right] + i\frac{\omega 4\pi}{c^2} \mathrm{Real}\,\sigma_+} \quad . \tag{86}$$

Let

$$S = \left[\left(\frac{m\pi}{Q}\right)^2 - \frac{\omega 4\pi}{c^2} \mathrm{Imag.}\,\sigma_+\right] \quad , \tag{87}$$

and

$$V = \frac{\omega 4\pi}{c^2} \mathrm{Real}\,\sigma_+ \quad . \tag{88}$$

Then we have that

$$\mathrm{Real}\left(\frac{E_t}{E_i}\right) = \frac{4\omega}{Qc} \sum_{m=1}^{\infty} \frac{(-1)^{m+1} V}{S^2 + V^2} \quad . \tag{89}$$

A computer program was run using the σ_+ we have just derived for two different cases. In one case, we chose a B-field range of 1,000 gauss to 10,000 gauss, $\omega = 10^6$ sec^{-1}, and $\tau = 10^{-9}$ sec. In the second case, we chose the same B-field range and frequency but made $\tau = 10^{-10}$ sec.

The sum in the expression $\mathrm{Real}\,(E_t/E_i)$ which is over m going from one to infinity was approximated by a sum going from one to seventy-five. An attempt was made to check the accuracy of this approximation in the following way. We ran a computer program to check the rate of convergence of

$$\sum_{m=M^*-X}^{M^*+X} \frac{(-1)^{m+1}\,V}{S^2+V^2}$$

where X equals an arbitrary integer. The results are given in Chart I. A sum was used over a finite number of m's centered about M*. The B-field range was from 7,000 gauss to 8,200 gauss. The number of terms included in each sum increased as B increased. However, the sum over 9 terms was also noted for each B-field so that a comparison could be made to a sum taken over more terms ranging from 19 to 37. The difference in these two sums was calculated, and for $\tau = 10^{-9}$ sec., there was a 1% difference or less while for $\tau = 10^{-10}$ sec., there was a difference as high as 115%. Thus, we could assume that for $\tau = 10^{-9}$ sec., there was rapid convergence while for $\tau = 10^{-10}$ sec., it was slow so that more terms than 9 would have to be included.

We must remember that the M* which makes S zero was defined only when $\omega_c\tau$ was infinite. We see that for $\tau = 10^{-9}$ sec, $\omega_c\tau \approx 17$ for B = 1,000 gauss and 170 for B = 10,000 gauss. For $\tau = 10^{-10}$ sec., $\omega_c\tau \approx 1.7$ for B = 1,000 gauss and 17 for B = 10,000 gauss. Since our values of $\omega_c\tau$ are not particularly large, we may doubt

CHART I

FOR RELAXATION TIME $\tau = 10^{-9}$ SEC.

B Field	Sum of 9 Terms	Final Sum	Number of Terms in Final Sum	Difference in Final Sum and Sum of Nine Terms
7000	-.326-02	-.326-02	19	0.0%
7100	-.223-02	-.223-02	23	0.0%
7200	-.178-03	-.180-03	23	1.1%
7300	+.545-04	+.529-04	25	3.0%
7400	+.369-03	+.367-03	27	0.5%
7500	+.184-02	+.184-02	27	0.0%
7600	+.258-02	+.259-02	31	0.4%
7700	+.484-03	+.486-03	31	0.4%
7800	+.103-03	+.104-03	31	1.0%
7900	-.792-04	-.776-04	33	2.1%
8000	-.365-03	-.363-03	35	0.6%
8100	-.160-02	-.160-02	35	0.0%
8200	-.263-02	-.263-02	37	0.0%
	FOR RELAXATION TIME $\tau = 10^{-10}$ SEC.			
7000	-.943-04	-.705-04	19	33.7%
7100	-.514-04	-.747-04	23	30.6%
7200	-.206-04	-.431-04	23	51.1%
7300	+.289-04	+.133-04	25	115.4%
7400	+.819-04	+.612-04	27	34.4%
7500	+.121-03	+.101-03	27	20.8%
7600	+.961-04	+.117-03	31	12.0%
7700	+.746-04	+.950-04	31	21.0%
7800	+.235-04	+.394-04	33	41.0%

the validity of using M* in a meaningful way. For $B = 1{,}000$ gauss, we have $M^* = 71$, and for $B = 10{,}000$ gauss, we have $M^* = 17$. Thus, it might seem that $\omega_c\tau$ for the case of $\tau = 10^{-10}$ sec. is not sufficiently large to use M* as that m which gives the largest contribution, thus leaving open the question as to what should be chosen as a centering point for the summation. Since our graphs of $\mathrm{Real}\,(E_t/E_i)$ versus B for $\tau = 10^{-9}$ sec. produced smooth regularly occuring waves, and a sum over an insufficient number of terms gave jagged irregular graphs, it was assumed that for the case of $\tau = 10^{-10}$ sec., we were summing over a sufficient number of terms if we got a smooth curve for our graphs. Our choice of summing from one to seventy-five gave us the desired results.

Graphs I through IV give the output for $\tau = 10^{-10}$ sec. Graphs V through IX give the output for $\tau = 10^{-9}$ sec.

Let us recall our predicted value of the magnetic field at which we expect to see helicon propagation start,

$$B = \frac{m^2 V_F^2 \pi \omega + Mc}{e} \quad . \tag{90}$$

From this definition we obtain $B = 5{,}800$ gauss. Thus, if we plot $\mathrm{Real}\,(E_t/E_i)$ versus B, we would expect to see helicon propagation around 5,800 gauss. From our graphs for $\tau = 10^{-9}$ sec., we see that helicon propagation is definitely starting at about this point. In the case of $\tau = 10^{-10}$ sec., our graph shows helicon propagation starting at about 6,200 gauss. This is not as close in agreement with 5,800 gauss as the previous case. However, as mentioned before, our $\omega_c\tau$ is also one order of magnitude smaller than before, and thus we would not expect a close agreement.

Let us describe the graphic results in more detail. First we consider the graphs for $\tau = 10^{-10}$ sec. On Graph I, we see the initiation of helicon propagation at about 6,300 gauss. Graphs II, III, and IV show the helicons increasing in amplitude and in distance between peaks. The curve has a smooth sinusoidal nature.

Now let us look at the graphs for $\tau = 10^{-9}$ sec. On Graph V we observe Gantmakher-Kaner oscillations. They have a constant period of 375 gauss. Recalling Equation (54), we find that a period of 375 gauss corresponds to $[m\bar{v}_z]_{EXT.} = 9.3 \times 10^{-20}$ gm-cm/sec. This, in turn, corresponds to a $k_{z\,EXT.}$ of $.88 \times 10^{+3}$ cm^{-1}. This is extremely close in value to KMAX, which was taken as $.9 \times 10^{8}$ cm^{-1}. We also note that the amplitude of the Gantmakher waves is smaller than the amplitude of the helicons by a factor of 10^{4}.

Graph VI is the same as Graph V with a slight increase in amplitude. Graph VII shows the start of helicon propagation. Graphs VIII and IX show the helicons gaining in amplitude and increasing in period. We notice that while the Gantmakher-Kaner oscillations were sinusoidal in shape, the helicons are not. They have more of a delta-function appearance about them. Recalling that for the same magnetic field range, the helicons for $\tau = 10^{-10}$ sec. were sinusoidal shaped, we conclude that the larger relaxation time has definitely caused a distinct change in curve shape.

Graphs X and XI are reproductions of experimental data taken by Wood[3] exhibiting these two distinct wave shapes. Here also, we notice the increasing amplitude and period of the helicons.

The relaxation time also affects the magnitude of the amplitudes. We notice that the amplitudes for $\tau = 10^{-10}$ sec. are two orders of magnitude smaller than the amplitudes for $\tau = 10^{-9}$ sec. in the area of helicon propagation.

GRAPH I

CALCULATED - SPHERICALLY SYMMETRIC

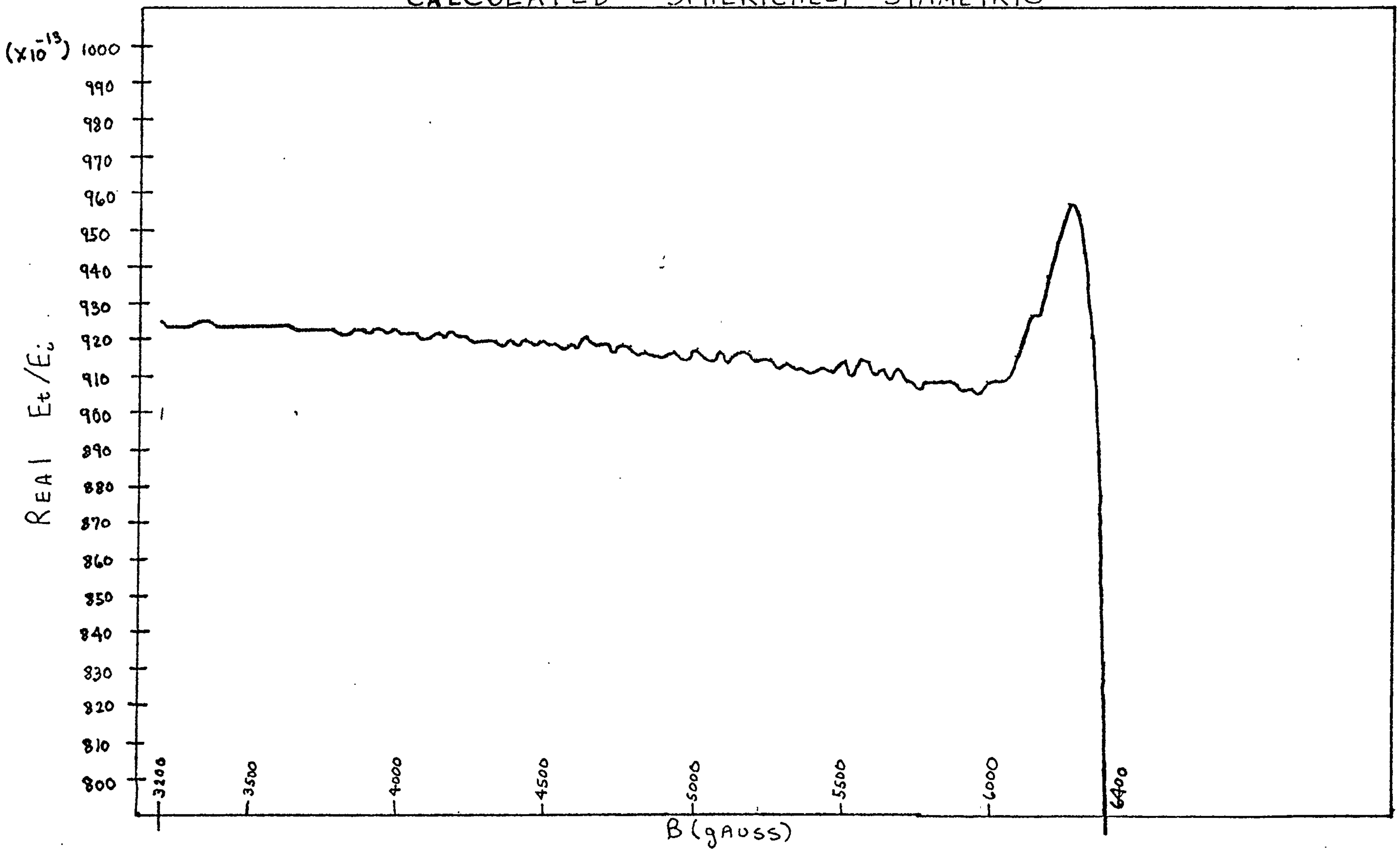

SODIUM

$\tau = 10^{-10}$ SEC $f = 10^{6}$ CYC/SEC

GRAPH II

CALCULATED - SPHERICALLY SYMMETRIC

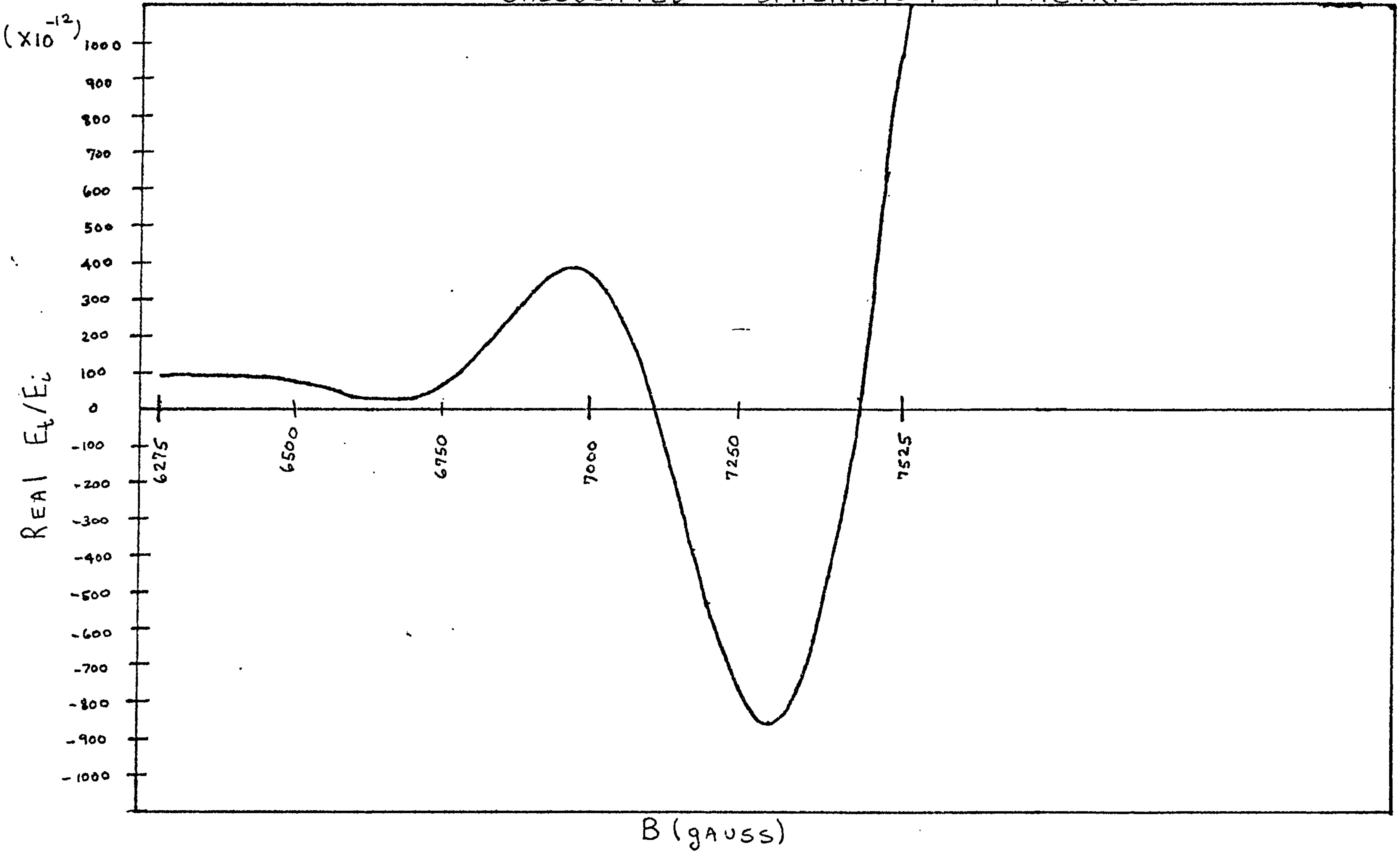

SODIUM

$\tau = 10^{-10}$ SEC $f = 10^{6}$ CYC/SEC

GRAPH III
CALCULATED SPHERICALLY SYMMETRIC

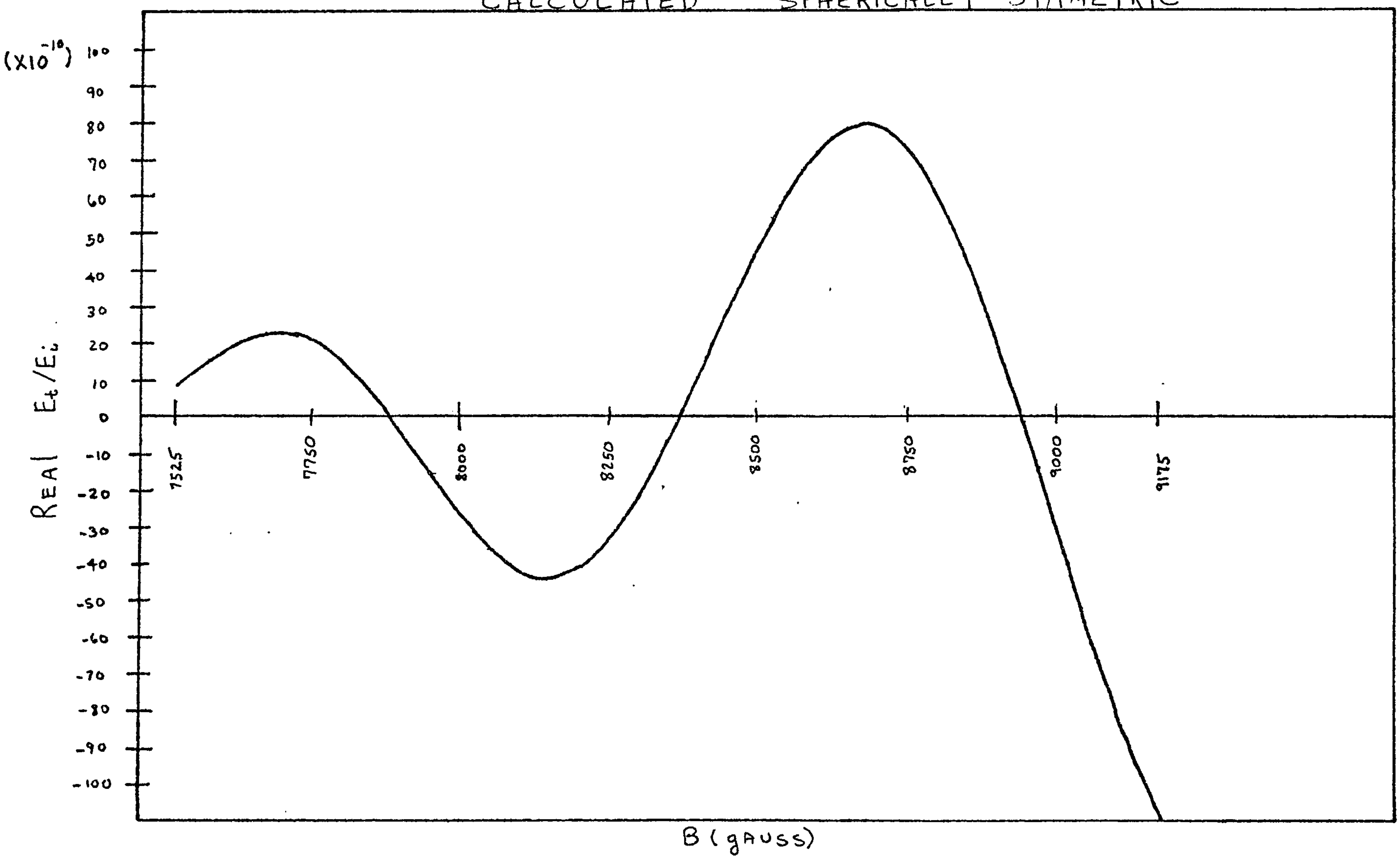

SODIUM

$\tau = 10^{-10}$ SEC $f = 10^{6}$ CYC/SEC

GRAPH IV

CALCULATED SPHERICALLY SYMMETRIC

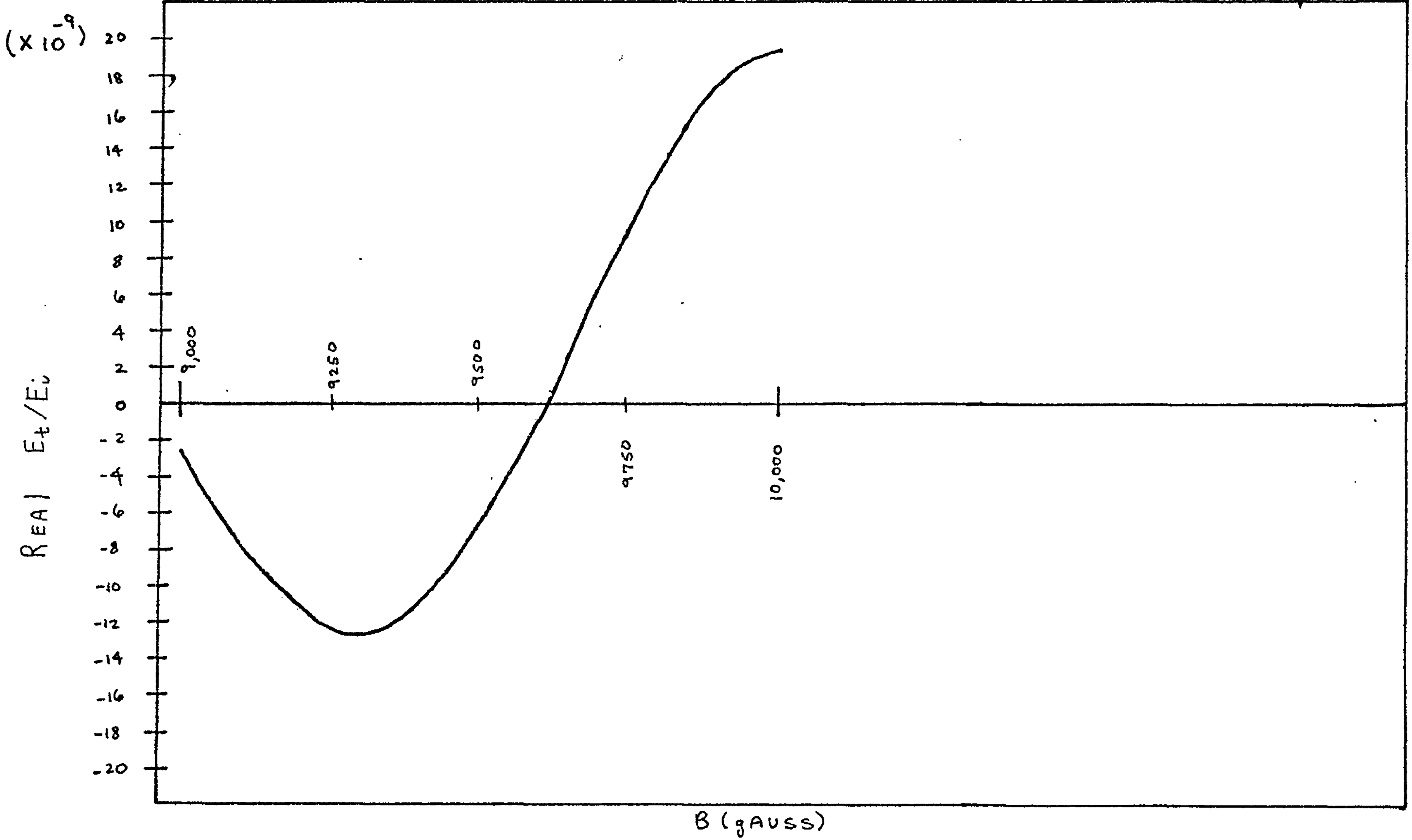

SODIUM

$\tau = 10^{-10}$ SEC $\quad f = 10^{6}$ CYC/SEC

GRAPH V

CALCULATED SPHERICALLY SYMMETRIC

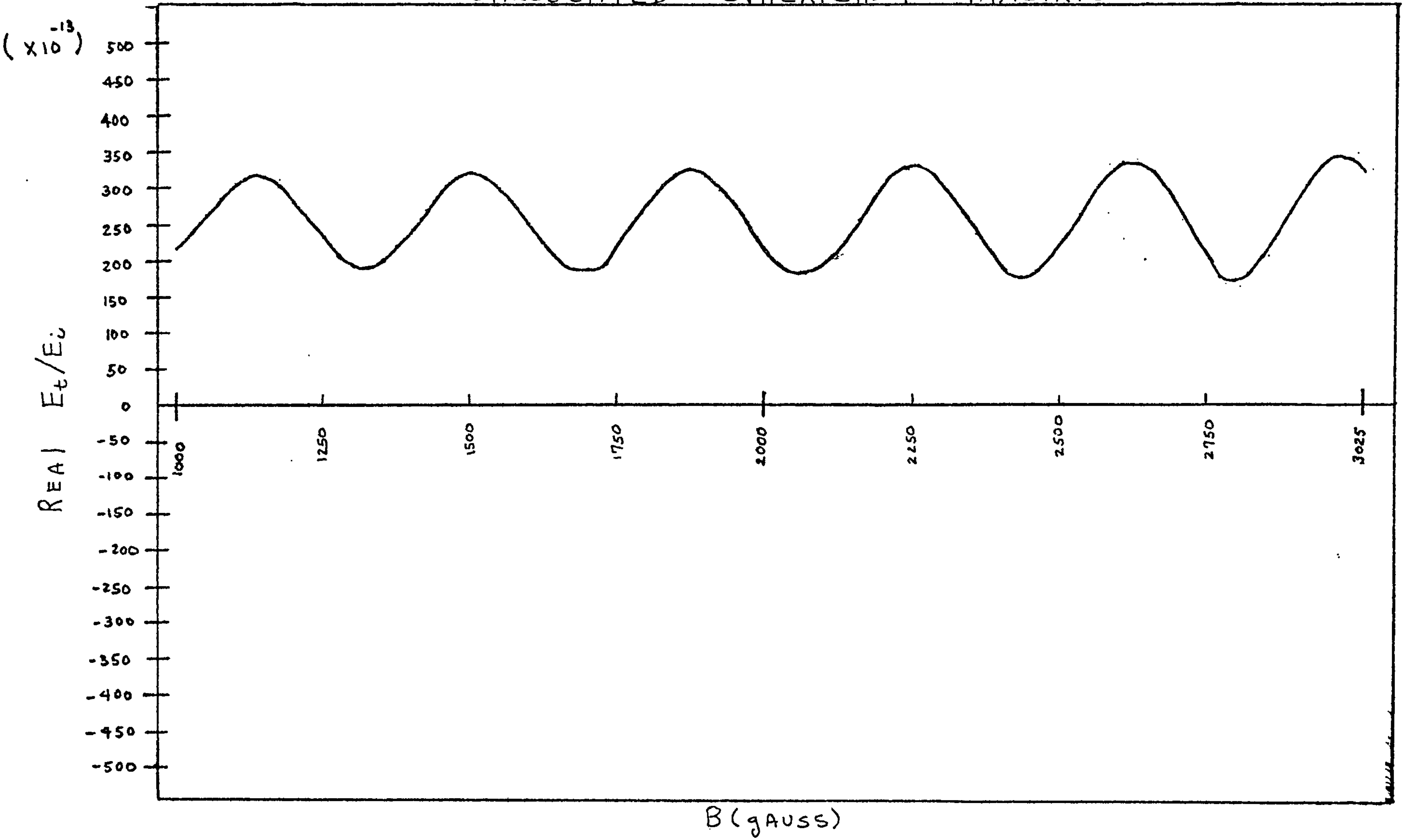

SODIUM

$\tau = 10^{-9}$ SEC $\quad f = 10^{6}$ CYC/SEC

GRAPH VI

CALCULATED SPHERICALLY SYMMETRIC

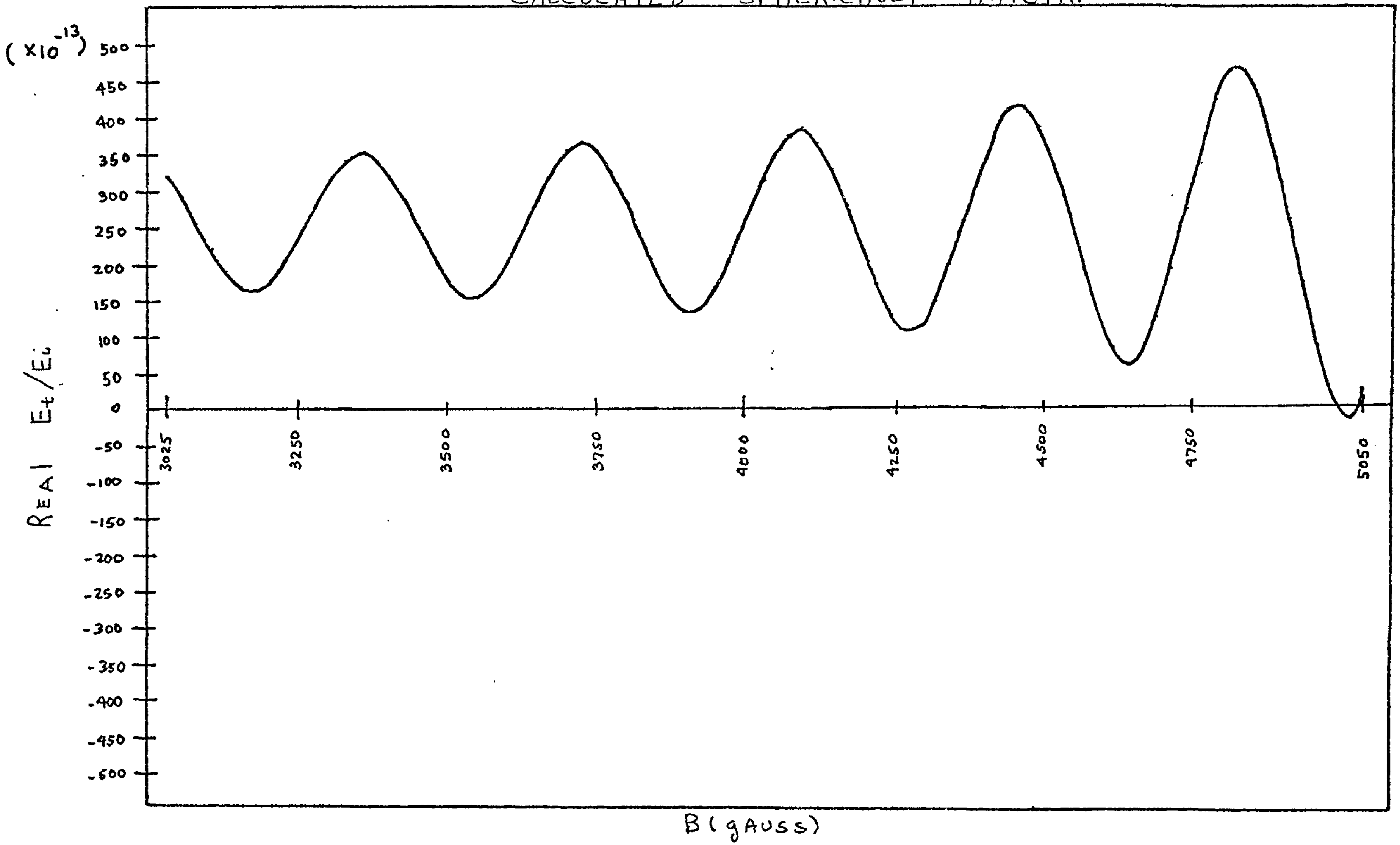

SODIUM

$\tau = 10^{-9}$ SEC $\quad f = 10^{6}$ CYC/SEC

GRAPH VII

CALCULATED SPHERICALLY SYMMETRIC

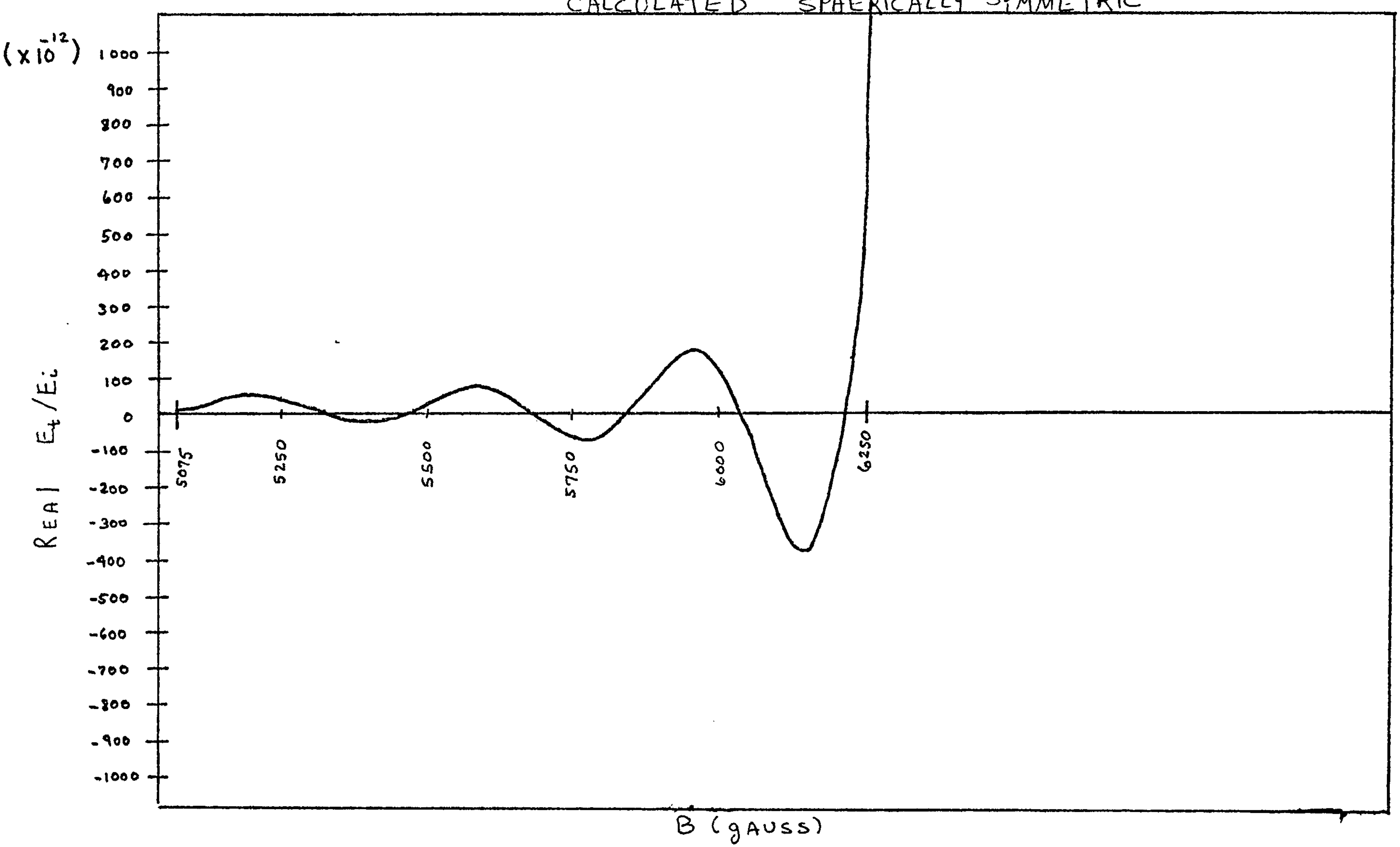

SODIUM

$T=10^{-9}$ SEC $f=10^{6}$ CYC/SEC

GRAPH VIII

CALCULATED SPHERICALLY SYMMETRIC

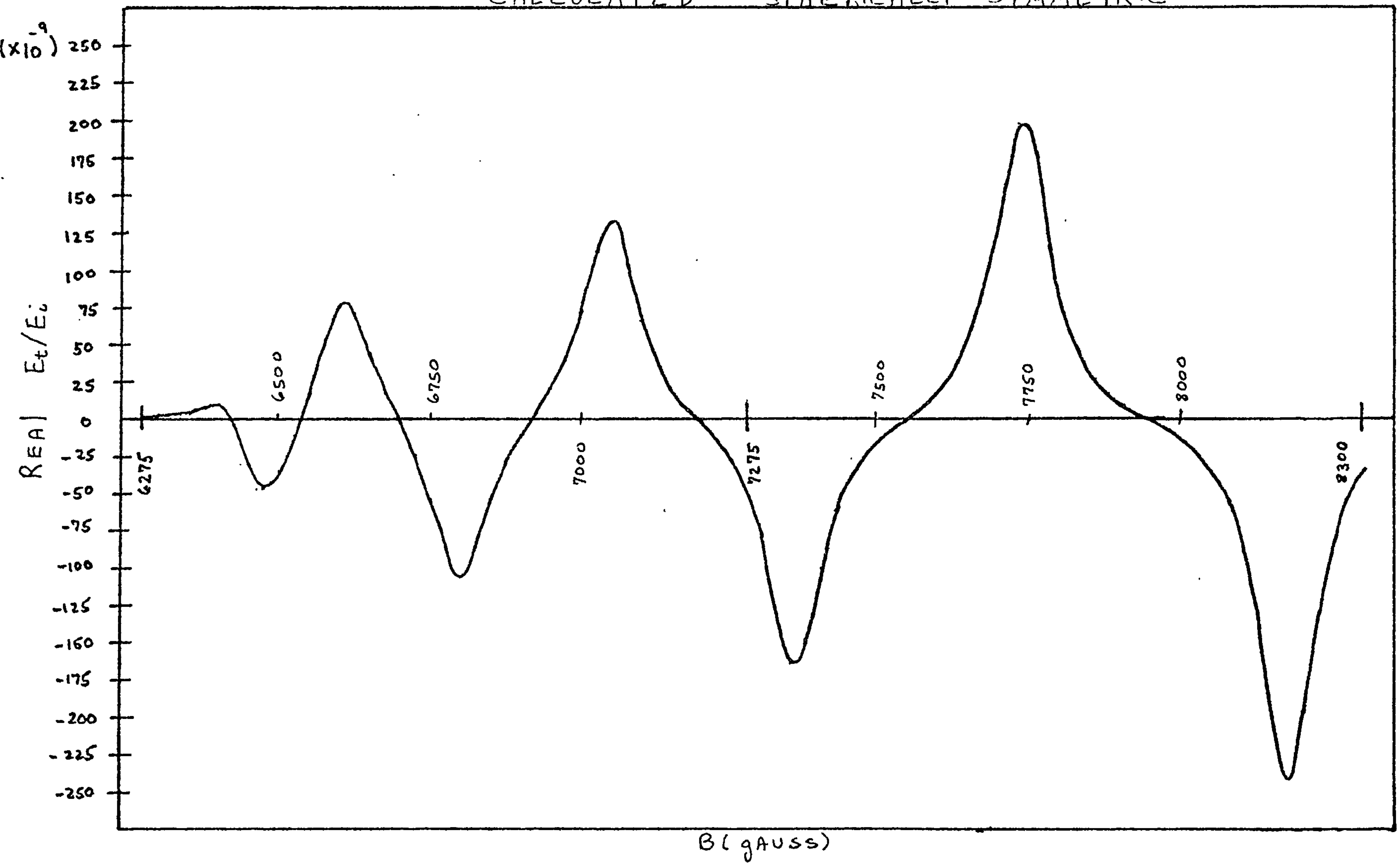

SODIUM

$\tau = 10^{-9}$ SEC $f = 10^{6}$ CYC/SEC

GRAPH IX

CALCULATED SPHERICALLY SYMMETRIC

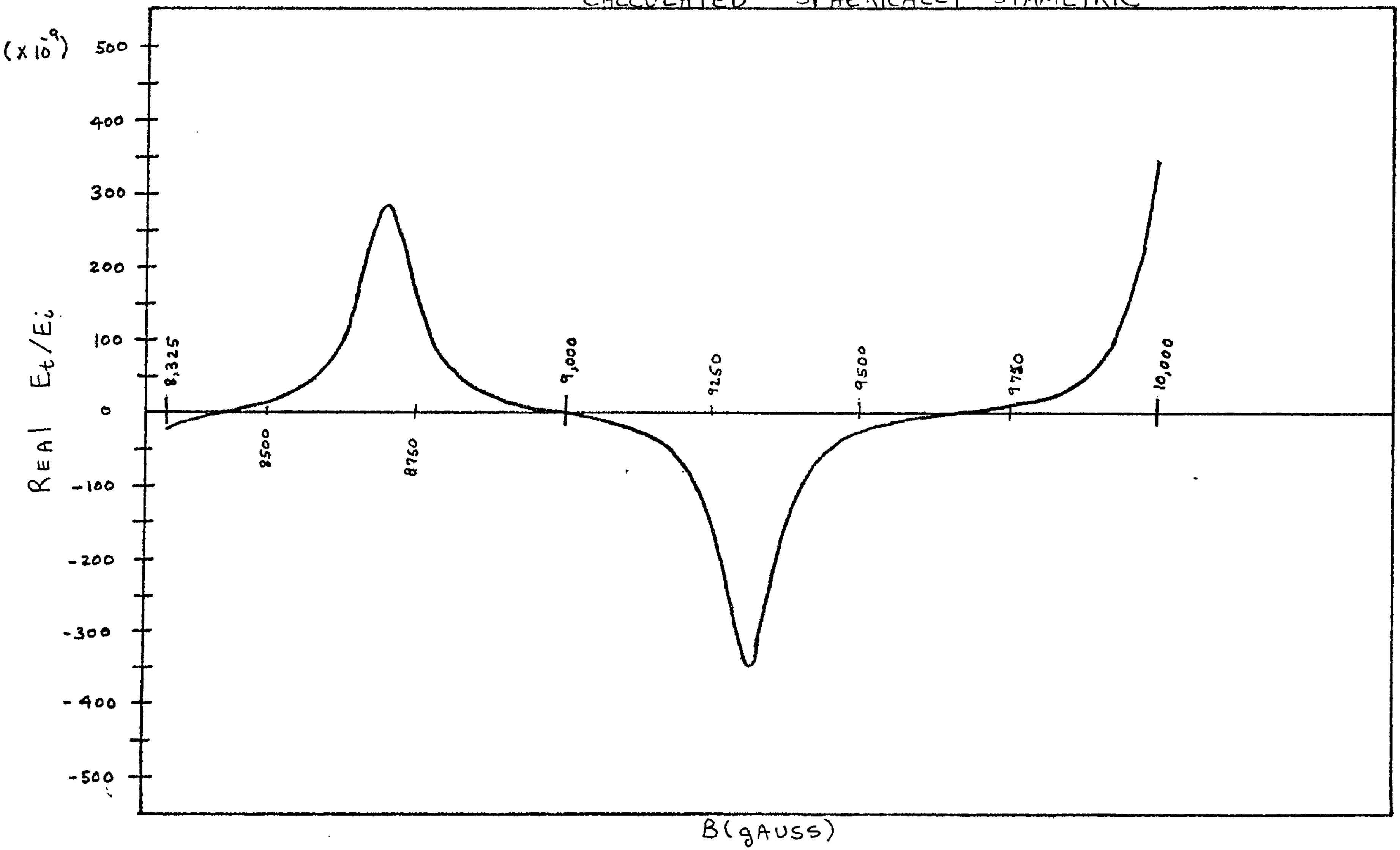

SODIUM

$\tau = 10^{-9}$ SEC $f = 10^{6}$ CYC/SEC

GRAPH V

EXPERIMENTAL SPHERICALLY SYMMETRIC

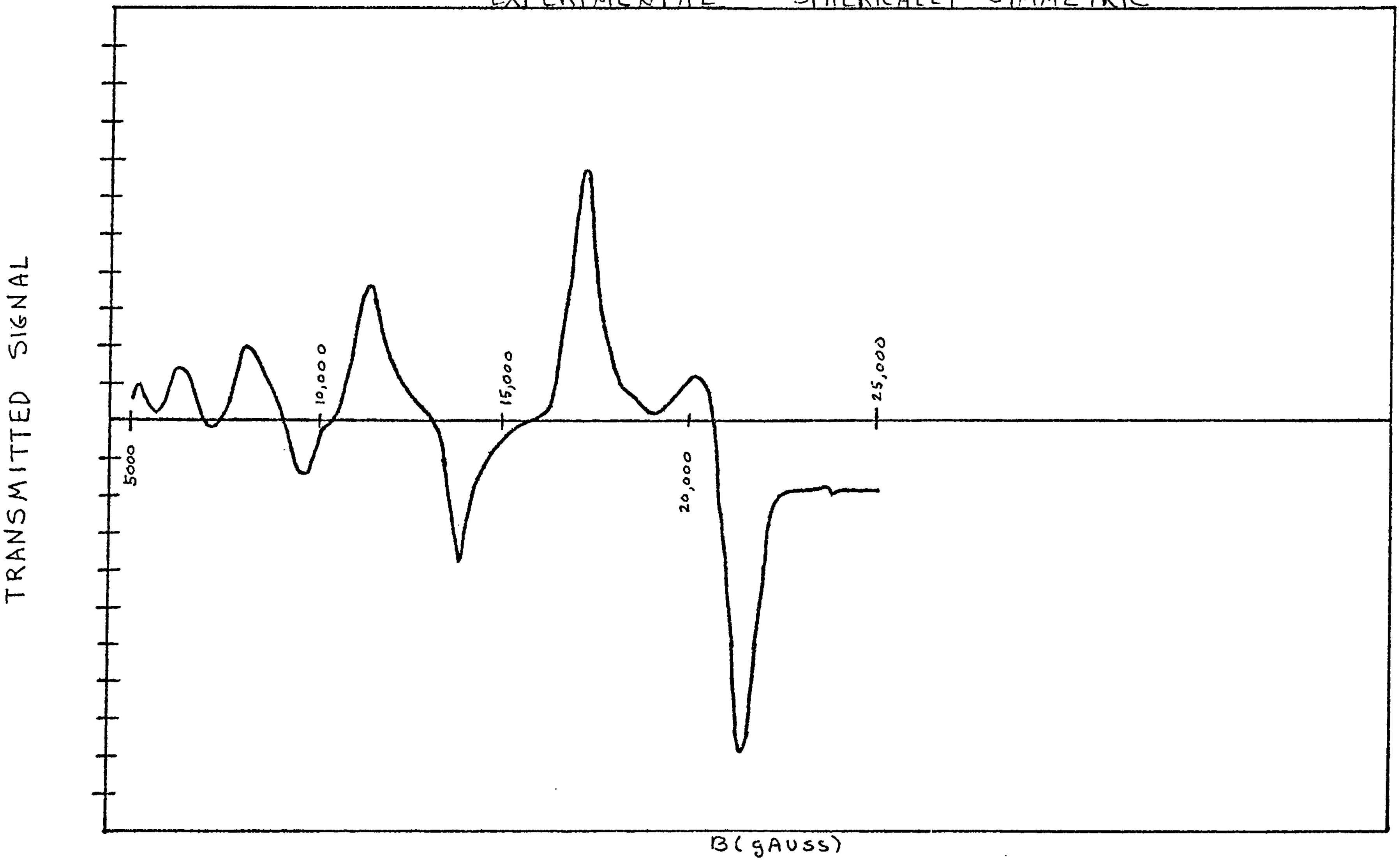

SODIUM

EXPERIMENTAL CURVE

$f = 50 \times 10^{3}$ CYC/SEC

GRAPH XI

EXPERIMENTALLY SPHERICALLY SYMMETRIC

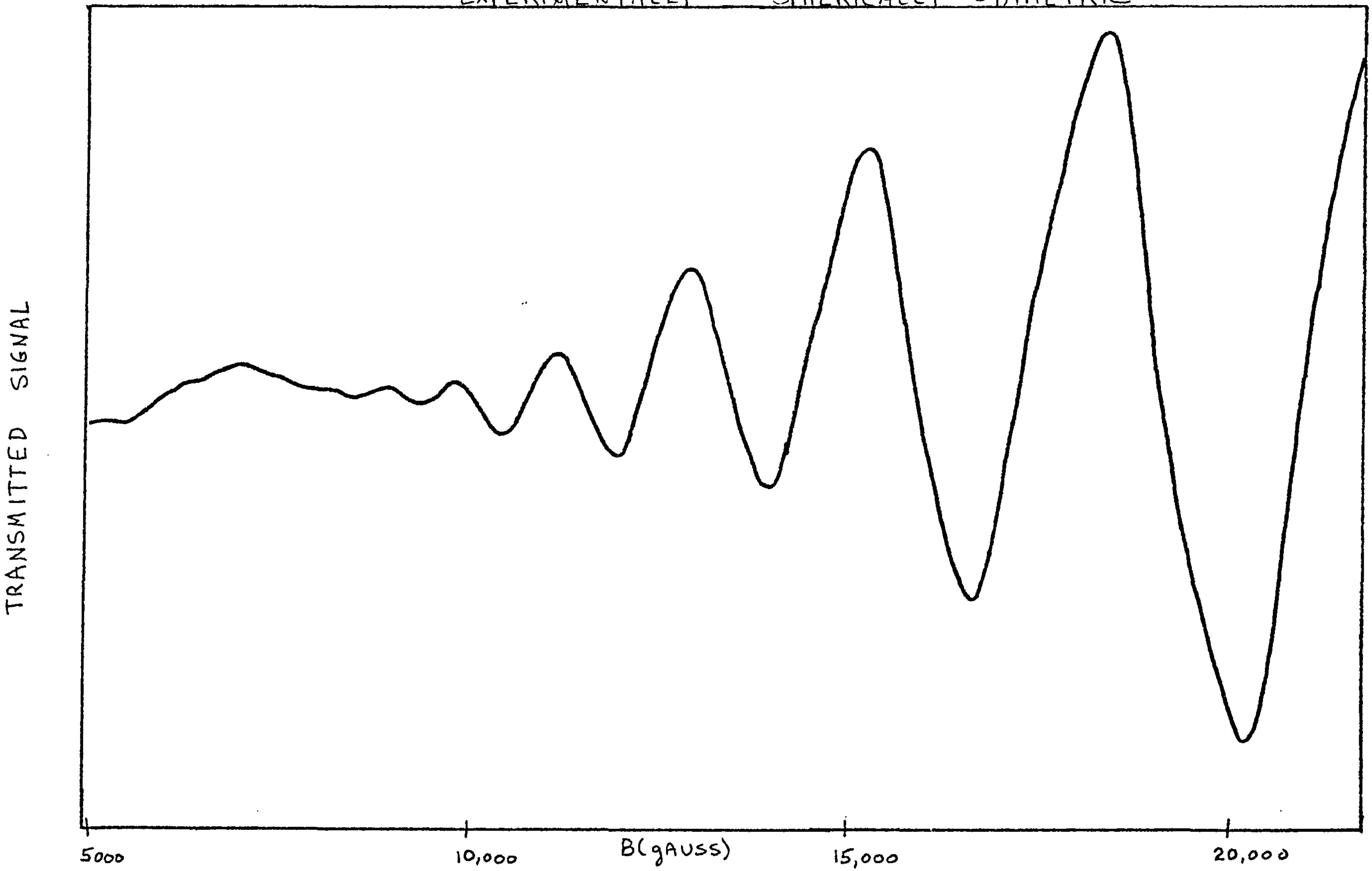

SODIUM

EXPERIMENTAL CURVE

$f = 242 \times 10^3$ CYC/SEC

Now we will advance to a cylindrically symmetric Fermi surface, which will include the spherical case. For cylindrically symmetric surfaces we have

$$V_x = V_\perp \cos\theta \quad , \tag{91}$$

$$V_y = V_\perp \sin\theta \quad , \tag{92}$$

$$V_z(\theta) = \bar{V}_z \quad , \tag{93}$$

where
$$V_\perp = (V_x^2 + V_y^2)^{1/2} \quad , \tag{94}$$

and
$$\hbar k_\perp = m V_\perp \quad . \tag{95}$$

Now again our equation for $\vec{V}_m$ simplifies to

$$V_{mx} = \frac{1}{2\pi}\int_0^{2\pi} V_\perp \cos\theta \, e^{-im\theta} \, d\theta \quad , \tag{96}$$

$$V_{mx} = (V_\perp/2)(\delta_{m,1} + \delta_{m,-1}) \quad , \tag{97}$$

and
$$V_{my} = (V_\perp/2i)(\delta_{m,1} - \delta_{m,-1}) \quad . \tag{98}$$

Now we have

$$\sigma_{xx} = \frac{e^2}{2\pi^2\hbar^2}\int_{-KMAX}^{+KMAX} m_c \, dk_z \sum_{m=-\infty}^{\infty} \frac{V_{mx} V_{mx}^*}{\frac{1}{\tau} + i(qV_z - \omega - m\omega_c)} \quad . \tag{99}$$

Again using the equations

$$a = \frac{1}{\tau} + iq\bar{V}_z - i\omega \quad , \tag{100}$$

and
$$b = \omega_c \quad , \tag{101}$$

we have that

$$\sigma_{xx} = \frac{e^2}{4\pi^2 m_c}\int_{-KMAX}^{+KMAX} \frac{a k_\perp^2 \, dk_z}{a^2 + b^2} \quad , \tag{102}$$

and

$$\sigma_{xy} = \frac{-e^2}{4\pi^2 m_c} \int_{-KMAX}^{+KMAX} \frac{b k_\perp^2 \, dk_z}{a^2 + b^2} \quad . \qquad (103)$$

Now we have that

$$\sigma_+ = \sigma_{xx} - i\,\sigma_{xy} \quad . \qquad (104)$$

Thus, we have

$$\sigma_+ = \frac{e^2 \tau}{4\pi^2 m_c} \int_{-KMAX}^{+KMAX} \frac{k_\perp^2 \, dk_z}{1 + i\tau(-\omega_c - \omega + q\bar{v}_z)} \quad . \qquad (105)$$

Now, as before, we have gotten around evaluating the integral expression of $\vec{v}_m$. However, while previously we had derived an exact expression for σ_+ , now it must be evaluated numerically.

We mentioned earlier that sodium was investigated mainly for the purpose of an accuracy check on our computer programs for copper. The integral expression for σ_+ was used to evaluate Real E_t/E_i over a magnetic field range of 8,800 gauss to 9,500 gauss. We then checked our results with the data gathered for the closed expression of σ_+ . This integral expression of σ_+ will later be used for copper, and from this check, we will know how accurate our results will be.

Now we rewrite our expression for σ_+ as:

$$\sigma_+ = \frac{e^2 \tau}{4\pi^3 m_c} \int_{-KMAX}^{+KMAX} \frac{(\pi k_\perp)^2 \, dk_z}{1 + i\tau(-\omega_c - \omega + q\bar{v}_z)} \quad . \qquad (106)$$

We are dealing with a spherical Fermi surface. Let us look at the drawing below.

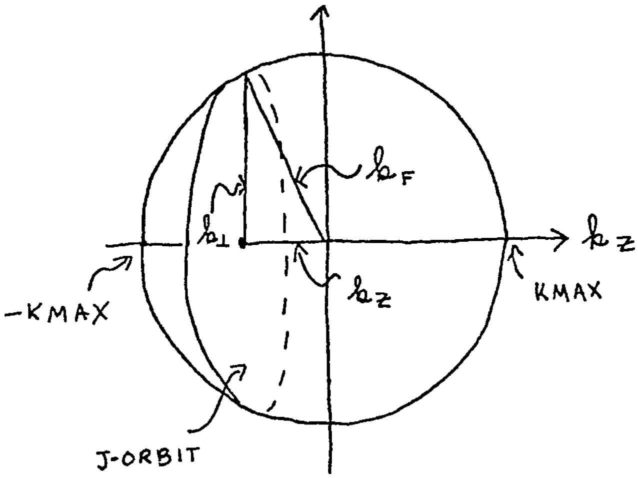

For a sphere, we have that KMAX equals the radius k_F . We divide the k_z -axis into 52 equally spaced intervals, so we will be evaluating the integrand of σ_+ at 53 points in the interval [-KMAX, +KMAX] . Thus, we will have 53 j-orbits. A typical j-orbit is shown. Now $(\pi k_\perp^2) = A_j$ is the cross-sectional area of a j-orbit. We know that for sodium KMAX = 0.9 X 10^8 cm^{-1}. Thus, from the drawing we can see that

$$A_j = \pi(k_F^2 - k_z^2) \quad . \tag{107}$$

Also recalling that for a Fermi sphere, we have for any j-orbit for which k_z = constant,

$$V_z = \frac{\hbar k_z}{m} \quad . \tag{108}$$

Thus, we can calculate all the data we need to evaluate σ_+ numerically. We used this expression of σ_+ in our

CHART II

Comparison of Real σ_+ and Imaginary σ_+ for Nine m's Centered About M*

NOTE: In number notation, +18 means 10^{+18}.

B = 8,900 gauss   M* = 23

Value of m	Real σ_+	Imaginary σ_+
19	.281+18	.412+20
20	.285+18	.414+20
21	.288+18	.416+20
22	.292+18	.417+20
23	.296+18	.419+20
24	.301+18	.421+20
25	.306+18	.424+20
26	.311+18	.426+20
27	.317+18	.428+20

B = 9,375 gauss   M* = 23

Value of m	Real σ_+	Imaginary σ_+
19	.251+18	.390+20
20	.253+18	.391+20
21	.256+18	.393+20
22	.259+18	.394+20
23	.263+18	.396+20
24	.266+18	.398+20
25	.270+18	.399+20
26	.274+18	.401+20
27	.279+18	.403+20

GRAPH XII

CALCULATED SPHERICALLY SYMMETRIC AND CYLINDRICALLY SYMMETRIC

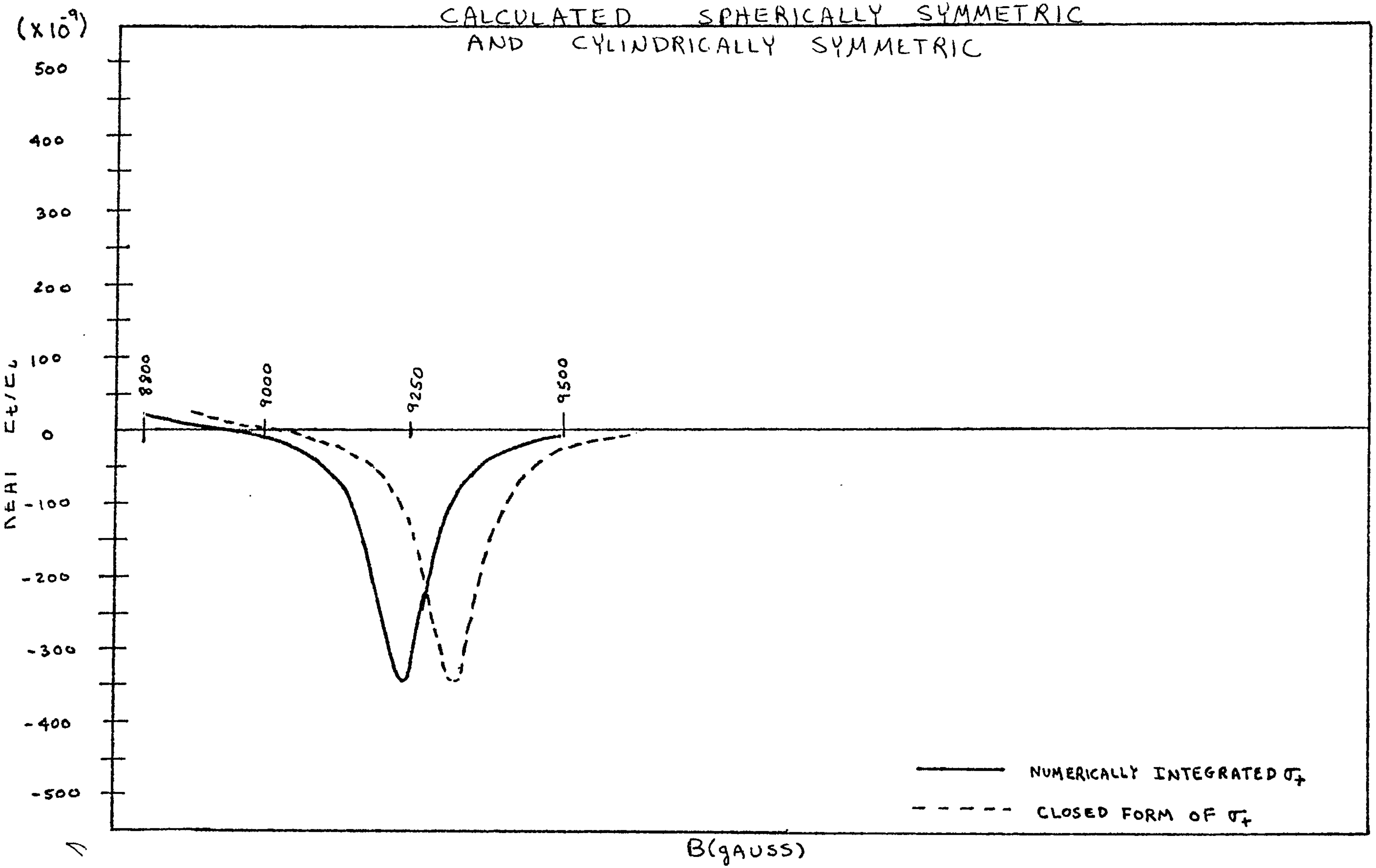

SODIUM

$\tau = 10^{-9}$ SEC $f = 10^{6}$ CYC/SEC

expression for Real E_t/E_i using a sum over m going from 1 to 75. Chart II shows a comparison of the real and imaginary parts of σ_+. We know that for helicon propagation $\mathrm{Img.}\, \sigma_+ \gg \mathrm{Real}\, \sigma_+$. Chart II verifies that this is so.

Graph XII shows a comparison of our data, written with a solid line, with the data obtained by our previous closed form expression of σ_+, drawn in a dotted line.

We see from the graphs that the numerically integrated σ_+ gives a curve shape identical with that which resulted from the closed form σ_+, except that the curves are out of phase with one another by about 85 gauss. This phase difference is probably caused by the fact that there is some error inherent in numerical integration techniques. In conclusion, we see that our numerical integrations are accurate enough to give us the correct shape of the curve which is what we are most concerned with.

We now advance to our most complicated fashion of calculating Real E_t/E_i. This method will be the one used to calculate E_t/E_i for copper using the true Fermi surface of that metal, but we now wish to check the accuracy of the computer program for the simpler case of sodium. The complication lies in that we must now evaluate $\vec{V}_m$ by numerical integration methods.

As before, we divide the k_z axis into fifty-two equally spaced intervals so that we will be evaluating σ_+ at 53 points in the interval [-KMAX, KMAX]. We then calculate the values of the x, y, and z components of the Fermi velocity at 45 different points equally spaced around each j-orbit. Thus, we will have the v_x, v_y, and v_z values for 45 points in the interval $[0, 2\pi]$. These Fermi velocity values were calculated as follows and as demonstrated in the diagram below:

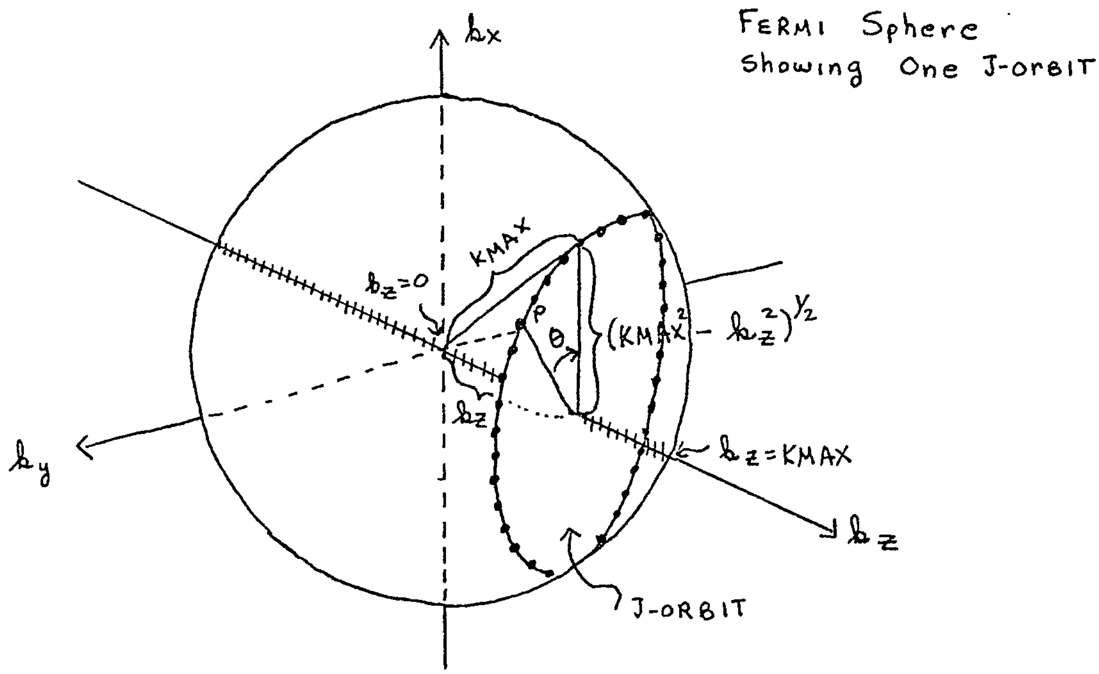

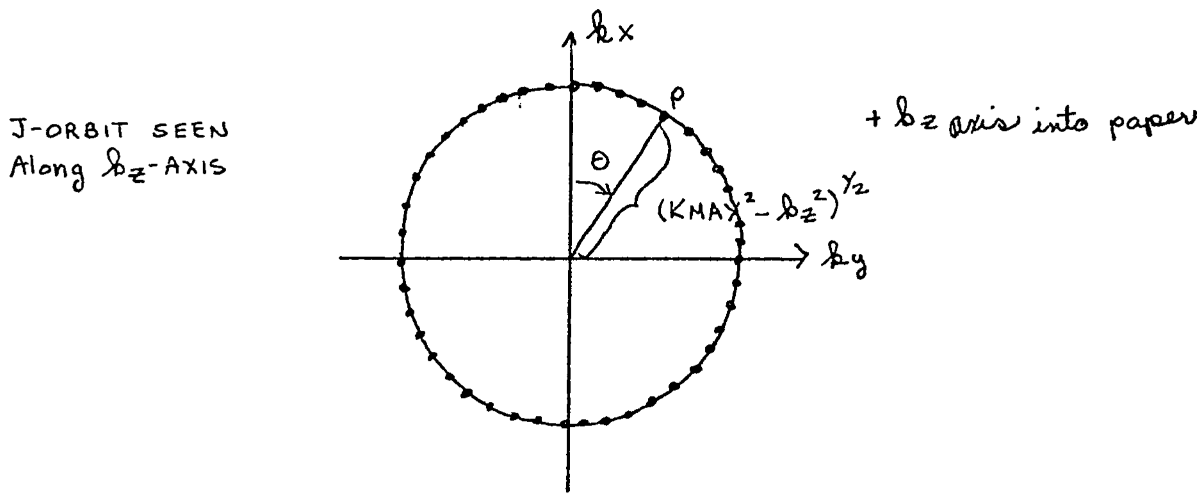

Thus, we have

$$V_{zP} = \frac{\hbar k_z}{m} \quad , \tag{109}$$

$$V_{xP} = \frac{\hbar}{m}(KMAX^2 - k_z^2)^{1/2}\cos\theta \quad , \tag{110}$$

and

$$V_{yP} = \frac{\hbar}{m}(KMAX^2 - k_z^2)^{1/2}\sin\theta \quad . \tag{111}$$

Now, let us recall that

$$\vec{V}_m = \frac{1}{2\pi}\int_0^{2\pi}\vec{V}(\theta)\, e^{-\frac{i}{\omega_c}\int_0^{\theta}\frac{m\pi}{Q}\{V_z(\theta'') - \bar{V}_z\} + m\omega_c\, d\theta''} d\theta \quad . \tag{112}$$

We have that

$$\bar{V}_z = \frac{1}{2\pi}\int_0^{2\pi} V_z(\theta)\, d\theta \quad . \tag{113}$$

For each j-orbit, we must do a numerical integration of $\bar{V}_z$. Let us store this value in an array called AVGVZ(J). Since we are going to do a numerical integration of V_{mx} and V_{my} , we must evaluate the integrand at the 45 different values of θ . Let us denote these angles by θ_n , where n goes from 1 to 45, and $\theta_1 = 0$ and $\theta_{45} = 2\pi$. Also, let

$$\frac{m\pi}{Q}\left\{V_z(\theta'') - \bar{V}_z\right\} = \mathcal{X}(\theta'') \quad . \tag{114}$$

We evaluate the expression

$$e^{-\frac{i}{\omega_c}\int_0^{\theta} \frac{m\pi}{Q}\{V_z(\theta'') - \bar{V}_z\} + m\omega_c \, d\theta''}$$

in the following way. For $\theta = \theta_1$, we have

$$e^{-\frac{i}{\omega_c}\int_0^{\theta_1} \mathcal{X}(\theta'') + m\omega_c \, d\theta''} = e^{-im\theta_1} e^{-\frac{i}{\omega_c}\int_0^{\theta_1} \mathcal{X}(\theta'')\,d\theta''} \quad . \tag{115}$$

For $\theta = \theta_2$, we have

$$e^{-\frac{i}{\omega_c}\int_0^{\theta_2} \mathcal{X}(\theta'') + m\omega_c \, d\theta''} = e^{-im\theta_2} e^{-\frac{i}{\omega_c}\int_0^{\theta_2} \mathcal{X}(\theta'')\,d\theta''} \quad , \tag{116}$$

or

$$e^{-\frac{i}{\omega_c}\int_0^{\theta_2} \mathcal{X}(\theta'') + m\omega_c \, d\theta''} = e^{-im\theta_2} e^{-\frac{i}{\omega_c}\int_0^{\theta_1} \mathcal{X}(\theta'')\,d\theta''} e^{-\frac{i}{\omega_c}\int_{\theta_1}^{\theta_2} \mathcal{X}(\theta'')\,d\theta''} \quad , \tag{117}$$

and so forth. We evaluate the integrals using the Trapezoidal Rule. Now, let

$$A_{p,r} = \int_{\theta_p}^{\theta_r} \mathcal{X}(\theta'')\,d\theta'' = \mathrm{EXPIN}(r) \quad . \tag{118}$$

Thus, we have

$$A_{4,5} = \mathrm{EXPIN}(5) = \int_{\theta_4}^{\theta_5} \mathcal{X}(\theta'')\,d\theta'' \quad , \tag{119}$$

and also

$$\int_0^{\theta_m} \mathcal{X}(\theta'')\,d\theta = A_{1,2} + A_{2,3} + \cdots + A_{m-1,m} = \mathrm{EXPIN}(2) + \mathrm{EXPIN}(3) + \cdots + \mathrm{EXPIN}(m) \quad , \tag{119}$$

and

$$\int_0^{\theta_{m-1}} \mathcal{X}(\theta'')\,d\theta = A_{1,2} + A_{2,3} + \cdots + A_{m-2,m-1} = \mathrm{EXPIN}(2) + \mathrm{EXPIN}(3) + \cdots + \mathrm{EXPIN}(m-1) \quad , \tag{120}$$

and so forth. Now let

$$\mathrm{PARTP}(m) = e^{-i/\omega_c \, \mathrm{SUM}_m} \tag{121}$$

and
$$PARTN(m) = e^{+\frac{i}{\omega_c} SUM_m} \quad , \tag{122}$$
where
$$SUM_m = \sum_{a=1}^{m} EXPIN(a) \quad . \tag{123}$$
If we now let
$$CART(m) = e^{-iN\Theta_m} \quad , \tag{124}$$
then at each of the 45 points, the value of the integrand will be given by the expressions
$$\begin{pmatrix} \text{Value of Integrand} \\ \text{for Points on the} \\ \text{Positive } k_z \text{ Axis} \end{pmatrix}_{mx} = V_x(\Theta_m)\, PARTP(m)\, CART(m) \quad , \tag{125}$$
and
$$\begin{pmatrix} \text{Value of Integrand} \\ \text{for Points on the} \\ \text{Negative } k_z \text{ Axis} \end{pmatrix}_{mx} = V_x(\Theta_m)\, PARTN(m)\, CART(m) \quad . \tag{126}$$
Now, let us recall Equations (73) and (74) which state
$$V_{mx} = V_F \sin Q_j/2 \, [\delta_{m,1} + \delta_{m,-1}] \, ,$$
and
$$V_{my} = V_F \sin Q_j/2i \, [\delta_{m,1} - \delta_{m,-1}] \quad .$$
Thus, we have that
$$\text{REAL } V_{1,x} = V_F \sin Q_j/2 \qquad \text{Imag. } V_{1,x} = 0 \quad , \tag{127}$$
$$\text{REAL } V_{-1,x} = V_F \sin Q_j/2 \qquad \text{Imag. } V_{-1,x} = 0 \quad , \tag{128}$$
$$\text{REAL } V_{1y} = 0 \qquad \text{Imag. } V_{1,y} = -V_F \sin Q_j/2 \, , \tag{129}$$
and
$$\text{REAL } V_{-1y} = 0 \qquad \text{Imag. } V_{-1,y} = V_F \sin Q_j/2 \, . \tag{130}$$

Now for sodium $V_F = 1.03 \times 10^8$ cm/sec, and for the j=1-orbit, $\theta_j = \pi/2$. Thus, we should expect the following values:

Real $V_{1,x} = .515 \times 10^8$	Imaginary $V_{1,x} = 0.0$
Real $V_{-1,x} = .515 \times 10^8$	Imaginary $V_{-1,x} = 0.0$
Real $V_{1,y} = 0.0$	Imaginary $V_{1,y} = -.515 \times 10^8$
Real $V_{-1,y} = 0.0$	Imaginary $V_{-1,y} = .515 \times 10^8$

Using data from a computer run for B= 7,000 gauss for the j=1 orbit or $k_z = 0.0$, we obtain Chart III. Thus, we have checked the accuracy of calculating the V_m's with our program and found an error of 1.1%.

In calculating E_t/E_i, we approximate the sum over m going to infinity with a sum of nine terms centered about M*, since it was shown earlier in Chart I that for $\tau = 10^{-9}$ sec., we had very rapid convergence of Real E_t/E_i . Recalling that during helicon propagation, Imag $\sigma_+ >$ Real σ_+ , we note the sample data given in Chart IV. The data given by our previous program, where the σ_+'s but not the V_m's were calculated numerically, is on the left. The data given by this last program, where both σ_+ and V_m are calculated numerically, is given on the right. The value of the magnetic field is 8,850 gauss. Helicons are propagating in this region, and we notice that Imag $\sigma_+ >$ Real σ_+ by a factor of 100. The close values of the σ_+ serve as another accuracy check of our last program.

NUMERICALLY INTEGRATED V_{NX} AND V_{NY}
VALUES FOR SODIUM AT B=7,000 G.

CHART III

N	Real V_{NX}	Imaginary V_{NX}	Real V_{NY}	Imaginary V_{NY}
-5	+.2440+03	-.2083-02	-.3605+00	+.1656+01
-4	+.2428+03	-.6373-01	+.1024+01	+.6730+00
-3	+.2423+03	-.3705+00	-.5982-01	+.3839-01
-2	+.2431+03	-.4984+00	-.1394+00	-.3860+00
-1	+.5209+08	+.2924+00	+.4569-02	+.5209+08
0	+.2427+03	+.0000	+.2924+00	.0000
+1	+.5209+08	-.2924+00	+.4569-02	+.3860+00
+2	+.2431+03	+.4984+00	-.1394+00	-.3839-01
+3	+.2423+03	+.3705+00	-.5982-01	-.6730+00
+4	+.2428+03	-.6373-01	+.1024+01	-.1656+01
+5	+.2440+03	+.2083-02	-.3605+00	+.1656+01

VALUES OF REAL σ_+ AND IMAGINARY σ_+ FOR SODIUM
FOR B=8,850 GAUSS AND M-RANGE OF 18 TO 26

CHART IV

M	σ_+ Calculated Without Numerically Integrated V_N's		σ_+ Calculated With Numerically Integrated V_N's	
	Real σ_+	Imaginary σ_+	Real σ_+	Imaginary σ_+
18	.2870+18	.4145+20	.292+18	.418+20
19	.2907+18	.4162+20	.296+18	.420+20
20	.2947+18	.4180+20	.300+18	.422+20
21	.2991+18	.4200+20	.310+18	.426+20
22	.3038+18	.4221+20	.316+18	.429+20
23	.3089+18	.4243+20	.322+18	.431+20
24	.3144+18	.4267+20	.328+18	.434+20
25	.3205+18	.4292+20	.335+18	.437+20
26	.3270+18	.4319+20	.352+18	.443+20

The program used is included in the appendix. We used a B-field range from 8,800 gauss to 9,450 gauss in order to check our graphic results with Graph XII. Our data is plotted on Graph XIII. Graph XII is superimposed on our data for comparison.

GRAPH XIII

CALCULATED - SPHERICALLY AND CYLINDRICALLY SYMMETRIC

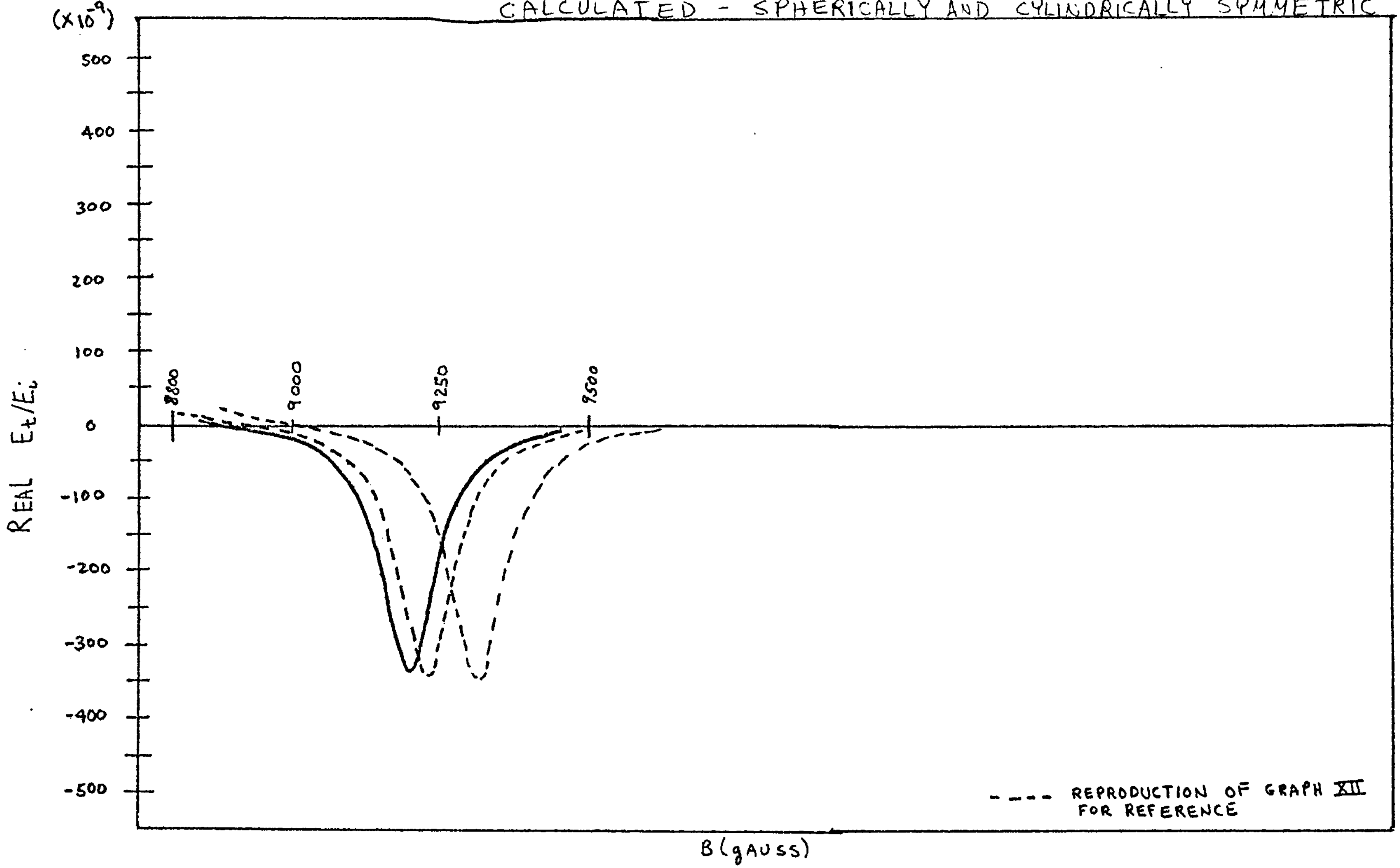

SODIUM

$\tau = 10^{-9}$ SEC $\quad f = 10^{6}$ CYC/SEC

E_t/E_i For Copper

Summarizing our approach to sodium, we found E_t/E_i by calculating σ_+ in three ways: (1) A closed form σ, (2) An integrated σ with closed expressions for the $\vec{V}_m$'s, and (3) An integrated σ with numerically integrated expressions of $\vec{V}_m$.

In the case of the true Fermi surface for copper, we have as a good approximation

$$V_z(\theta) = \overline{V}_z + a(p_z)\cos 4\theta\,, \tag{131}$$

and

$$V_x = b\sin\theta\,, \qquad b \neq b(p_z) \neq b(\theta) \tag{132}$$

$$V_y = -b\cos\theta\,, \tag{133}$$

for p_z parallel to the [001] direction (see Figure I). Thus, our expression for $\vec{V}_m$ would be

$$V_{mx} = \frac{b}{2\pi}\int_0^{2\pi} \sin\theta\, e^{-i\frac{a}{4\omega_c}\sin 4\theta}\, e^{-im\theta}\, d\theta\,, \tag{134}$$

and

$$V_{my} = \frac{-b}{2\pi}\int_0^{2\pi} \cos\theta\, e^{-i\frac{a}{4\omega_c}\sin 4\theta}\, e^{-im\theta}\, d\theta\,. \tag{135}$$

This is not a simple expression to evaluate, as in the case of sodium where the V_{mx} and V_{my} were evaluated as delta functions. Therefore, methods (1) and (2) are eliminated for use with the true Fermi surface of copper. This leaves method (3) for use. However, as an accuracy check we can use a cylindrically symmetric approximation of the copper Fermi surface with method (2). We have already described method (2) in the previous section on sodium. Our equation for σ_+ was given as

$$\sigma_+ = \frac{e^2\tau}{4\pi^3 m_c}\int_{-KMAX}^{+KMAX}\frac{(\pi k_\perp)^2\,dk_z}{1+i\tau(-\omega_c-\omega+q\bar{v}_z)}\ , \tag{136}$$

which can be rewritten as

$$\sigma_+ = \frac{e^2\tau}{4\pi^3 m_c}\int_{-KMAX}^{+KMAX}\frac{A(k_z)\,dk_z}{1+i\tau\left(-\omega_c-\omega-\frac{\hbar}{2\pi m}\frac{\partial A}{\partial k_z}\right)}\ , \tag{137}$$

where

$$\pi k_\perp^2 = A(k_z)\ , \tag{138}$$

and

$$m v_z = -\frac{\hbar}{2\pi}\frac{\partial A}{\partial k_z}\ , \tag{139}$$

where $A(k_z)$ is the cross-sectional area made by a plane perpendicular to the k_z axis intersecting the Fermi surface.

We did computations for the directions [001] and [111]. From Wood, data for $A(k_z)$ and $\frac{\partial A}{\partial k_z}$ for these two directions was available. The drawing below shows the orientation of the k_z-axis with the Fermi surface for these two directions.

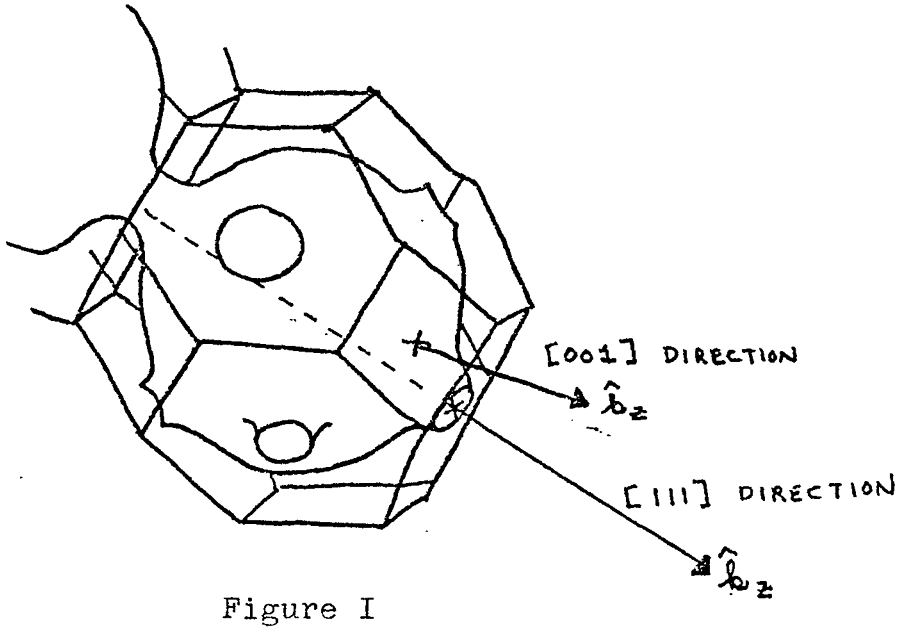

Figure I

Let us first examine the [111] direction. A τ of 10^{-9} sec. was used, and two different frequencies $f = 395.2 \times 10^3$ cycles/sec. and $f = 6 \times 10^5$ cycles/sec. were investigated.

Graph XIV is experimental data obtained by Wood for a frequency of 400.0×10^3 cycles/sec. and a B-field range of 10 to 30 thousand gauss. We see Gantmakher-Kaner oscillations with a B-field period of 600 gauss. However, the graph displays beats, and thus there must be present two Gantmakher-Kaner waves of slightly different frequencies. Our frequencies are expressed in the units cycles per unit gauss magnetic field.

If we have two waves expressed as

$$y_1 = A \cos(2\pi f_1 t + \phi_1) \quad , \tag{140}$$

and

$$y_2 = A \cos(2\pi f_2 t + \phi_2) \quad , \tag{141}$$

then, adding, we get

$$y = y_1 + y_2 = A[\cos(2\pi f_1 t + \phi_1) + \cos(2\pi f_2 t + \phi_2)] \quad . \tag{142}$$

Making use of the trigonometric identity

$$\cos a + \cos b = 2\left[\cos \tfrac{1}{2}(a+b)\right]\left[\cos \tfrac{1}{2}(a-b)\right] \quad , \tag{143}$$

we obtain

$$y = 2A \cos\left[2\pi\left(\frac{f_1 - f_2}{2}\right)t + \left(\frac{\phi_1 - \phi_2}{2}\right)\right] \cos\left[2\pi\left(\frac{f_1 + f_2}{2}\right)t + \left(\frac{\phi_1 + \phi_2}{2}\right)\right] \quad . \tag{144}$$

The composite wave may be regarded as having a frequency equal to $\frac{1}{2}(f_1 + f_2)$, which is the average of the frequencies of the original waves. The amplitude of the composite wave is given by the quantity in the first set of brackets in Equation (144). The amplitude varies with a frequency of $\frac{1}{2}(f_1 - f_2)$, and the number of beats per second is given as (f_1 - f_2). The drawing below is a typical representation of the presence of beats.

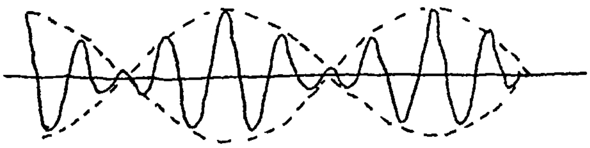

Graphs XV and XVI show the results for a frequency of 395.2 X 10^3 cycles/sec. for a B-field range of 2,000 to 14,000 gauss. Graph XVII displays the beats which begin at 5,700 gauss and end at about 13,700 gauss. The results for a frequency of 6 X 10^5 cycles/sec. are shown in Graphs XVIII through XX for a B-field range of 100 to 20,000 gauss. Graph XXI displays the beats which begin at 6,400 gauss and end at about 18,000 gauss. In both cases, the envelope of the wave is irregular in shape, but still displays the periodic recurrence of increasing and decreasing wave amplitudes. Since our Gantmakher-Kaner oscillations do not have the simple forms of Equations (140) and (141) and may not have the same amplitude, we understand why our graphic results

GRAPH XIV

EXPERIMENTAL

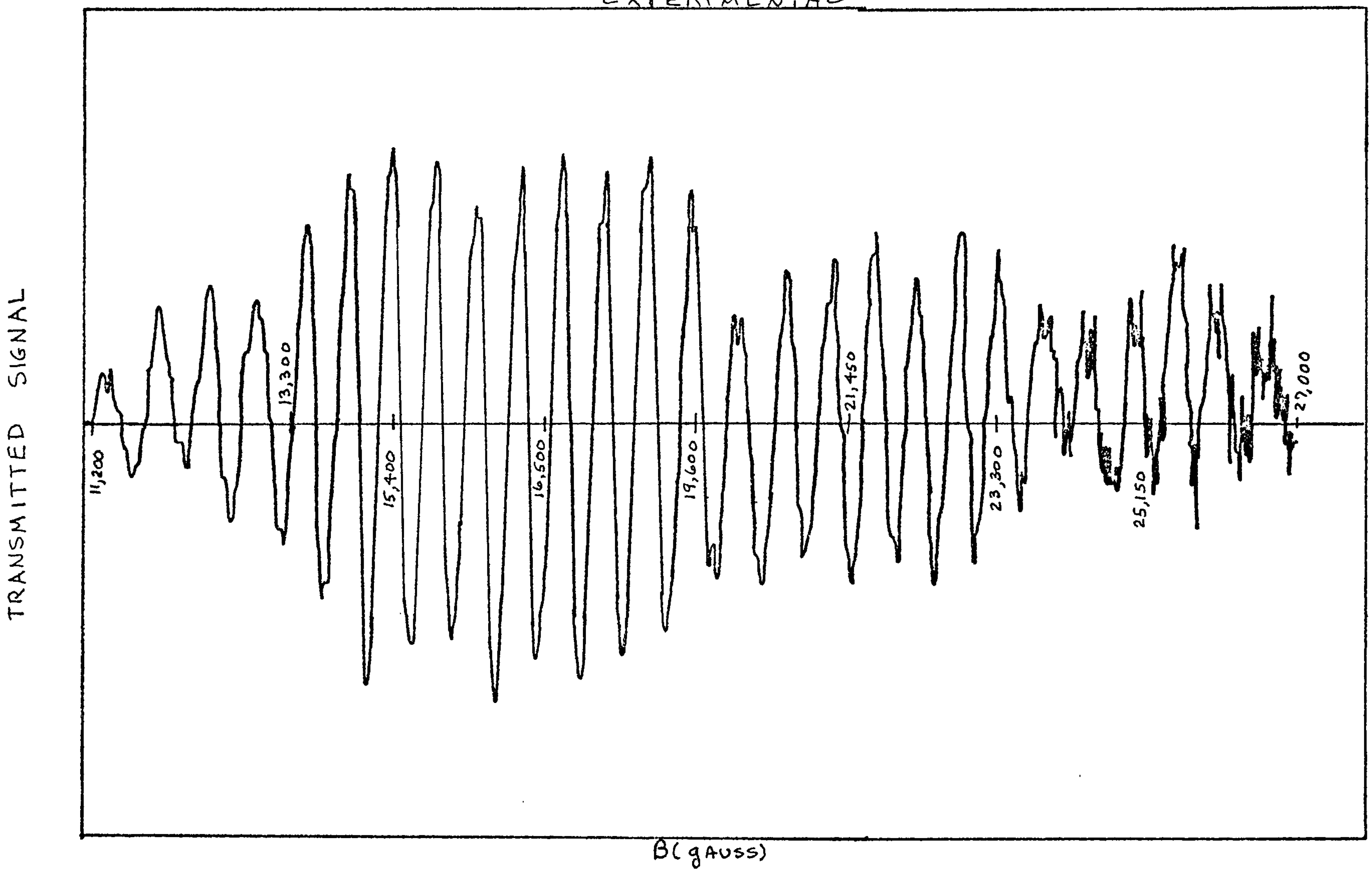

COPPER [111]

EXPERIMENTAL CURVE $f = 400.0 \times 10^{3}$ CYC/SEC

GRAPH XV

CALCULATED - CYLINDRICALLY SYMMETRIC

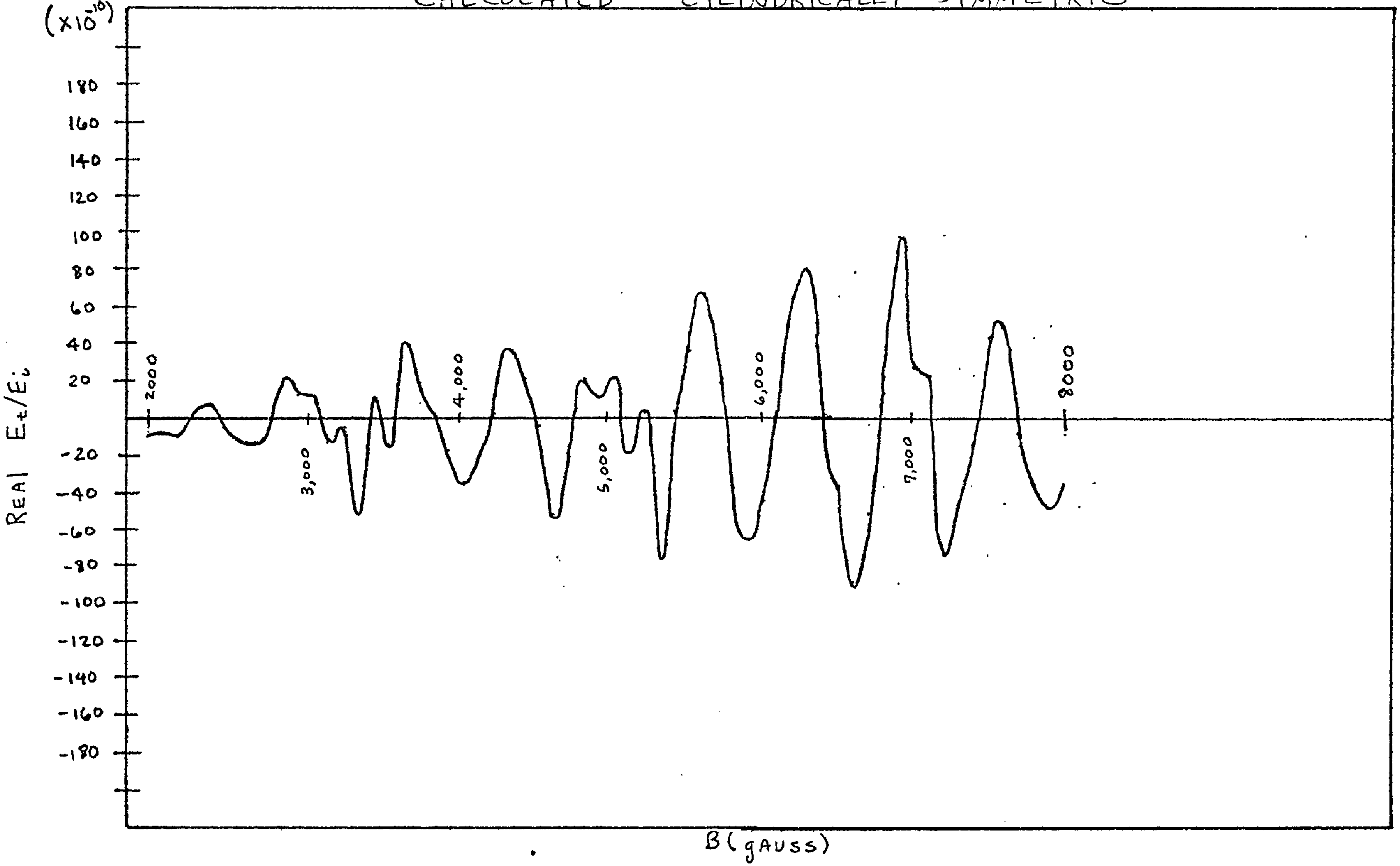

COPPER [111]

$\tau = 10^{-9}$ SEC $\quad f = 395.2 \times 10^{3}$ CYC/SEC

GRAPH XVII

CALCULATED CYLINDRICALLY SYMMETRIC

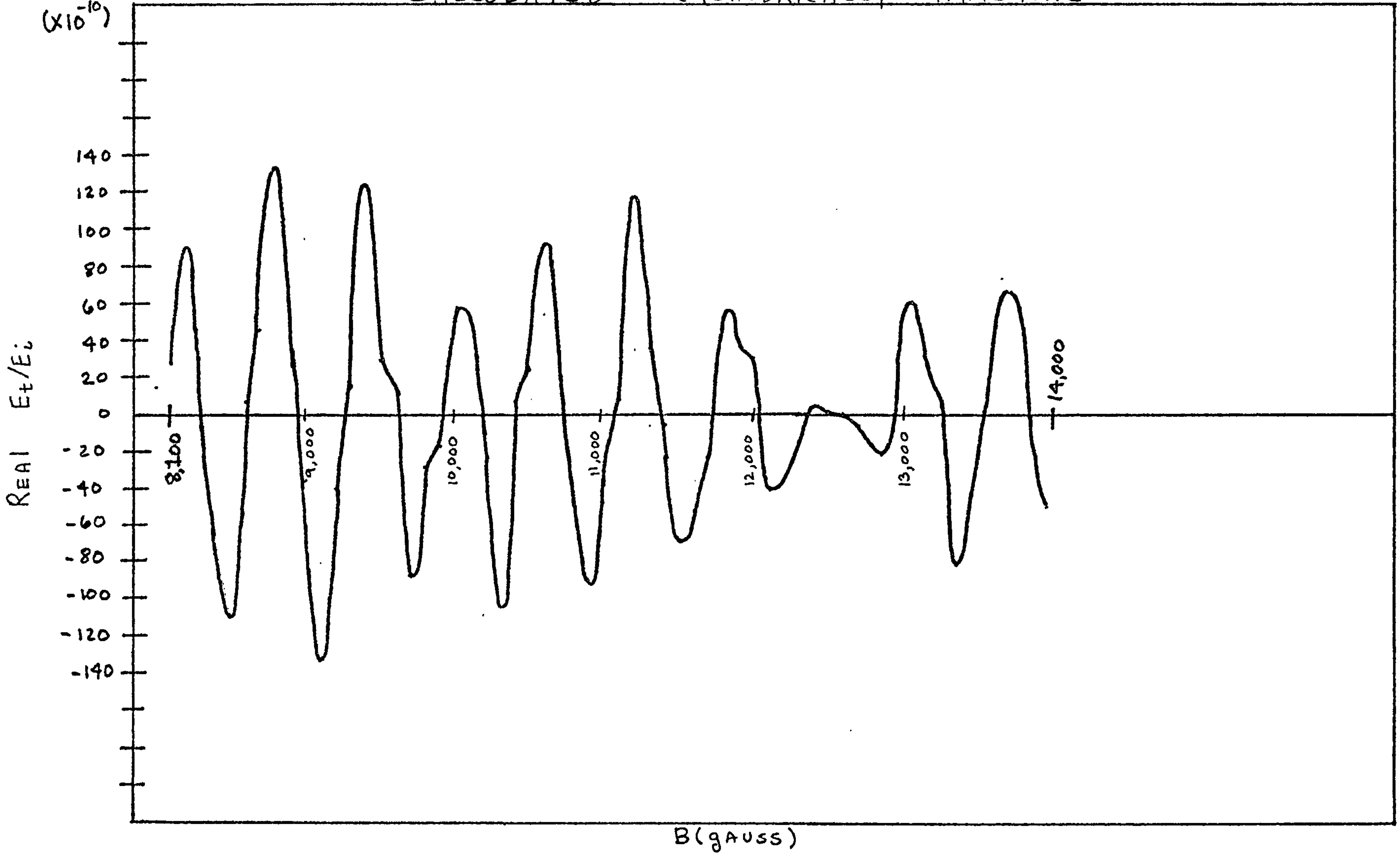

COPPER [111]

$\tau = 10^{-9}$ SEC $\quad f = 395.2 \times 10^{3}$ CYC/SEC

GRAPH XVII

CALCULATED CYLINDRICALLY SYMMETRIC

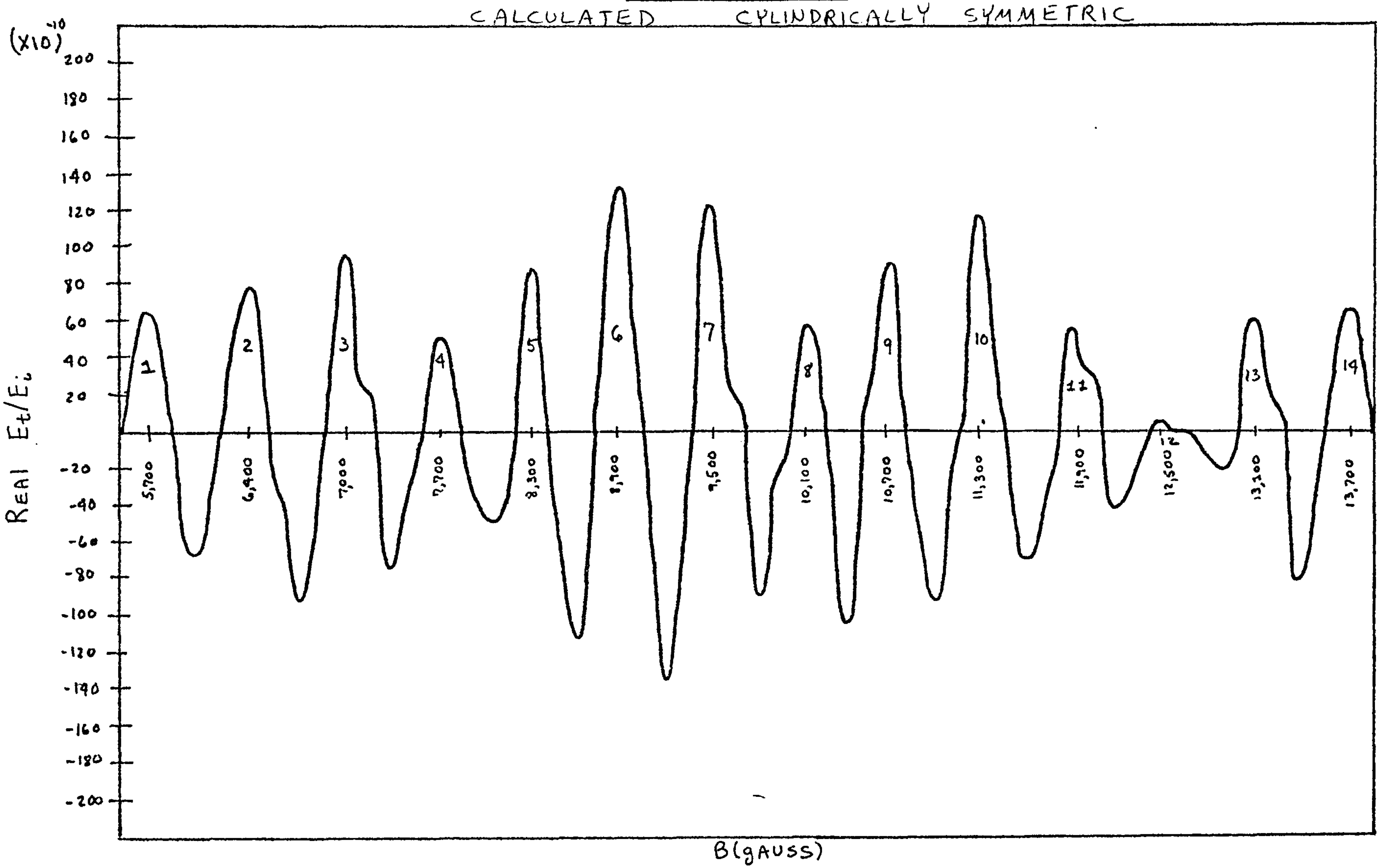

COPPER [111]

$\tau = 10^{-9}$ SEC $\qquad f = 395.2 \times 10^{3}$ CYC/SEC

GRAPH XVIII

CALCULATED CYLINDRICALLY SYMMETRIC

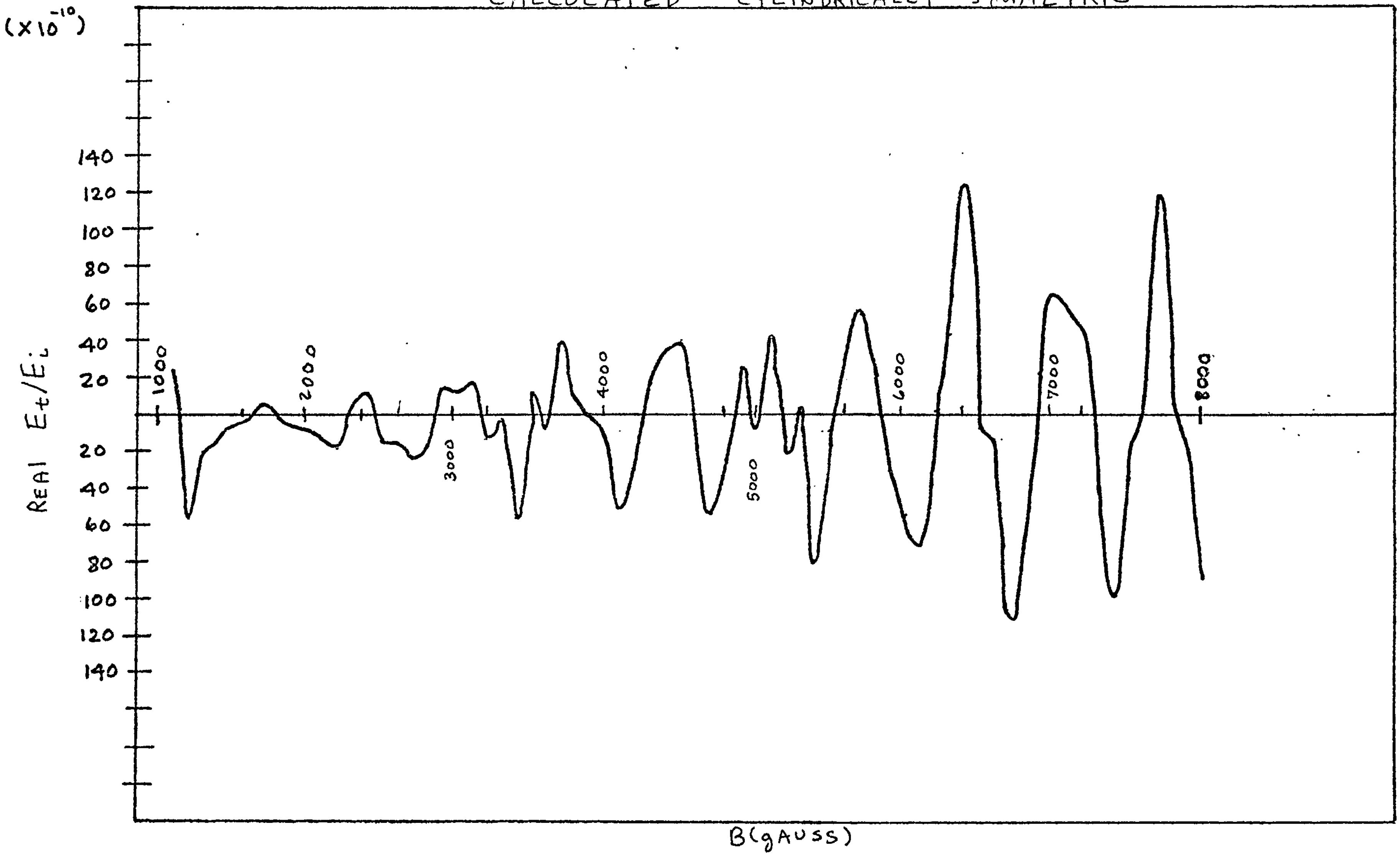

COPPER [111]

$\tau = 10^{-9}$ SEC $\quad f = 6 \times 10^{5}$ CYC/SEC

GRAPH XIX

CALCULATED CYLINDRICALLY SYMMETRIC

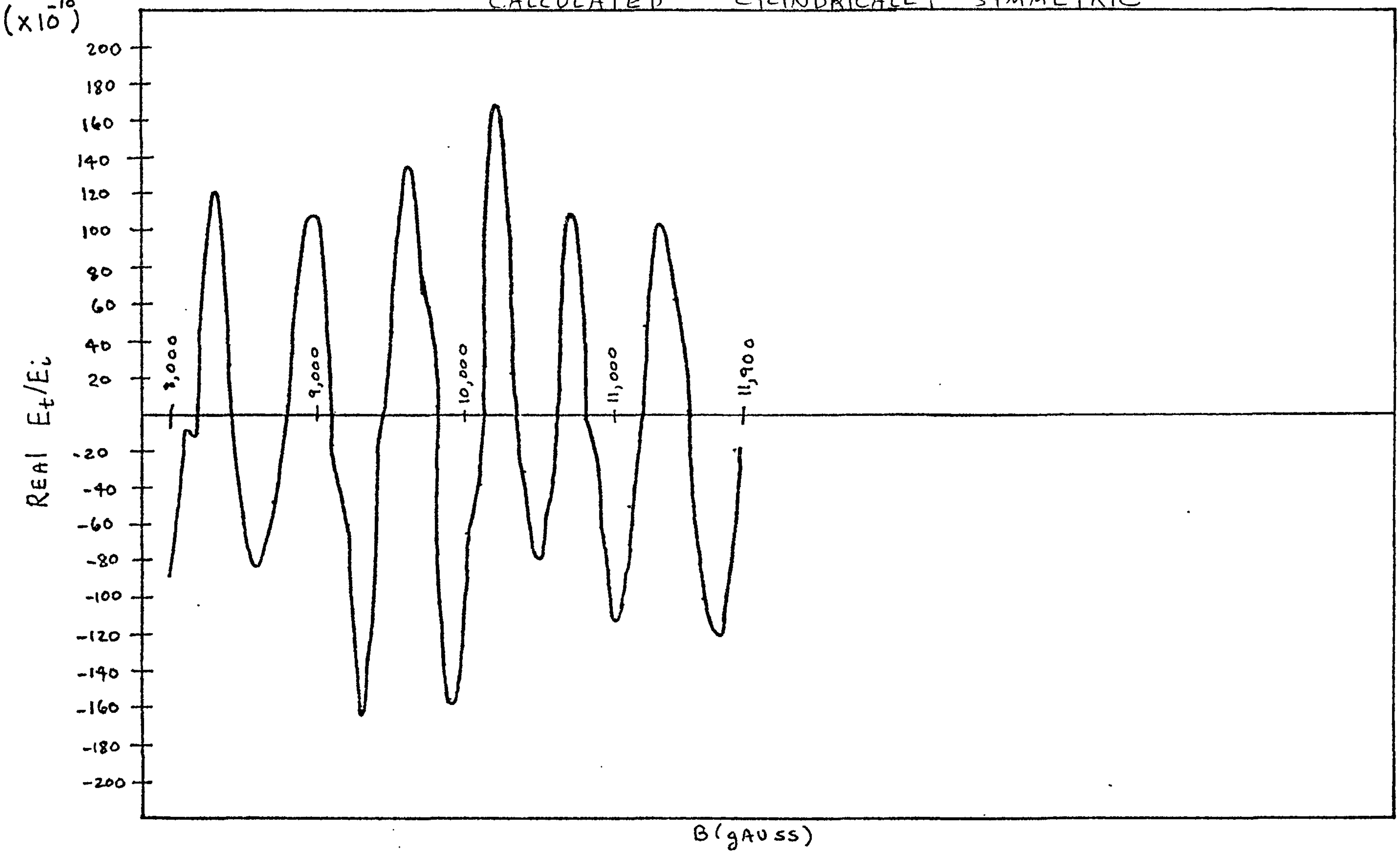

COPPER [111]

$\tau = 10^{-9}$ SEC $\quad f = 6 \times 10^{5}$ CYC/SEC

GRAPH XX

CALCULATED CYLINDRICALLY SYMMETRIC

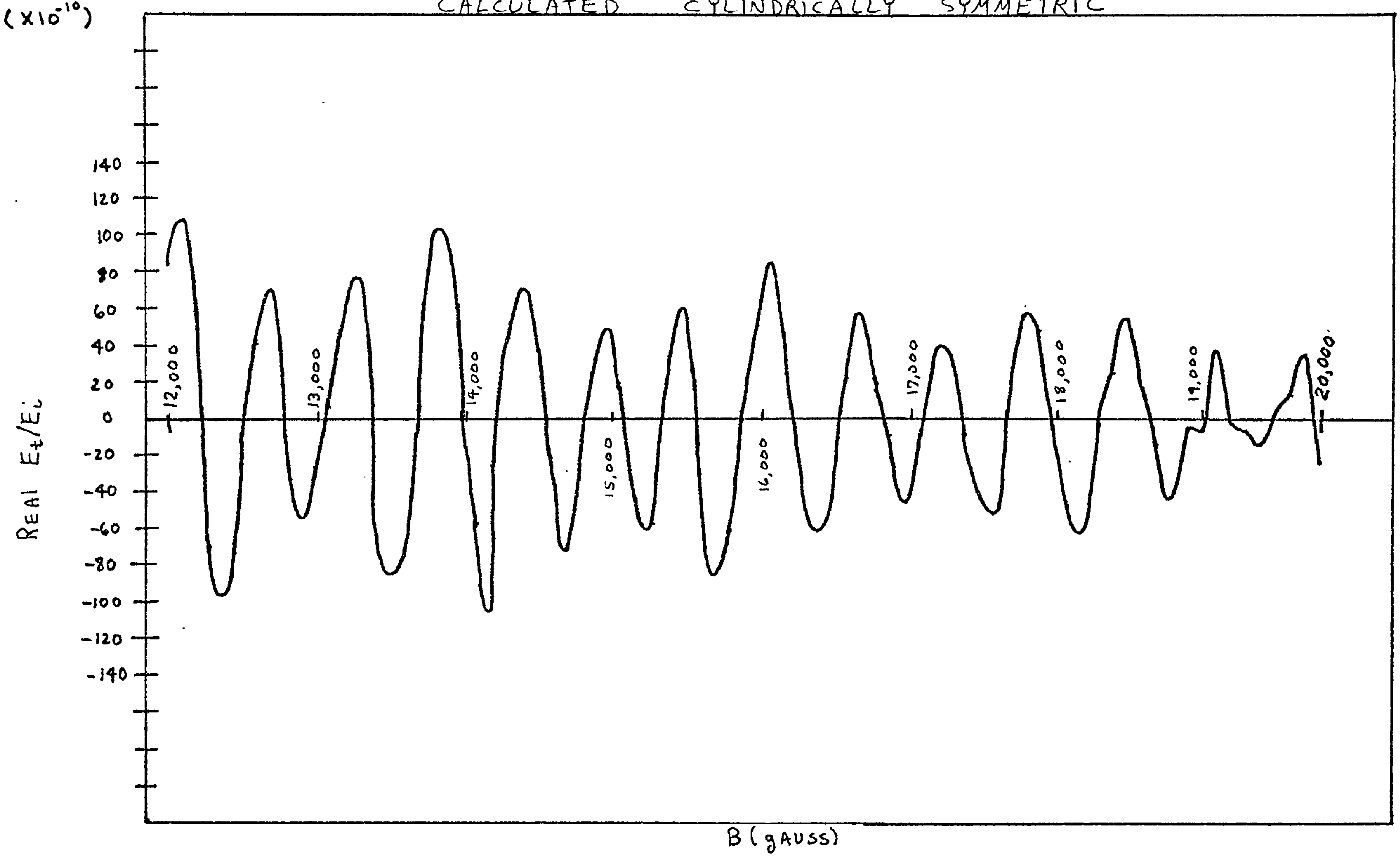

COPPER [111]

$\tau = 10^{-9}$ SEC $\quad f = 6 \times 10^5$ CYC/SEC

GRAPH XXI

CALCULATED CYLINDRICALLY SYMMETRIC

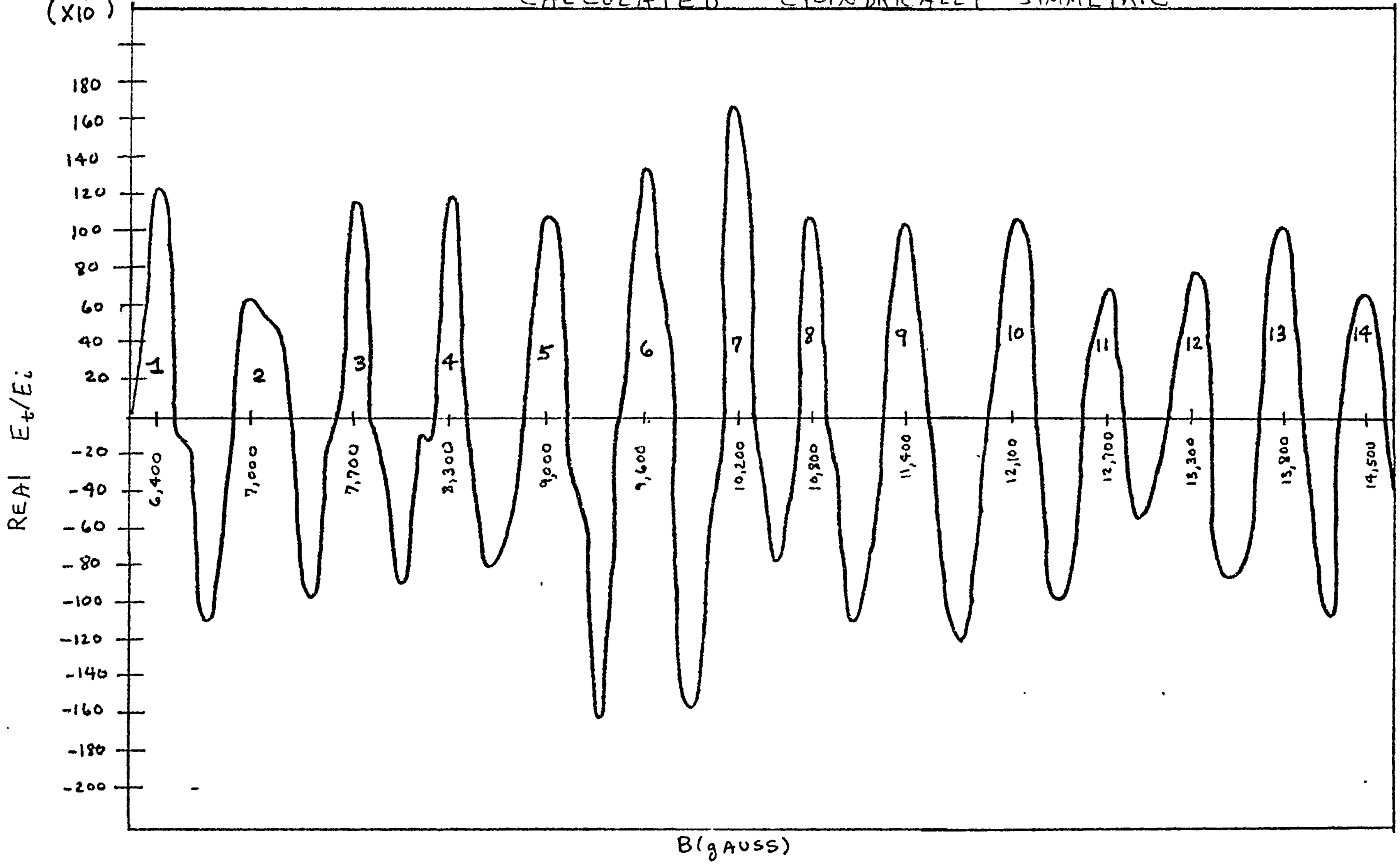

COPPER [111]

$T = 10^{-9}$ SEC $\quad f = 6 \times 10^{5}$ CYC/SEC are not as symmetric as the above drawing. The irregular envelope of the wave which we see would probably result mathematically by summing the two Gantmakher-Kaner waves expressed as Fourier series. Because of the irregularity of the envelope, we are unable to determine the beat frequency accurately from the graph.

Charts V and VI show the calculation of the period of the Gantmakher-Kaner waves, both cases of frequency giving a period of about 600 gauss. This agrees with the experimental data mentioned before.

Recall Equation (54) which states that

$$(\Delta B)\frac{eQ}{2\pi c} = [m_c V_z]_{EXT.} = -\frac{\hbar}{2\pi}\frac{\partial A}{\partial k_z} \quad ,$$

where $\Delta B = B/m$ = the period of the G-K wave. Now, Graph A shows a plot of $\partial A/\partial K_z$ versus $a|k_z|$ for the [111] direction of copper. We see two extremal values of the function $\partial A/\partial K_z$ which have been labeled P_1 and P_2 . P_1 corresponds to $\partial A/\partial K_z$ equaling 6.57×10^8 cm^{-1}, and P_2 corresponds to $\partial A/\partial K_z$ equaling 8.1×10^8 cm^{-1}. Thus, there are two values of $[m V_z]_{EXT.}$ which should give Gantmakher-Kaner waves, each having a different period. For P_1 , we obtain ΔB = 538 gauss, and for P_2 , we obtain ΔB = 664 gauss.

Calculation of Frequency of Waves
for the [111] Direction of Copper
for $f = 395.2 \times 10^3$ cyc/sec

CHART V

Peak No. on Graph	Value of E_t/E_i	B-Field	Period in Gauss
1	64×10^{-10}	5,700	
			700
2	78×10^{-10}	6,400	
			600
3	98×10^{-10}	7,000	
			700
4	49×10^{-10}	7,700	
			600
5	89×10^{-10}	8,300	
			600
6	132×10^{-10}	8,900	
			600
7	122×10^{-10}	9,500	
			600
8	58×10^{-10}	10,100	
			600
9	91×10^{-10}	10,700	
			600
10	117×10^{-10}	11,300	
			600
11	55×10^{-10}	11,900	
			600
12	46×10^{-10}	12,500	
			600
13	60×10^{-10}	13,100	
			600
14	63×10^{-10}	13,700	

Calculation of Frequency of Waves
for the [111] Direction of Copper
for $f = 6 \times 10^5$ cyc/sec

CHART VI

Peak No. on Graph	Value of E_t/E_i	B-Field	Period in Gauss
1	123×10^{-10}	6,400	
2	65×10^{-10}	7,000	600
3	119×10^{-10}	7,700	700
4	121×10^{-10}	8,300	600
5	107×10^{-10}	9,000	700
6	135×10^{-10}	9,600	600
7	167×10^{-10}	10,200	600
8	107×10^{-10}	10,800	600
9	103×10^{-10}	11,400	600
10	108×10^{-10}	12,100	700
11	69×10^{-10}	12,700	600
12	75×10^{-10}	13,300	600
13	101×10^{-10}	13,800	500
14	70×10^{-10}	14,500	700
-	48×10^{-10}	15,100	600
-	61×10^{-10}	15,700	600
-	85×10^{-10}	16,300	600
-	55×10^{-10}	16,900	600
-	37×10^{-10}	17,400	500
-	55×10^{-10}	18,000	600

$|\partial A/\partial k_z|$ VERSUS $a|k_z|$ FOR [111] DIRECTION OF COPPER

GRAPH A

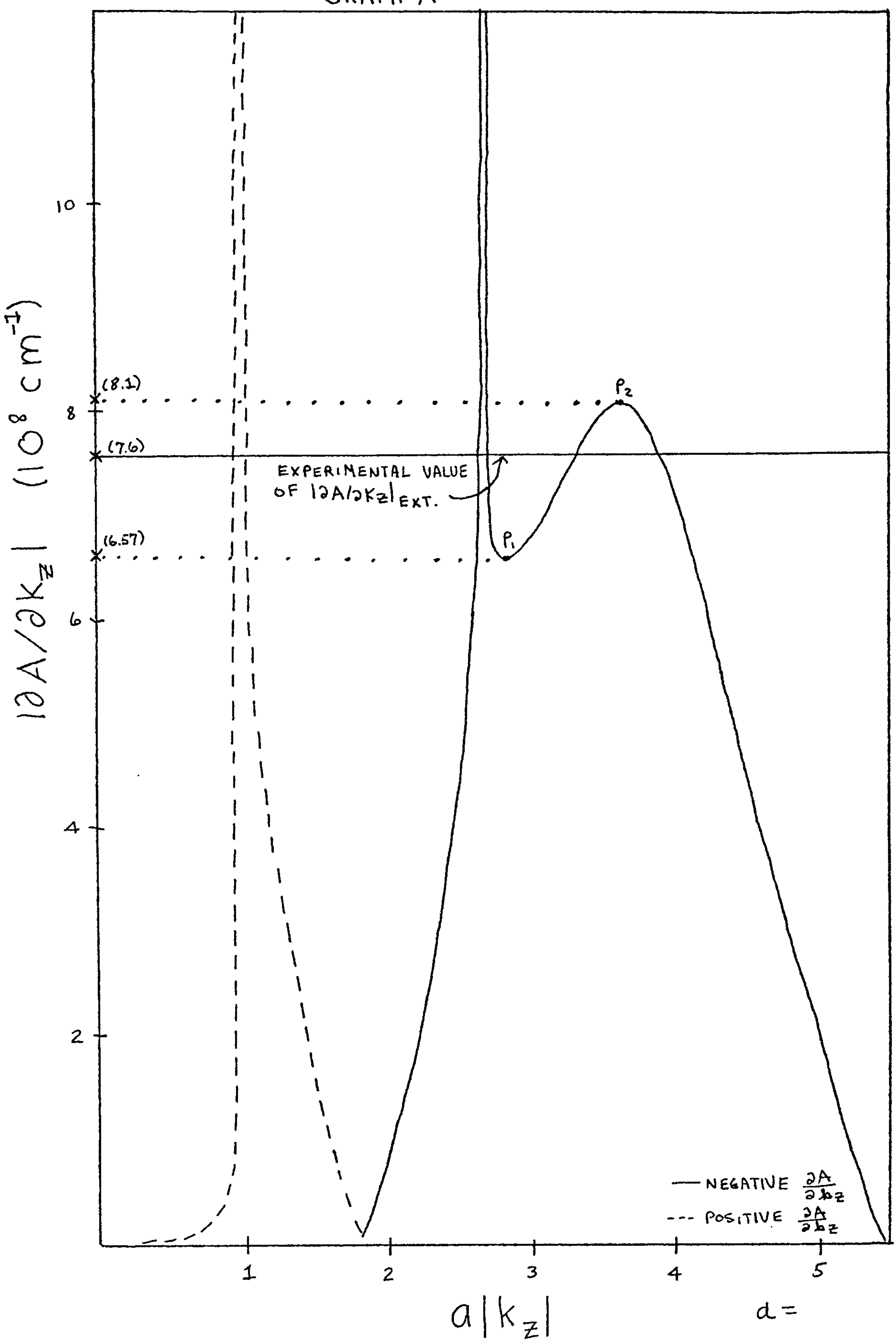

Now the frequency is related to the period by

$$f = \frac{1}{(\Delta B)} \quad . \tag{145}$$

Thus, we have that

$$f_1 = 1/538 \ \text{gauss}^{-1} = .0018 \ \text{gauss}^{-1},$$

and

$$f_2 = 1/664 \ \text{gauss}^{-1} = .0015 \ \text{gauss}^{-1}.$$

Therefore, the frequency of the composite wave is given by

$$f^* = \tfrac{1}{2}(.0018 + .0015) \ \text{gauss}^{-1} \quad ,$$

or

$$f^* = .00165 \ \text{gauss}^{-1} \quad .$$

Now the ΔB from the graph was 600 gauss, corresponding to a frequency of .0016 gauss^{-1}. Thus, we have a perfect agreement with theory. That is, the two frequencies of the Gantmakher-Kaner waves making up the beats are .0015 gauss^{-1} and .0018 gauss^{-1}. We also note that the experimental value of the frequency of the composite Gantmakher-Kaner wave corresponds to a value of $\partial A/\partial k_z$ of $7.6 \times 10^8 \ \text{cm}^{-1}$ on Graph A. This corresponds to a frequency of .0016 gauss^{-1}. Thus, our data agrees with experimental data as well.

Let us now look at the results for the [001] direction of copper. Graph XXXII is an experimental curve obtained by Wood showing helicon propagation starting at about 16,000 gauss.

We have computed data for a frequency of 395.2×10^3 hz. for $\tau = 10^{-9}$ sec. and $\tau = 10^{-10}$ sec. Graphs XXII through XXVII show the results for $\tau = 10^{-9}$ sec. for a B-field range of 8,000 to 19,000 gauss. Helicons begin propagating at about 15,275 gauss as seen from Graph XXV. The helicons have a delta function shape, just as the helicons for sodium had at $\tau = 10^{-9}$ sec. Graphs XXII through XXV show waves which are not constant in period nor increase in amplitude. These can be called neither helicons nor Gantmakher-Kaner oscillations. Their source is unknown to us.

Graph B is a graph of $\partial A/\partial k_z$ versus k_z for the [001] direction of copper. We see an extremal value of $\partial A/\partial k_z$ equal to 2.2×10^8 cm^{-1}, which means that we would expect a Gantmakher-Kaner wave contribution from those electrons having a V_z velocity corresponding to this value of $\partial A/\partial k_z$. However, experimentally, no Gantmakher-Kaner oscillations are seen. Realizing that experimental results would come from use of the true

EXPERIMENTAL CURVE (TRUE FERMI SURFACE)

$f = 395.2 \times 10^3$ CYC/SEC

GRAPH XXXII

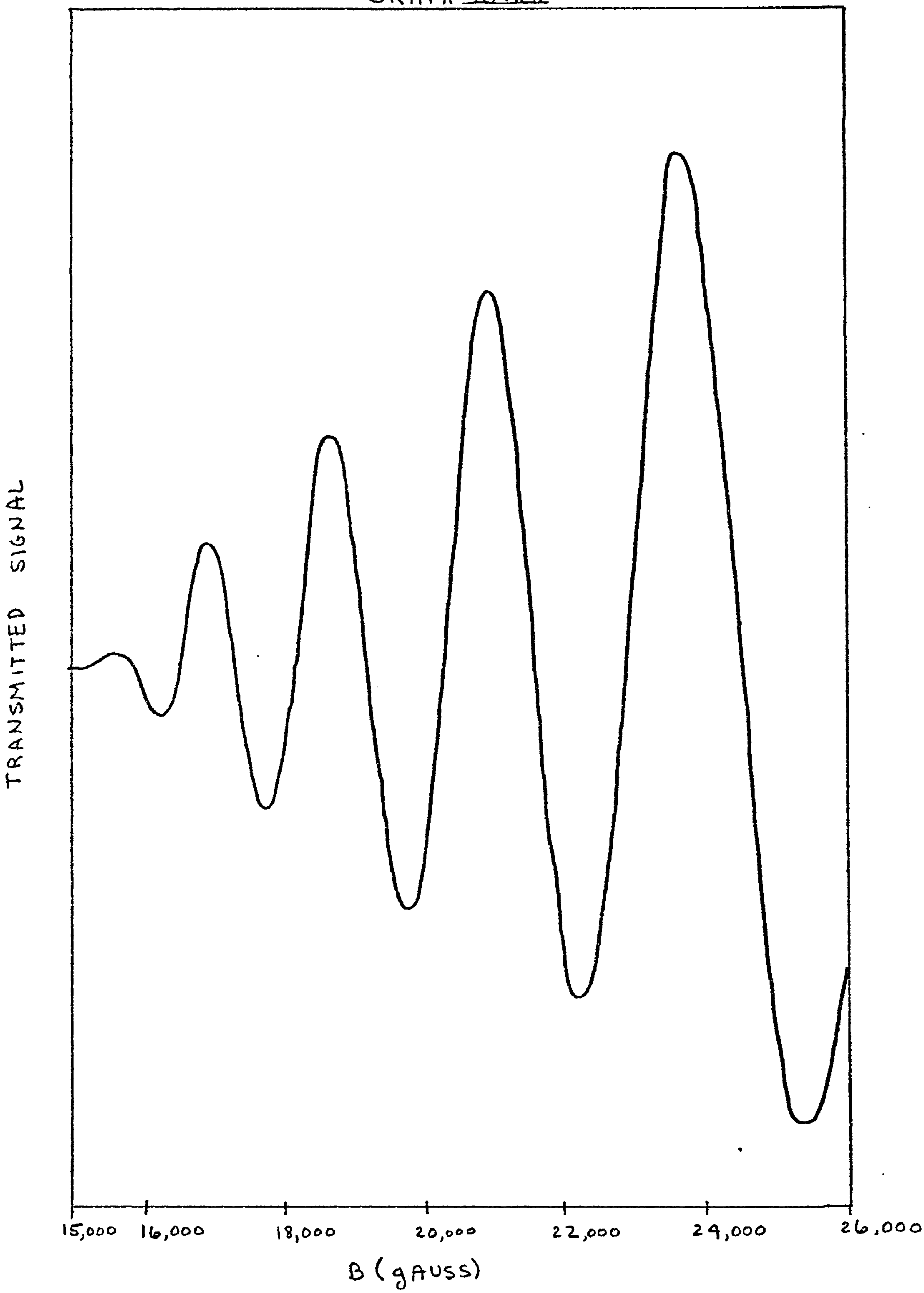

GRAPH XXII

CALCULATED CYLINDRICALLY SYMMETRIC

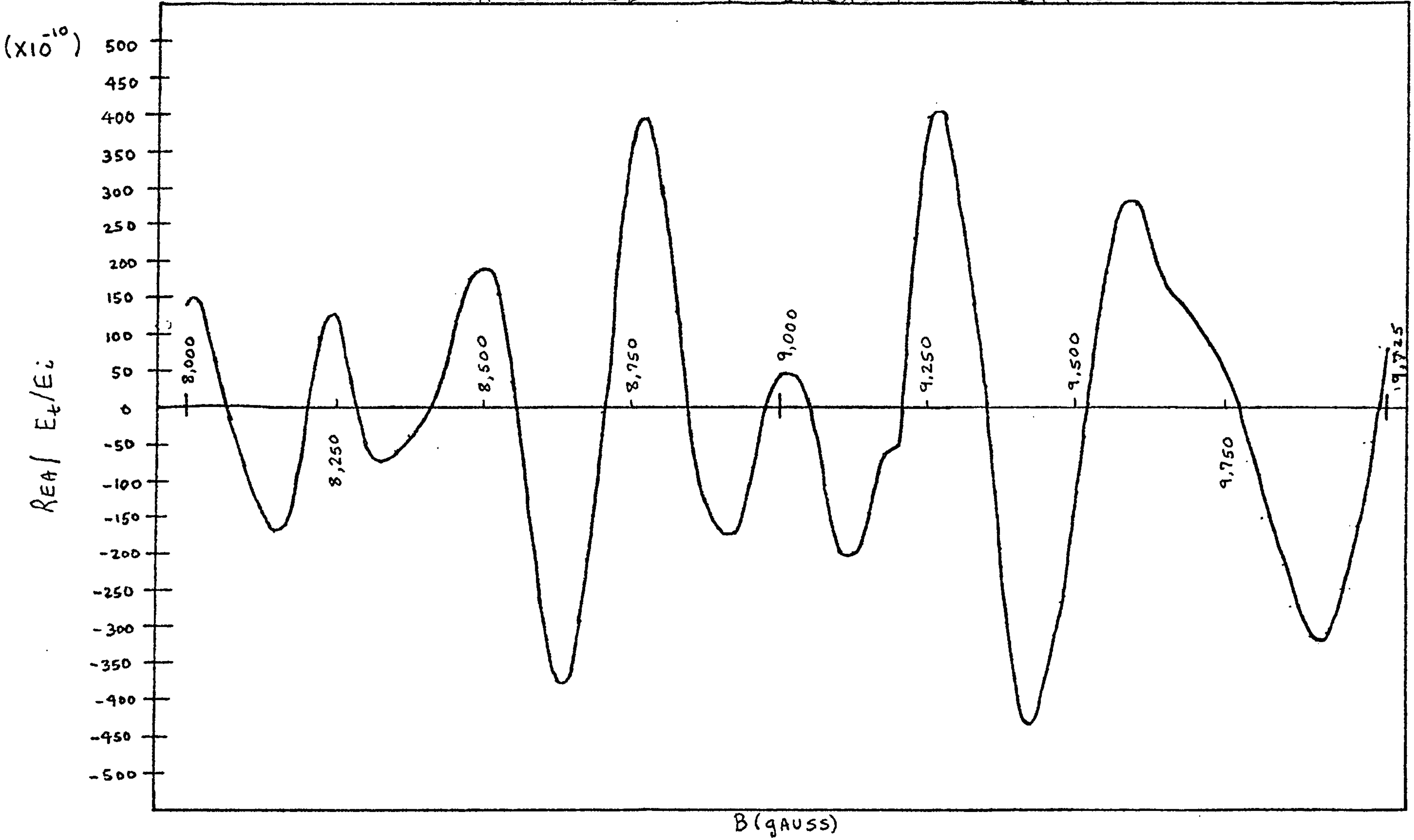

COPPER [001]

$\tau = 10^{-9}$ SEC $f = 395.2 \times 10^{3}$ CYC/SEC

GRAPH XXIII

CALCULATED CYLINDRICALLY SYMMETRIC

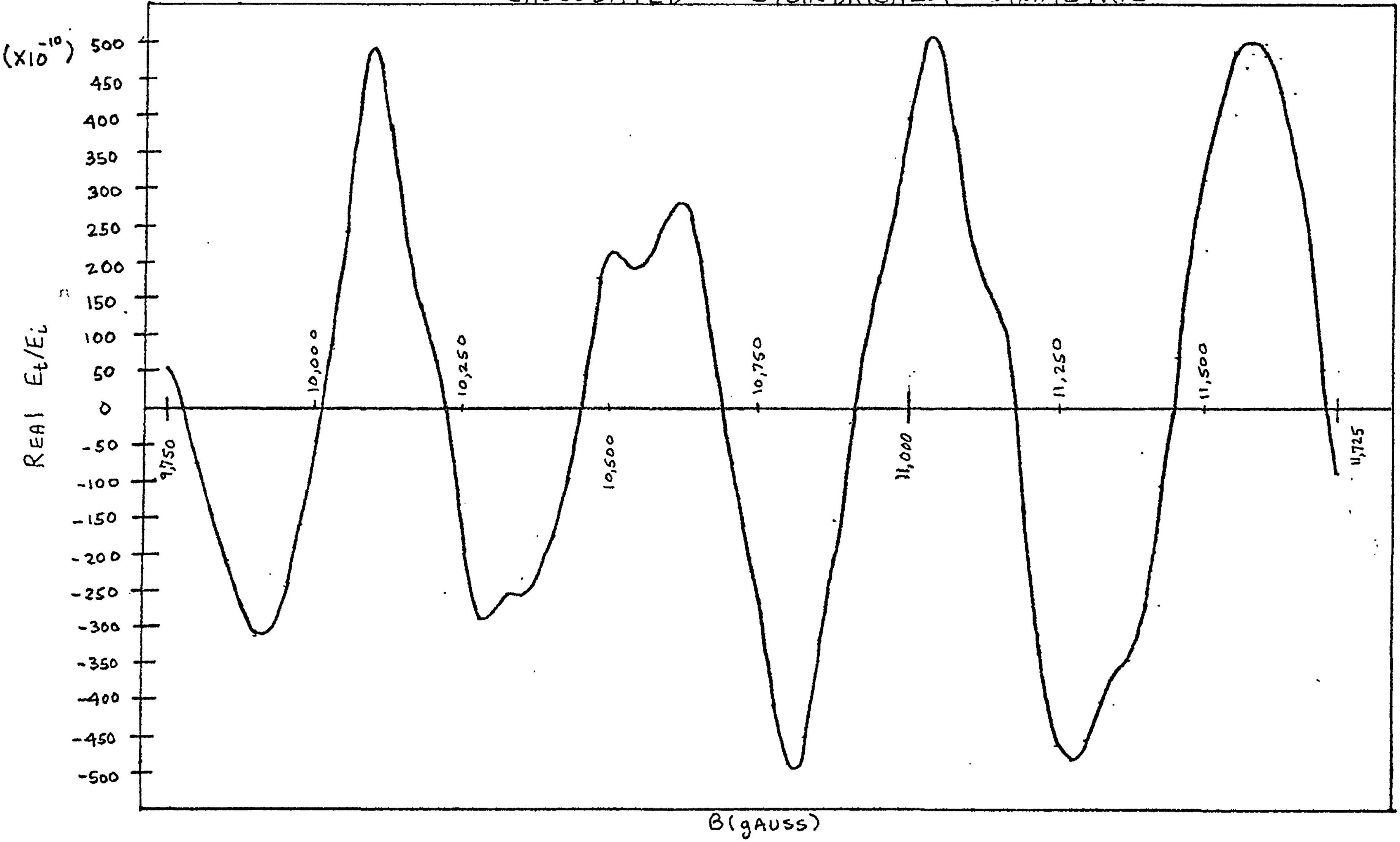

COPPER [001]

$\tau = 10^{-9}$ SEC $\quad f = 395.2 \times 10^{3}$ CYC/SEC

GRAPH XXIV

CALCULATED CYLINDRICALLY SYMMETRIC

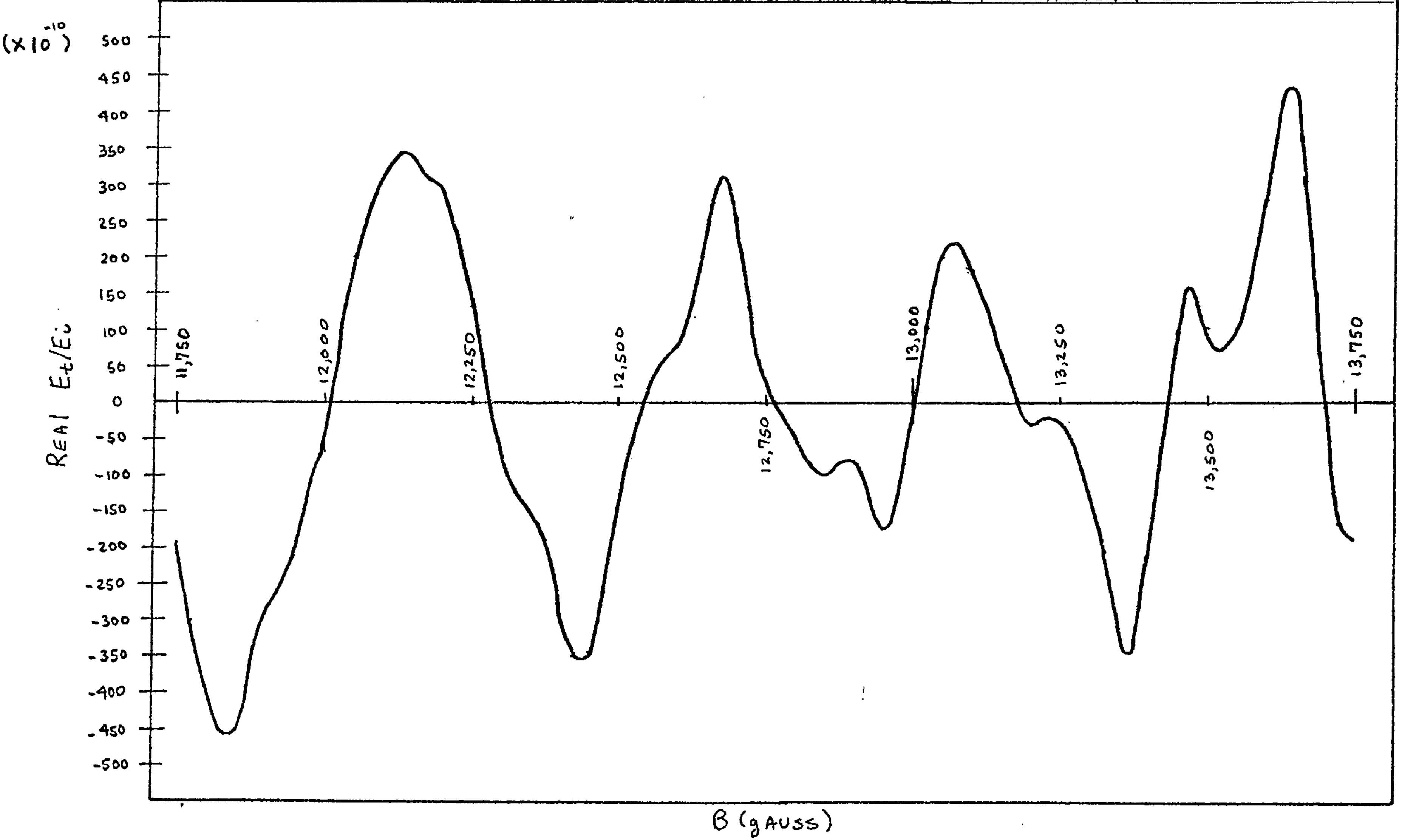

COPPER [001]

$T = 10^{-9}$ SEC $f = 395.2 \times 10^{3}$ CYC/SEC

GRAPH XXV

CALCULATED CYLINDRICALLY SYMMETRIC

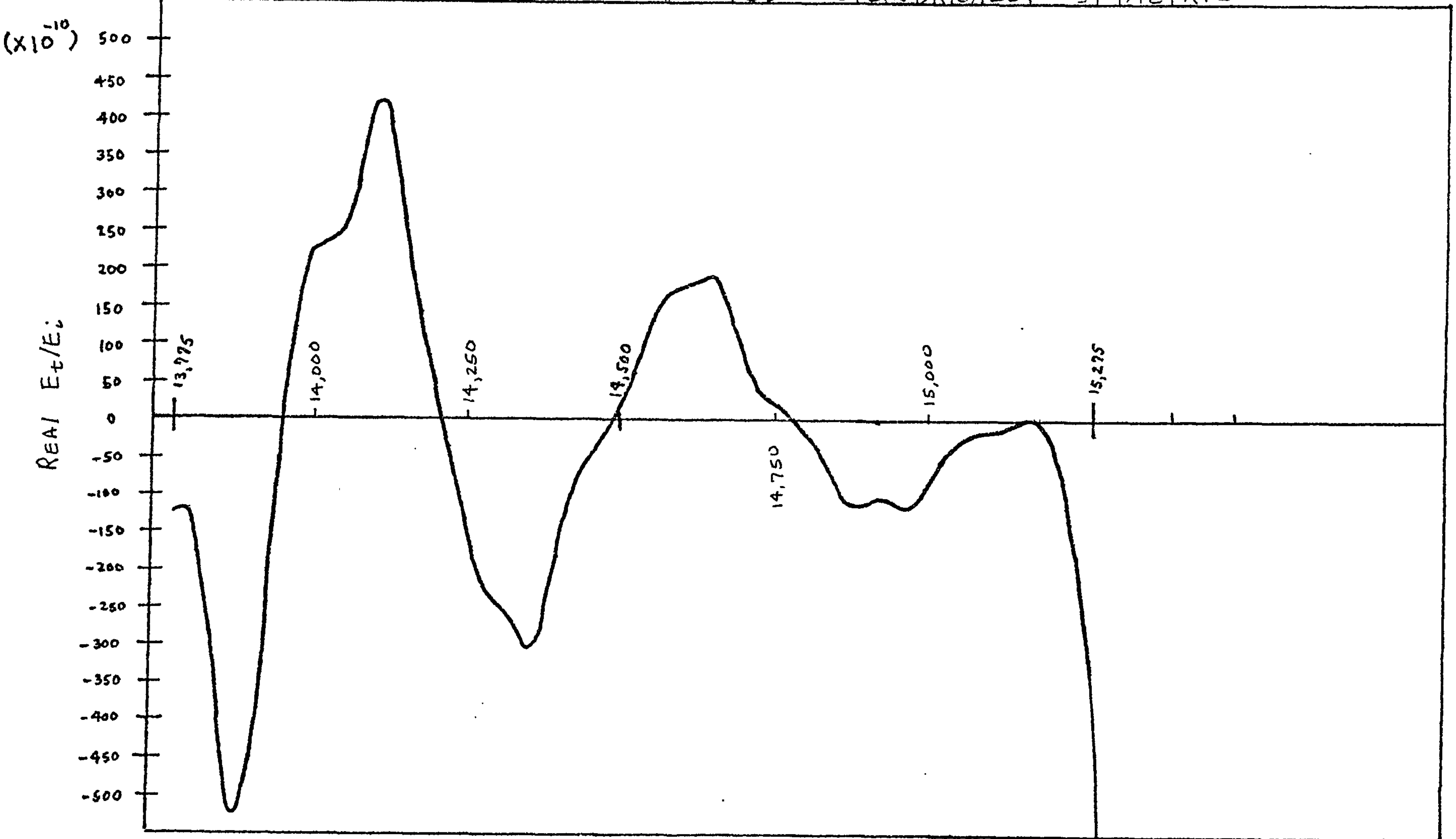

COPPER [001]

$\tau = 10^{-9}$ SEC $\quad f = 395.2 \times 10^{3}$ CYC/SEC

GRAPH XXVI

CALCULATED CYLINDRICALLY SYMMETRIC

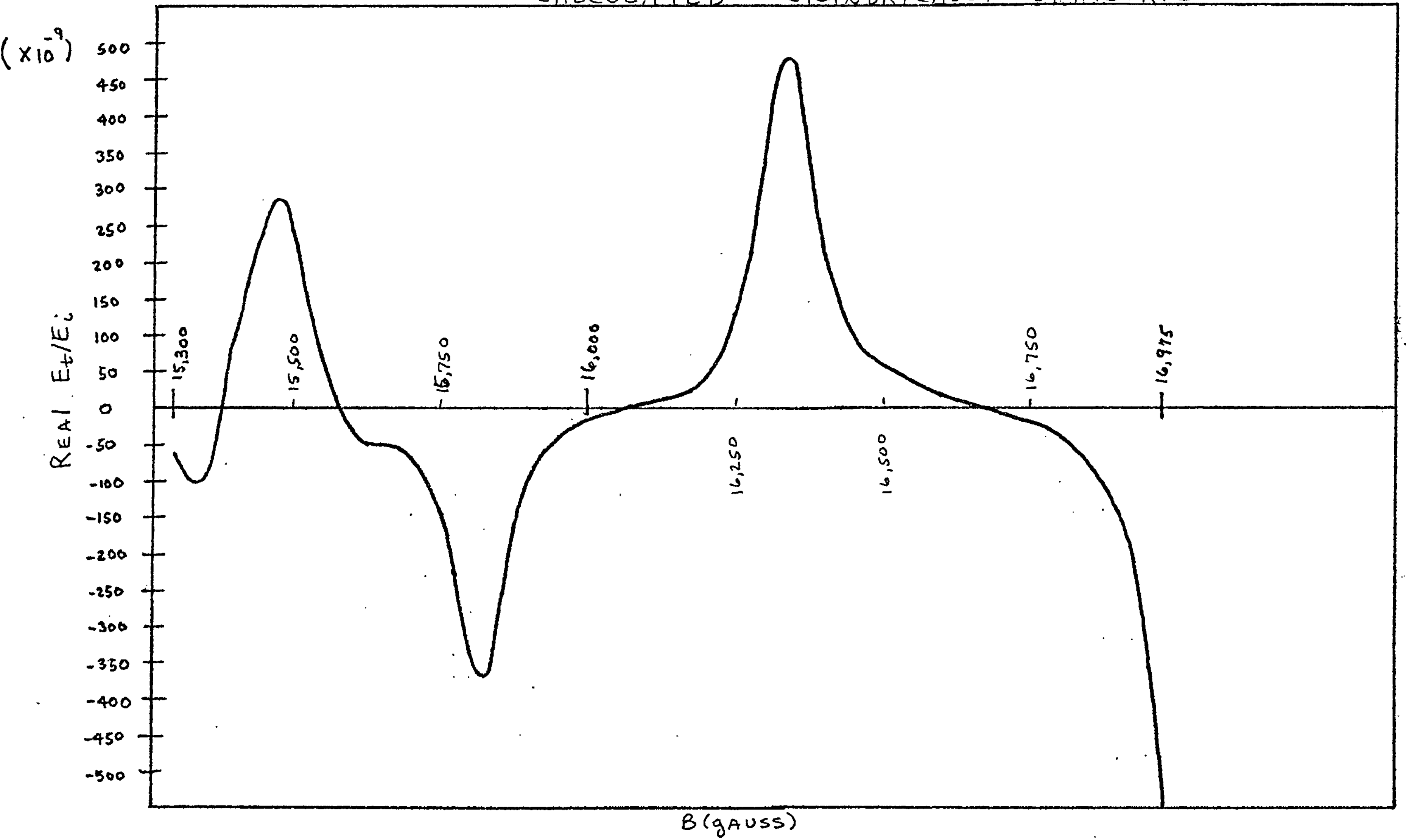

COPPER [001]

$T = 10^{-9}$ SEC $f = 395.2 \times 10^{3}$ cyc/sec

GRAPH XXVIII

CALCULATED CYLINDRICALLY SYMMETRIC

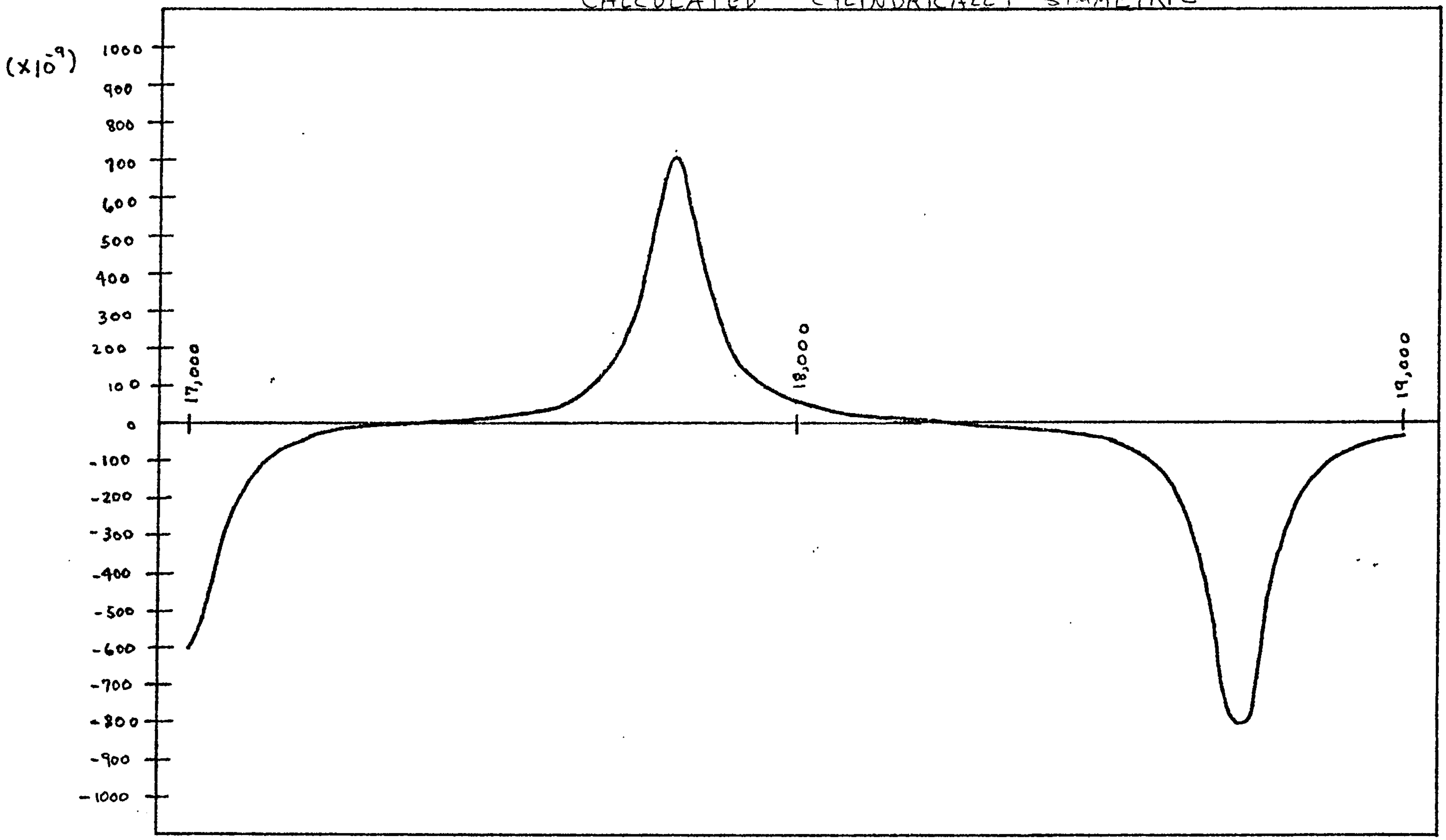

COPPER [001]

$T = 10^{-9}$ SEC $f = 395.2 \times 10^{3}$ CYC/SEC

noncylindrically symmetric Fermi surface, one might suspect that our assumption of a cylindrically symmetric Fermi surface, which Graph B describes, causes the Gantmakher-Kaner oscillations. This will be discussed further in the data analyzation of the copper calculations using the true Fermi surface values.

On Graph B we also note the value of $|\partial A/\partial k_z|_{MAX}$, which is responsible for the absorption edge. The value of $[\partial A/\partial k_z]_{MAX}$ is 9.4 X 10^8 cm^{-1}. Using the equation

$$\omega_c = eB/mc = \omega_e = \omega + q V_z \quad , \tag{146}$$

we saw that the last group of electrons which can experience Doppler - shifted cyclotron resonance are those having the velocity V_{zMAX}. Now since $\omega \ll q V_z$, we have

$$eB^*/mc = q V_{zMAX} \quad , \tag{147}$$

or

$$B^* = q V_{zMAX}\, mc/e = q c \hbar (\partial A/\partial k_z)/2\pi e \quad . \tag{148}$$

Thus, B* is the value of B at which we would expect helicons to start propagating. Using $[\partial A/\partial k_z]_{MAX} = 9.4$ X 10^8 cm^{-1}, we obtain that

$$B^* = 15{,}700 \quad ,$$

where m = 41 for $q = m\pi/Q$. This value of m corresponds to M*, defined earlier as that value of m in $\vec{q}$ which

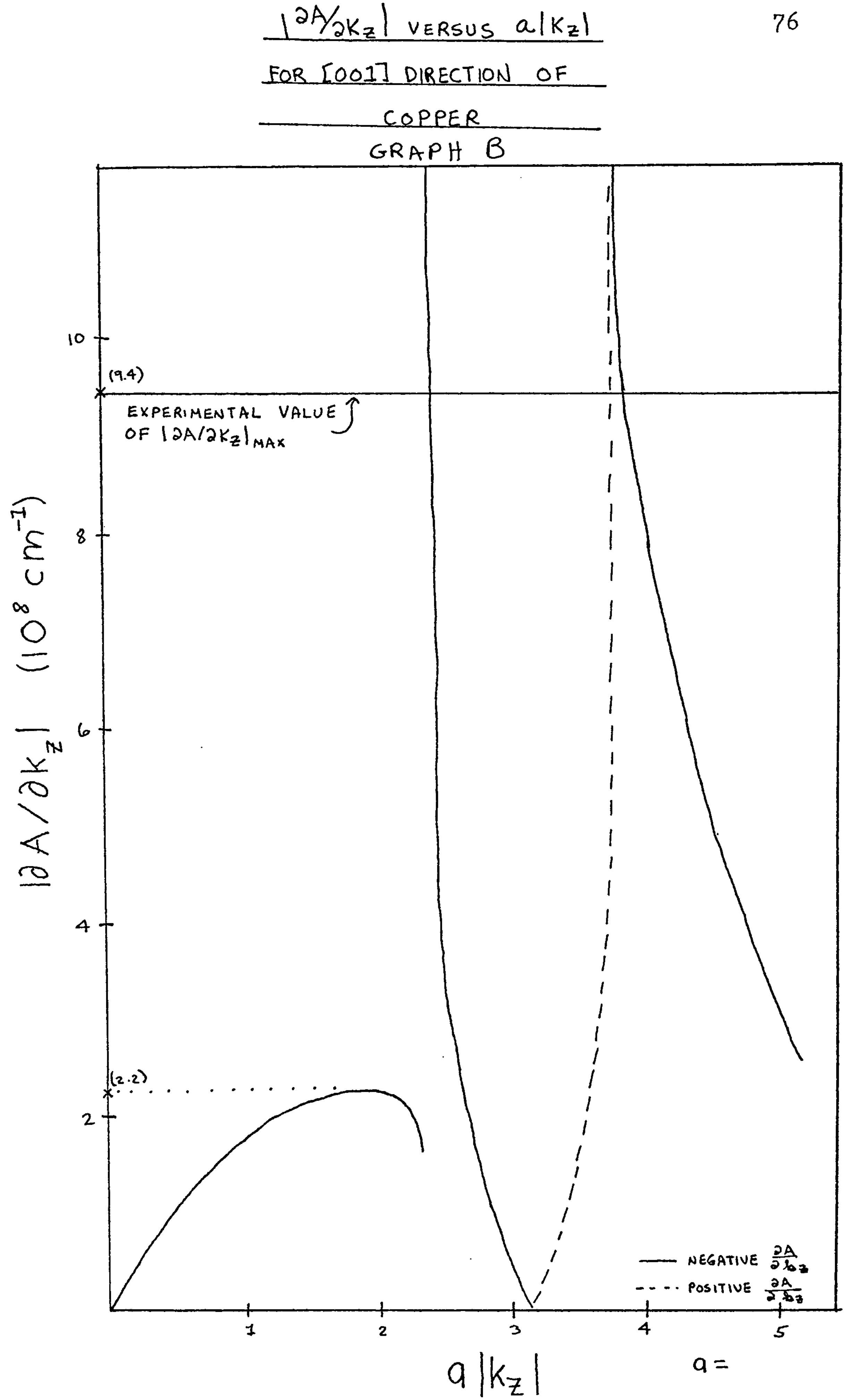

|∂A/∂Kz| VERSUS a|Kz|
FOR [001] DIRECTION OF
COPPER
GRAPH B
|∂A/∂kz| (10^8 cm^-1)
10
8
6
4
2
(9.4)
EXPERIMENTAL VALUE OF |∂A/∂Kz|MAX
(2.2)
1
2
3
4
5
a|kz|
a =
NEGATIVE ∂A/∂kz
POSITIVE ∂A/∂kz

gives the largest contribution to REAL E_t/E_i . Helicons are seen to start at about 15,275 gauss; however, as usual, the exact point is impossible to locate.

Data was calculated for $\tau = 10^{-10}$ sec. for a B-field range of 13,250 to 17,500 gauss. Graphs XXVIII through XXX show the data. Helicons are seen to begin propagating at about 15,750 gauss, which is in good agreement with the experimental data. We also note the smooth sinusoidal-like shape of the helicons, differing from the delta shaped peaks for the previous τ . This result from the change of τ is identical with that seen in sodium.

GRAPH XXVIII

CALCULATED CYLINDRICALLY SYMMETRIC

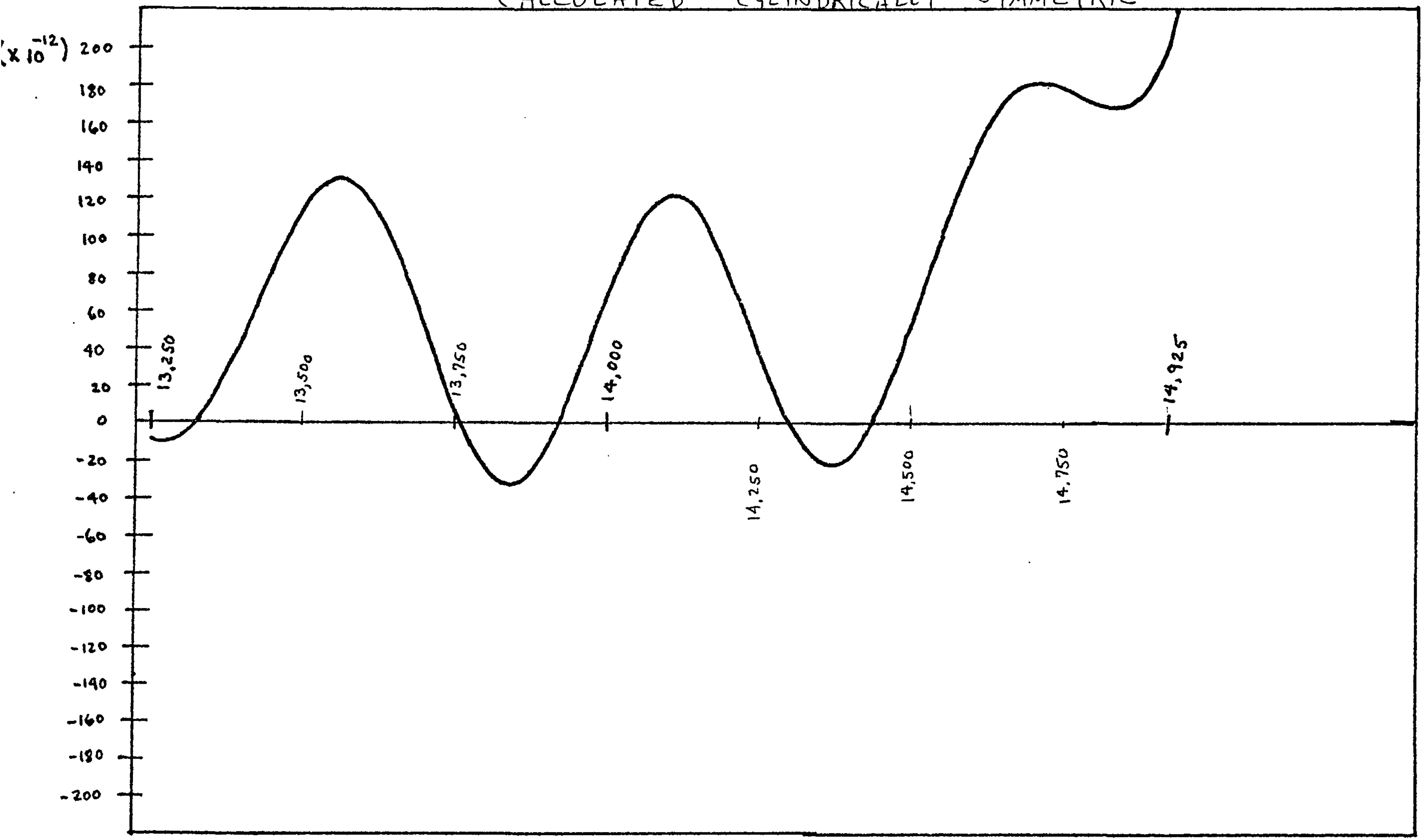

COPPER [001]

$\tau = 10^{-10}$ SEC $f = 395.2 \times 10^{3}$ CYC/SEC

GRAPH XXIV

CALCULATED CYLINDRICALLY SYMMETRIC

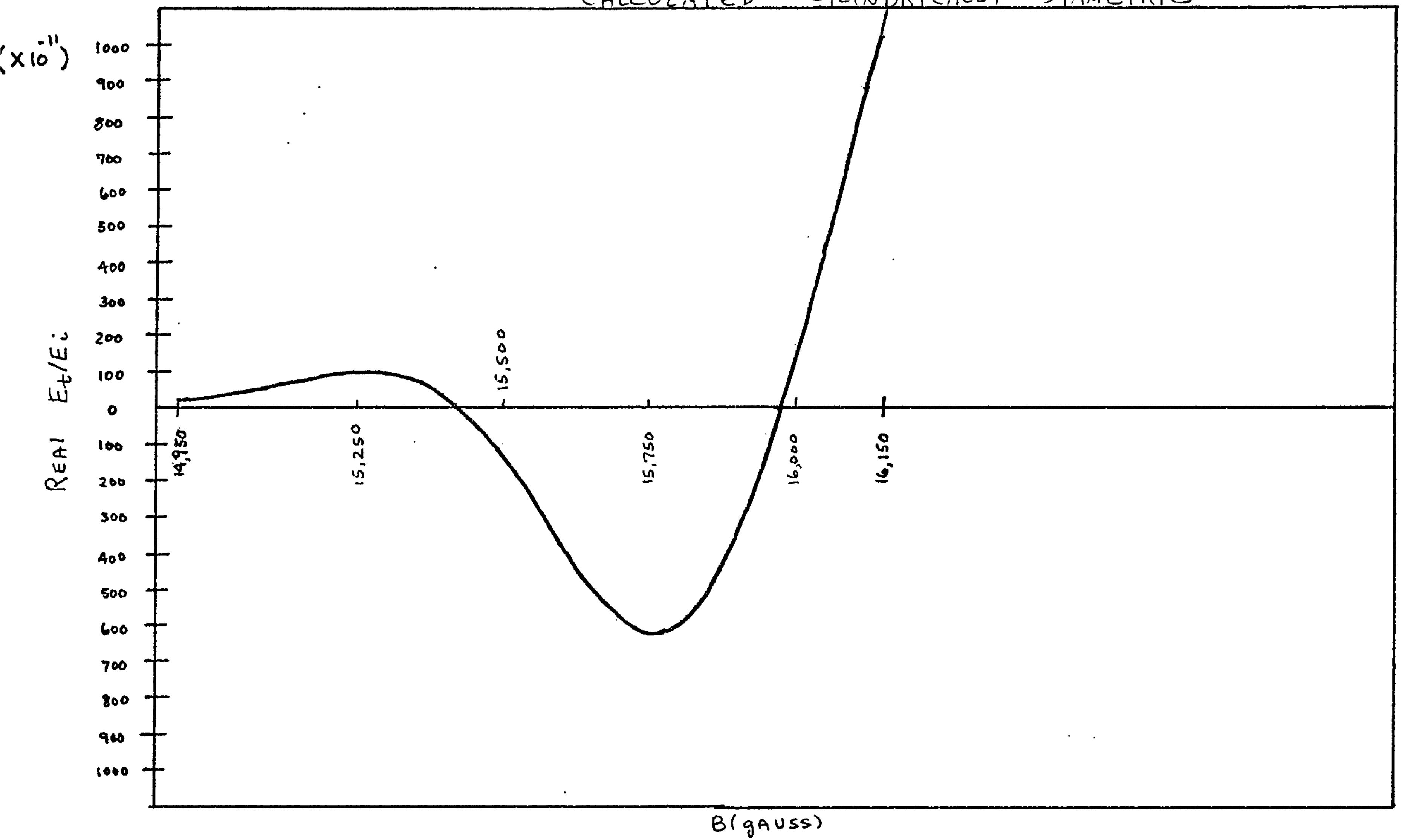

COPPER [001]

$\tau = 10^{-10}$ SEC $f = 395.2 \times 10^{3}$ CYC/SEC

GRAPH XXX

CALCULATED CYLINDRICALLY SYMMETRIC

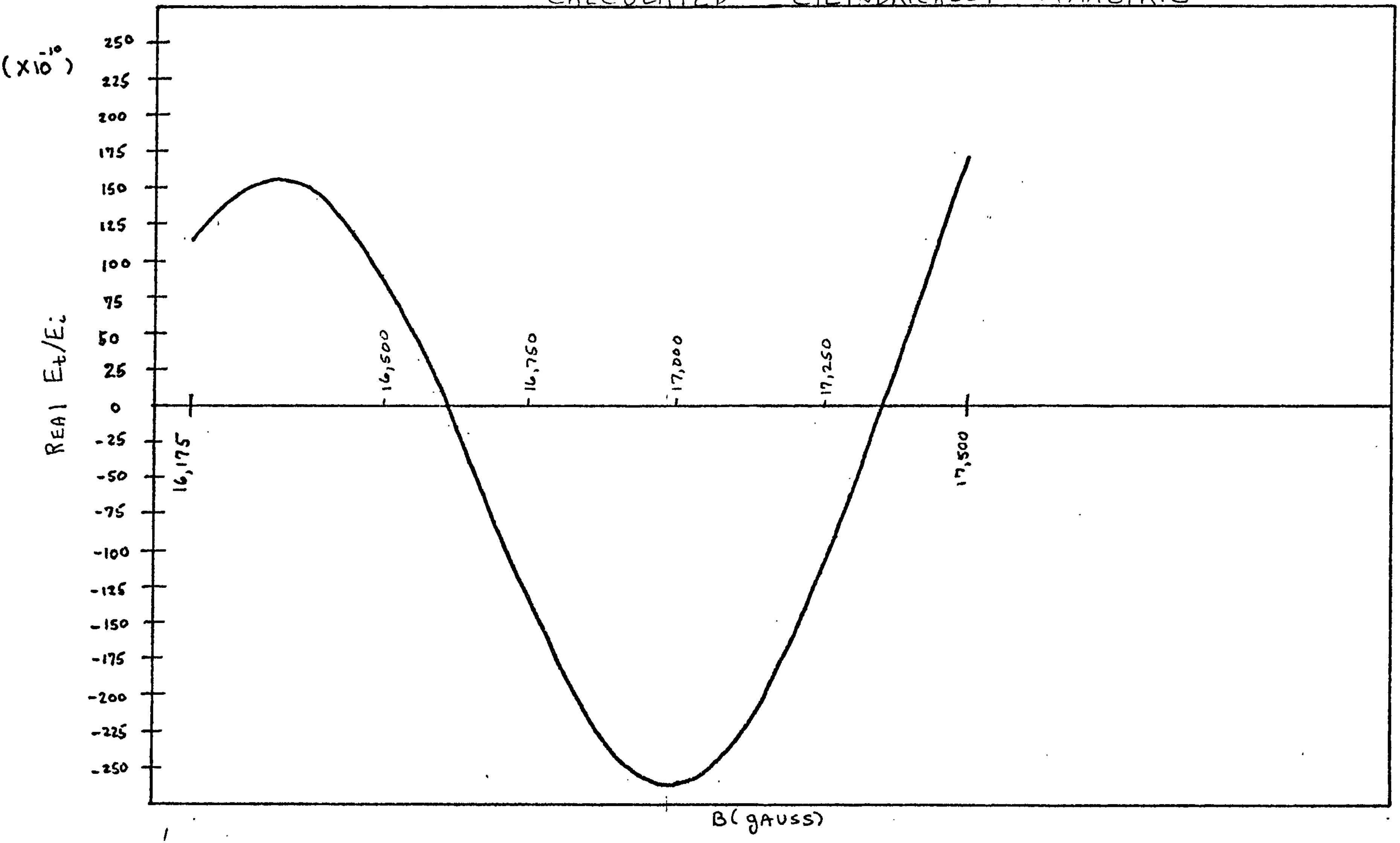

COPPER [001]

$T = 10^{-10}$ SEC $f = 395.2 \times 10^{3}$ CYC/SEC

We now conclude this thesis with the results for the final case of copper in which we use the true Fermi surface. Again we use the computer program included in the appendix in which the $\vec{V}_{mx}$ and $\vec{V}_{my}$ are evaluated by numerical integrations. The values of the V_x , V_y , and V_z components of the velocity for an electron on the Fermi surface were made available by Wood. Recalling that

$$\vec{V} = \frac{1}{\hbar}\left(\frac{\partial \mathcal{E}(\vec{k})}{\partial \vec{k}}\right) ,$$

and that

$$\vec{V} = \lim_{\Delta \vec{k} \to 0} \frac{1}{\hbar} \frac{\mathcal{E}(\vec{k}+\Delta\vec{k}) - \mathcal{E}(\vec{k})}{\Delta \vec{k}} , \quad (149)$$

we see that it is necessary to know the constant energy surface $\Delta\vec{k}$ away from the Fermi surface. In the calculation of the velocity by Wood, it was assumed that the constant energy surface $\Delta\vec{k}$ away from the Fermi surface was concentric in shape with the Fermi surface. If this is not a valid assumption, then our velocity on the Fermi surface is not accurate at all points and a difference in the data results and the experimental curve might be expected.

The results are shown on Graphs XXXI and XXXIII. A frequency of 395.2×10^3 hertz and a τ of 10^{-9} sec. was used. Graph XXXI displays a B-field range of 16,500 gauss to 17,500 gauss, and Graph XXXIII shows a B-field range of 11,100 to 11,900 gauss. The [001] direction of copper was investigated; thus, we were able to compare our data with Graphs XXIII, XXIV, XXVI, and XXVII which show the data for the cylindrically symmetric Fermi surface approximation. The amplitudes of the peaks of Graphs XXXI and XXXIII are smaller by two orders of magnitude than the amplitudes of their respective peaks on Graphs XXIII, XXIV, XXVI, and XXVII. The numerical integration techniques used in the program cannot be responsible for the decrease since their accuracy was checked in the case of sodium. Recalling Graph XII, we see an amplitude for a helicon calculated by our numerical integrations which is identical with that calculated by the earlier two methods in which numerical integrations were not used.

Graph XXXI does, however, show the familiar delta shape due to the relaxation time of 10^{-9} sec. and agrees with the experimental curve on Graph XXXII in that helicons are propagating in this B-field region. Graph XXXIII does not agree with the experimental curve which shows nothing propagating in this region. Our only explanation of this is that the velocity on the Fermi surface is not accurate at all points due to a non-concentric constant energy surface $\Delta \vec{k}$ away from the Fermi surface. Also, the loss of cylindrical symmetry of the Fermi surface is believed to be the cause of the reduction in amplitude of the peaks by a factor of 10^{-2} which was mentioned earlier. As for the case of sodium, limited computer time forced us to investigate only small B-field ranges in this final case.

GRAPH XXXI

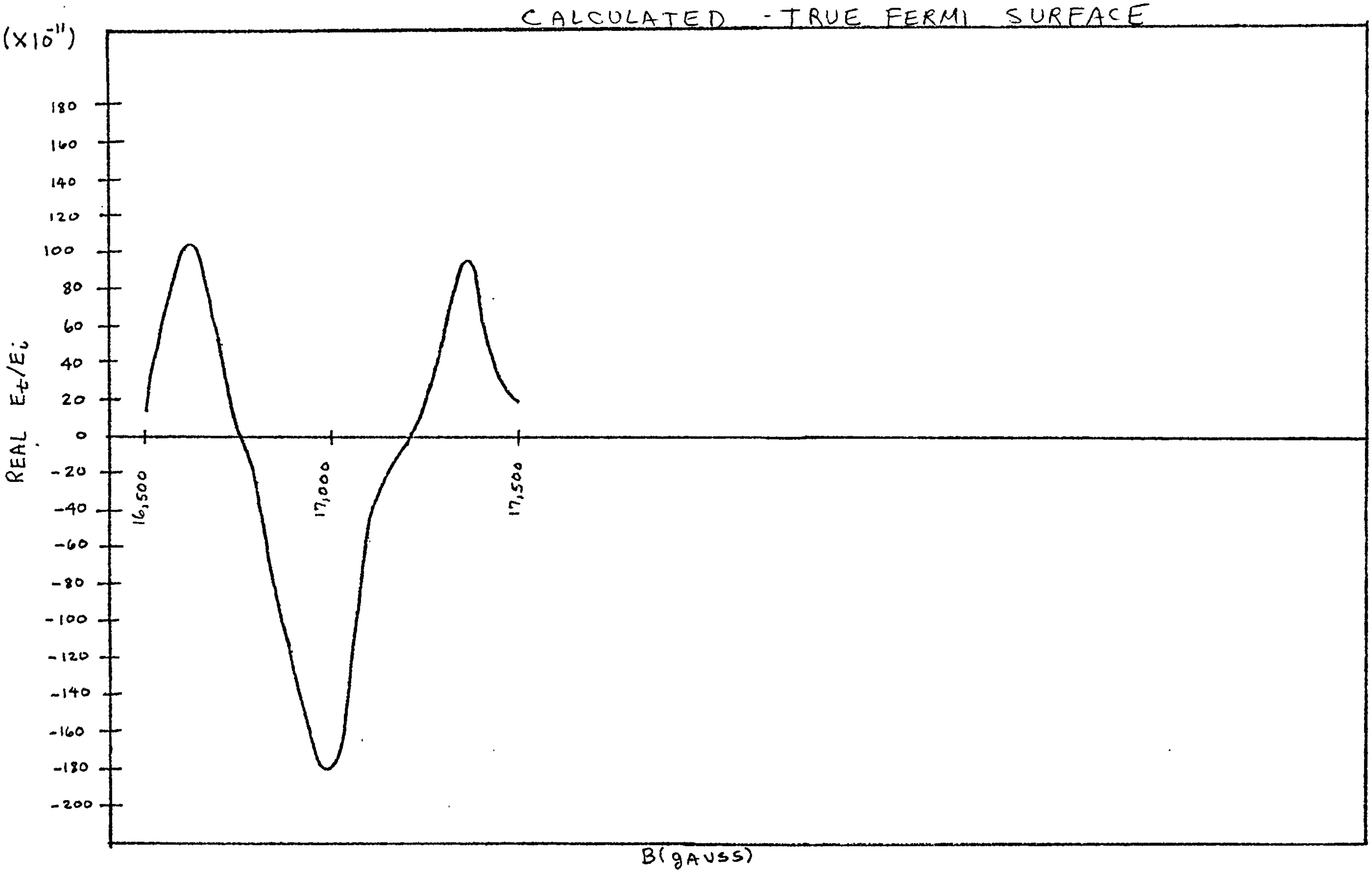

COPPER [001] DIRECTION

$\tau = 10^{-9}$ SEC $f = 395.2 \times 10^{3}$ CYC/SEC

GRAPH XXXIII

CALCULATED TRUE FERMI SURFACE

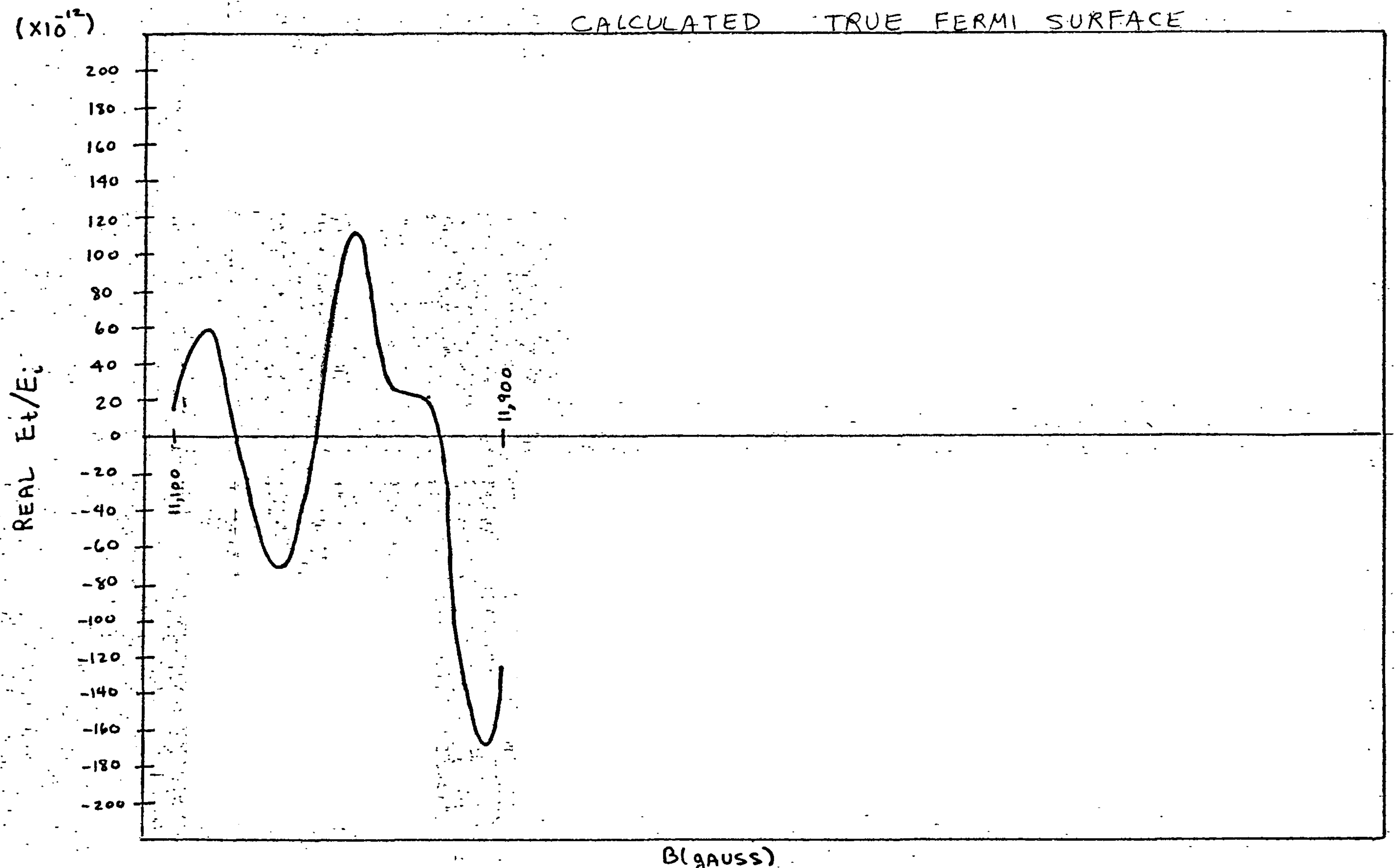

COPPER [001] DIRECTION

$\tau = 10^{-9}$ SEC $f = 395.2 \times 10^{3}$ cyc/sec

COMPUTER PROGRAM FOR THE CALCULATION OF THE RATIO OF THE MAGNITUDE OF THE TRANSMITTED ELECTRIC FIELD TO THE INCIDENT ELECTRIC FIELD

The following are the variables contained in the program:

Q= thickness of metal slab (cm.)
AMXK= maximum value of the wave vector in the z-direction
W= frequency of incident electromagnetic wave
T= relaxation time
PE= electron density
KPS= the number of magnetic field values for which we are evaluating E_t/E_i
BO= the lowest magnetic field value that we are using
SU= the step interval between consecutive magnetic field values
IO= the number of integers which when added to IPED is considered as a sufficient approximation to the infinite sum in the expression for E_t/E_i
JS= number of orbits into which the Fermi Surface has been divided between k_z=0.0 and k_z= AMXK
J= DO-LOOP index for orbits
N= number of Fermi surface data points for an orbit. N may be even or odd, but the points are assumed as evenly distributed in the interval
K= DO-LOOP index for wave number.
F= wave number = K*PI/Q
KS= integer which gives maximum wave number
NN= DO-LOOP index for the sum contained in the expression
NNO= the sum in the expression which goes from plus to minus infinity is replaced by a sufficiently approximate sum going from plus to minus (NNO-1)/2
NT= IO + 1

The values of the variables in the program for sodium that were used are as follows:

$Q = 0.1$ cm

$AMXK = 0.9 \times 10^{8}$ cm^{-1}

$W = 10^{6}$ hz.

$PE = 2.5 \times 10^{22}$ electrons/cm^3

$IO = 5$

$JS = 27$

$N = 45$

$NNO = 11$

$NNT = 6$

Values of Variables for Copper

The values of the variables in the program for copper that were used are as follows:

$Q = 0.084$ cm

$AMXK = 1.44 \times 10^{8}$ cm^{-1}

$W = 10^{6}$ hz.

$PE = 8.5 \times 10^{22}$ electrons/cm^{3}

$IO = 4$

$JS = 27$

N = variable

$NNO = 9$

$NT = 5$

COMPUTER PROGRAM

```
      DOUBLE PRECISION A, ANSRX, ANSRY, ANSIX, ANSIY, BETA,
      GAMMA, S, V, DET, DARTR, DARTI, ETEIR, ETEII
      COMPLEX CART, CSUMA, CSUMB, CSUMC, CSUMD, PARTP, PARTN,
      SUMAXN, SUMAYN, SUMBXN, SUMBYN, SUMCXN, SUMAXP, SUMAYP,
      SUMBXP, SUMBYP, SUMCXP, SUMCYP, SUMCYN, DENOMP, DENOMN,
      DENM, DENP, VNXPP, VNYPP, VNXNN, VNYNN, VNXN, VNYN, VNYP,
      VNXP, SAXX, SAXY, SBXXA, SBXXB, SBXYA, SBXYB, SIGXX, SIGXY,
      CIA, CVYXX, CVYXY
      DIMENSION  DENP(NNO), DENM(NNO), VNXPP(NNO), VNYPP(NNO),
      VNXNN(NNO), VNYNN(NNO), VX(NMAX), VY(NMAX), VZ(NMAX),EXPIN(NMAX),
      PARTP(NMAX), PARTN(NMAX), CART(NMAX), NAN(JS), WC(JS),
      ARRAY(JS), AVGVZ(JS), ARMC(JS), CVYXX(JT,KS), CVYXY(JT,KS)
      Q=
      AMXK=
      CIA= (0.0,1.0)
      H= 1.0545E-27
      TM= 9.11E-28
      R= 9.11E-28
      W=
      T=
      D= 2.99E+10
      E= 4.8E-10
      PE=
      PI= 3.1416
      ST=(W*PE*E)/(PI*D)
      A=((E**2)*AMXK)/((H**2)*(PI**2)*((2*JS)-2))
      REWIND 8
      DO 1000 KP=1,KPS
      B=(BO + SU*(KP-1))
      PEB=(2.0*Q*SQRT(ST))/SQRT(B)
      IPEC=INT(PEB)
      IPED=IPEC + IO
      IPEG=IPEC - IO
      DO 265 J=1,JS
      READ(8) ARRAY(J), NAN(J)
      N=NAN(J)
      READ(8) (VX(I),I=1,N)
      READ(8) (VY(I),I=1,N)
      READ(8) (VZ(I),I=1,N)
C     CALCULATION OF THE ARRAY AVGVZ
      IF(N-2*(N/2)) 110,115,110
115   SUMA= VZ(1) + VZ(N-1)
      SUMB=0.0
      KN=N-2
      DO 111 L=2,KN,2
111   SUMB=SUMB + VZ(L)
      SUMC=0.0
      KN=N-3
      DO 112 L=3,KN,2
```

```
112   SUMC=SUMC + VZ(L)
      SUMD=(VZ(N-1) + VZ(N))/(2.0*(N-1))
      AVGVZ(J)=(SUMA + 4.0*SUMD + 2.0*SUMD)/(3.0*(N-1)) + SUMD
      GO TO 120
110   SUMA=VZ(1) + VZ(N)
      SUMB=0.0
      KN=N-1
      DO 116 L=2,KN,2
116   SUMB=SUMB + VZ(L)
      SUMC=0.0
      KN=N-2
      DO 117 L=3,KN,2
117   SUMC=SUMC + VZ(L)
      AVGVZ(J)=(SUMA + 4.0*SUMB + 2.0*SUMC)/(3.0*(N-1))
      GO TO 120
120   CONTINUE
      CALCULATION OF THE ARRAYS ARMC(J) AND WC(J)
      ARMC(J)=1.37*R*(NAN(J)*1.0)/(NAN(1)*1.0)
      WC(J)=(E*B)/(D*ARMC(J))
      DO 600 K=IPEG, IPED
      F= (K*PI)/Q
      EXPIN(1)=0.0
      DO 125 M=2,N
125   EXPIN(M)=(VZ(M) + VZ(M-1)-2.0*AVGVZ(J))*F*PI/((N-1))
      SUM=0.0
      DO 130 M=1,N
      SUM=SUM + EXPIN(M)
      PARTN(M)=CEXP(CIA*SUM/WC(J))
130   PARTP(M)=CEXP((-1.0*CIA*SUM)/WC(J))
      CART(1)=(1.0,0.0)
      DO 12 NN=1,NNO
      DO 135 M=2,N
135   CART(M)=CEXP(-2.0*CIA*(-NNT + NNO)*PI*(M-1)/((N-1)*1.0)
      IF (N-2*(N/2)) 181,182,181
182   SUMAXP=VX(1)*PARTP(1)*CART(1) + VX(N-1)*PARTP(N-1)*CART(N-1)
      SUMAYP=VY(1)*PARTP(1)*CART(1) + VY(N-1)*PARTP(N-1)*CART(N-1)
      SUMAXN=VX(1)*PARTN(1)*CART(1) + VX(N-1)*PARTN(N-1)*CART(N-1)
      SUMAYN=VY(1)*PARTN(1)*CART(1) + VY(N-1)*PARTN(N-1)*CART(N-1)
      SUMBXP=(0.0,0.0)
      SUMBYP=(0.0,0.0)
      SUMBXN=(0.0,0.0)
      SUMBYN=(0.0,0.0)
      KN=N-2
      DO 146 L=2,KN,2
      SUMBXP=SUMBXP + VX(L)*PARTP(L)*CART(L)
      SUMBYP=SUMBYP + VY(L)*PARTP(L)*CART(L)
      SUMBXN=SUMBXN + VX(L)*PARTN(L)*CART(L)
146   SUMBYN=SUMBYN + VY(L)*PARTN(L)*CART(L)
      SUMCXP=(0.0,0.0)
```

```
      SUMCYP=(0.0,0.0)
      SUMCXN=(0.0,0.0)
      SUMCYN=(0.0,0.0)
      KN=N-3
      DO 147 L=3,KN,2
      SUMCXP=SUMCXP + VX(L)*PARTP(L)*CART(L)
      SUMCYP=SUMCYP + VY(L)*PARTP(L)*CART(L)
      SUMCXN=SUMCXN + VX(L)*PARTN(L)*CART(L)
147   SUMCYN=SUMCYN + VY(L)*PARTN(L)*CART(L)
      SUMDXP=(VX(N-1)*PARTP(N-1)*CART(N-1)+VX(N)*PARTP(N)*CART(N))
      /(2.0*(N-1))
      SUMDYP=(VY(N-1)*PARTP(N-1)*CART(N-1)+VY(N)*PARTP(N)*CART(N))
      /(2.0*(N-1))
      SUMDXN=(VX(N-1)*PARTN(N-1)*CART(N-1)+VX(N)*PARTN(N)*CART(N))
      /(2.0*(N-1))
      SUMDYN=(VY(N-1)*PARTN(N-1)*CART(N-1)+VY(N)*PARTN(N)*CART(N))
      /(2.0*(N-1))
      VNXP=(SUMAXP + 4.0*SUMBXP +2.0*SUMCXP)/(3.0*(N-1))+(SUMDXP)
      VNYP=(SUMAYP + 4.0*SUMBYP +2.0*SUMCYP)/(3.0*(N-1))+(SUMCYP)
      VNXN=(SUMAXN + 4.0*SUMBXN +2.0*SUMCXN)/(3.0*(N-1))+(SUMDXN)
      VNYN=(SUMAYN + 4.0*SUMBYN +2.0*SUMCYN)/(3.0*(N-1))+(SUMDYN)
      GO TO 60
181   SUMAXP=VX(1)*PARTP(1)*CART(1) + VX(N)*PARTP(N)*CART(N)
      SUMAYP=VY(1)*PARTP(1)*CART(1) + VY(N)*PARTP(N)*CART(N)
      SUMAXN=VX(1)*PARTN(1)*CART(1) + VX(N)*PARTN(N)*CART(N)
      SUMAYN=VY(1)*PARTN(1)*CART(1) + VY(N)*PARTN(N)*CART(N)
      SUMBXP=(0.0,0.0)
      SUMBYP=(0.0,0.0)
      SUMBXN=(0.0,0.0)
      SUMBYN=(0.0,0.0)
      KN=N-1
      DO 141 L=2,KN,2
      SUMBXP= SUMBXP + VX(L)*PARTP(L)*CART(L)
      SUMBYP= SUMBYP + VY(L)*PARTP(L)*CART(L)
      SUMBXN= SUMBXN + VX(L)*PARTN(L)*CART(L)
141   SUMBYN= SUMBYN + VY(L)*PARTN(L)*CART(L)
      SUMCXP=(0.0,0.0)
      SUMCYP=(0.0,0.0)
      SUMCXN=(0.0,0.0)
      SUMCYN=(0.0,0.0)
      KN=N-2
      DO 142 L=3,KN,2
      SUMCXP=SUMCXP + VX(L)*PARTP(L)*CART(L)
      SUMCYP=SUMCYP + VY(L)*PARTP(L)*CART(L)
      SUMCXN=SUMCXN + VX(L)*PARTN(L)*CART(L)
142   SUMCYN=SUMCYN + VY(L)*PARTN(L)*CART(L)
      VNXP=(SUMAXP + 4.0*SUMBXP + 2.0*SUMCXP)/(3.0*(N-1))
      VNYP=(SUMAYP + 4.0*SUMBYP + 2.0*SUMCYP)/(3.0*(N-1))
      VNXN=(SUMAXN + 4.0*SUMBXN + 2.0*SUMCXN)/(3.0*(N-1))
```

```
      VNYN=(SUMAYN + 4.0*SUMBYN + 2.0*SUMCYN)/(3.0*(N-1))
 60   EN=NN
      DENOMP=(1.0/T)+CIA*(F*AVGVZ(J)-W-((-NNT*1.0+EN)*WC(J)))
      DENOMN=(1.0/T)-CIA*(F*AVGVZ(J)+W+((-NNT*1.0+EN)*WC(J)))
      VNXPP(NN)=VNXP
      VNYPP(NN)=VNYP
      VNXNN(NN)=VNXN
      VNYNN(NN)=VNYN
      DENP(NN)=DENOMP
 12   DENM(NN)=DENOMN
      CALCULATION OF SUMS FOR SIGXX AND SIGXY
      CSUMA=(0.0,0.0)
      CSUMB=(0.0,0.0)
      CSUMC=(0.0,0.0)
      CSUMD=(0.0,0.0)
      DO 10 NN=1,NNO
      CSUMA=CSUMA + VNXNN(NN)*CONJG(VNXNN(NN))/DENM(NN)
      CSUMB=CSUMB + VNXNN(NN)*CONJG(VNYNN(NN))/DENM(NN)
      IF (J-1) 275,276,275
275   CSUMC=CSUMC + VNXPP(NN)*CONJG(VNXPP(NN))/DENP(NN)
      CSUMD=CSUMD + VNXPP(NN)*CONJG(VNYPP(NN))/DENP(NN)
276   CONTINUE
 10   CONTINUE
      CVYXX(JS+1-J,K)=CSUMA
      CVYXY(JS+1-J,K)=CSUMB
      CVYXX(JS-1-J,K)=CSUMC
      CVYXY(JS-1-J,K)=CSUMD
600   CONTINUE
265   CONTINUE
      REWIND 8
      DO 700 K=IPEG,IPED
      F=(K*PI)/Q
      SAXX=ARMC(JS)*CVYXX(1,K) + ARMC(JS)*CVYXX(2*JS-1,K)
      SAXY=ARMC(JS)*CVYSY(1,K) + ARMC(JS)*CVYXY(2*JS-1,K)
      SBXXB=ARMC(1)*CVYXX(JS,K)
      SBXYB=ARMC(1)*CVYXY(JS,K)
      SBXXA=(0.0,0.0)
      SBXYA=(0.0,0.0)
      DO 285 L=2,JS-1,2
      SBXXA=SBXXA + ARMC(JS+1-L)*CVYXX(L,K)+ARMC(L)*CVYXX(JS-1+L,K)
285   SBXYA=SBXYA + ARMC(JS+1-L)*CVYXY(L,K)+ARMC(L)*CVYXY(JS-1+L,K)
      DO 290 L=3,JS-2,2
      SBXXB=SBXXB + ARMC(JS+1-L)*CVYXX(L,K)+ARMC(L)*CVYXX(JS-1+L,K)
290   SBXYB=SBXYB + ARMC(JS+1-L)*CVYXY(L,K)+ARMC(L)*CVYSY(JS-1+L,K)
      SIGXX=(SAXX + 4.0*SBXXA + 2.0*SBXXB)/3.0
      SIGXY=(SAXY + 4.0*SBXYA + 2.0*SBXYB)/3.0
      ANSRX=REAL(SIGXX)*A
      ANSRY=REAL(SIGXY)*A
      ANSIX=AIMAG(SIGXX)*A
```

```
      ANSIY=AIMAG(SIGXY)*A
      V=(4.0*PI*W*(ANSRX + ANSIY))/(D**2)
      S=(F**2)-((W*4.0*PI*(ANSIX-ANSRY))/(D**2))
      DET=(S**2) + (V**2)
      IF (K-2*(K/2)) 15,16,15
   16 PNO=-1.0
      GO TO 500
   15 PNO= 1.0
  500 DARTR=PNO*V/DET
      DARTI=PNO*S/DET
      IF (K-IPEG) 801,800,801
  800 BETA= 0.0
      GAMMA= 0.0
  801 BETA=BETA + DARTR
      GAMMA=GAMMA + DARTI
  700 CONTINUE
      ETEII=(4.0*W*GAMMA)/(Q*D)
      ETEIR=(4.0*W*BETA)/(Q*D)
      WRITE(6,900) ETEIR, ETEII, B
  900 FORMAT(1X,6HETEIR=,D14.3,4X,6HETEII=,D14.3,4X,2HB=,F10.2)
 1000 CONTINUE
      REWIND 8
      END
```

REFERENCES

1. P. R. Antoniewicz, L. T. Wood, and J. D. Gavenda, Physical Review Letters 21, 998 (1968).
2. J. Mertsching, Phys. Stat. Sol. 14, 3 (1966).
3. L. T. Wood, thesis, University of Texas (1969).
4. J. C. McGroddy, J. R. Stanford, and E. A. Stern, Phys. Rev. 141, 437 (1966).